Steel Joist System Reliability Report

Kubilay Cicek, Graduate Research Assistant

Hannah B. Blum, Alain H. Peyrot Associate Professor

Department of Civil and Environmental Engineering

University of Wisconsin - Madison

August 2025

Revised February 2026

This report was prepared for Steel Joist Institute

Abstract

Current steel design codes primarily adopt member-based resistance factors, which could lead to overly conservative or inefficient designs for structural systems. This study investigates the reliability of steel joists to develop system-based resistance factors that better reflect real structural behavior. Using advanced statistical techniques, Latin hypercube sampling, and structural reliability methods, the influence of various uncertainties on the performance of these systems were evaluated. Sensitivity studies assess the impact of material properties, and geometric imperfections on system stability. The results provide target reliability indices and system-based resistance factors, which can enhance design efficiency while maintaining safety. This research is supported by collaborations with the Steel Joist Institute and the Steel Deck Institute, ensuring that the findings are aligned with industry needs. The proposed system-based resistance factors will contribute to the refinement of design provisions in steel construction codes, offering cost-effective and structurally optimized solutions. Ultimately, this study bridges the gap between theoretical reliability assessment and practical engineering applications, facilitating more efficient and reliable steel structures.

Contents

List of Figures

List of Tables

1. Introduction

Steel joists are widely used in structural engineering due to their efficiency, lightweight nature, and high load-carrying capacity. The design of reliable structures requires comprehensive knowledge of material behavior, robust predictive models, identification of possible failure modes, and rigorous reliability assessment. This study integrates finite element modeling, statistical analyses, and sensitivity studies to evaluate the performance of steel joists under realistic conditions, ensuring structural safety and efficient material use in high-performance applications.

The primary objective of this study is to establish system-based resistance factors and target reliability indices that better reflect the true behavior of steel joists. Current design codes predominantly rely on member-based resistance factors, which may not fully capture the interaction effects, system-level dependencies and more importantly the redundancy in the systems (Galambos, [4] and Hendawi, S. and Frangopol, D. M. [5]). By leveraging advanced computational models and probabilistic methods, this study aims to provide insights into joist reliability and proposes adjustments to design methodologies to improve structural efficiency and safety.

The research methodology involves stochastic input generation, finite element modeling (FEM) using shell and beam elements, and nonlinear second-order analyses to accurately capture failure modes. Stochastic variables for material properties, cross-section dimensions, and weld lengths are generated using the Latin Hypercube Sampling method, based on collected data from manufacturing plants. These randomized datasets are then used to drive finite element analyses for different failure scenarios.

Detailed computational models (FEM) are employed to simulate stress distributions and

predict failure onset across the structure. Both beam and shell element models are utilized for validation purposes. The study examines multiple potential failure modes, including chord and web buckling, to determine the critical conditions for system integrity. A significant aspect of this research is its focused investigation into the resistance (R) component of the reliability equation. To demonstrate how the results of this resistance-focused analysis can be translated into engineering practice, the framework of AISI S100 [6] Chapter K is employed to calculate specific resistance factors (ϕ) across a range of target reliability indices (β_o). This approach not only quantifies the inherent variability of the joist capacity but also provides a clear methodology for integrating these probabilistic findings into standardized design procedures. By merging high-fidelity simulations with stochastic calibration, this study extends conventional deterministic methods into a probabilistic domain to enhance the robustness and efficiency of steel joist design.

2. Input Variables

In reliability analyses of structural systems, accurately characterizing input variables is essential for generating realistic stochastic models. This chapter presents the statistical evaluation of key input parameters used in the analyses, including material properties, cross-sectional dimensions, and weld lengths. The data were collected from various sources, normalized by their nominal values, and fitted to appropriate probability distributions to ensure consistency across different design scenarios. The selection of the best-fit distributions was based on empirical data and statistical fitting methods, with distribution parameters provided for each dataset. The following sections detail the statistical distributions of material properties for cold-formed and hot-rolled steel sections, cross-sectional imperfection measurements, and weld length variations, along with the rationale behind their selection.

The figures related to data distributions in this section consist of two subplots. The upper plot presents a histogram of the data along with the probability density function (PDF) of the fitted distribution, while the lower plot shows the cumulative distribution function (CDF) of the data and the empirical cumulative distribution function (ECDF) of the fitted distribution. The ECDF is an empirical measure of this probability based on observed data points.

The best-fit distributions were determined for each variable, including types such as Lognormal, Burr, Stable, and Generalized Extreme Value (GEV). Since these distributions are characterized by different mathematical parameters, a unified four-column structure is used in Table 2.2 to present the results consistently.

In this structure, the parameters are categorized based on their functional roles: the first

column represents Location, the second represents Scale, and the third and fourth columns provide Shape 1 and Shape 2 parameters, respectively. For example, while the Lognormal distribution is defined by mean (location) and standard deviation (scale), the GEV distribution includes an additional shape parameter (k) in the third column. Similarly, more complex distributions like Burr or Stable utilize the remaining columns to provide their specific shape or stability factors.

This organized approach ensures that all probabilistic inputs are clearly documented regardless of their distribution type. Table 2.2 provides the complete list of fitted parameters, while Table 2.4 summarizes the minimum and maximum ratios observed in the data after filtration. Furthermore, Table 2.3 presents the equivalent mean and standard deviation values derived from these distributions. These values are provided to facilitate a direct comparison with conventional structural design assumptions and to offer a simplified statistical overview of the data's central tendency and dispersion, even when the underlying distribution is non-Gaussian.

2.1. Material Properties

Joists are manufactured using Cold Formed Steel (CFS) and Hot Rolled Steel (HRS) sections. Tensile test results conducted by SJI member companies' plants for both HRS and CFS were randomly collected, analyzed, and fitted to distributions for random variable input generation. A nominal yield strength of 50 ksi was assumed for design purposes in the SJI joist designs; therefore, tensile test results for 50 ksi sections were specifically collected from SJI member companies. Despite focusing on 50 ksi material, the dataset includes various grades of both CFS and HRS sections, with their nominal ultimate stresses provided in Table 2.1. The ratios of measured values to nominal values for both yield stress and ultimate stresses were calculated.

Table 2.1: Material grades and nominal ultimate stresses

	CFS		HRS			
Grade	A1018	A1011	A529-A529NM	A572	A992	A500
F_u **(ksi)**	65	65	70	65	58	65

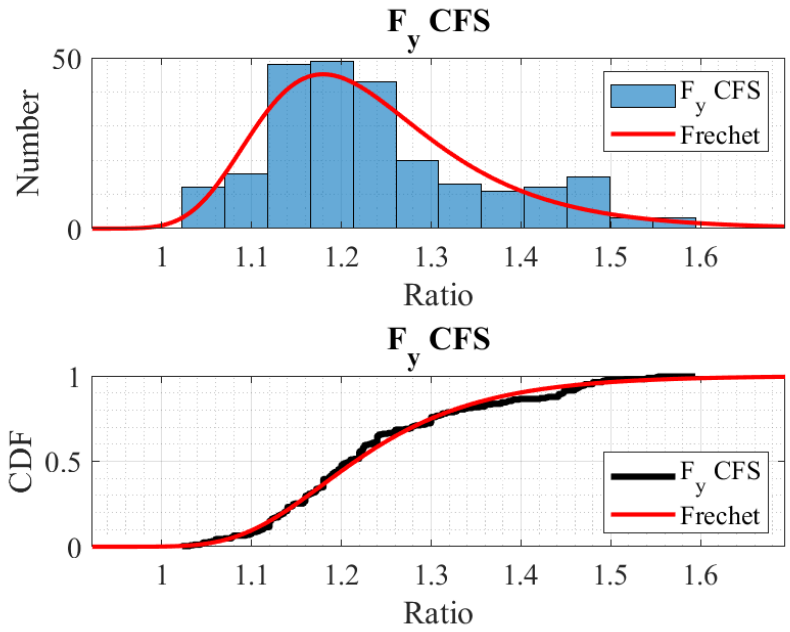

Figure 2.1: Yield stress distribution for CFS sections

2.1.1 Cold Formed Steel Material Data

The combined tensile test data, collected from different manufacturers, consists of 265 tensile test results. Figure 2.1 shows the histogram and best fit distribution of the collected data for CFS sections tensile test yield strength results. While there is a high dispersion in the collected data, a clear distribution fitting was achieved despite a small data concentration of data between ratios of 1.4 and 1.5. The best fit was obtained using Frechet distribution. Also Figure 2.2 shows the histogram and best fit distributions for ultimate stress data.

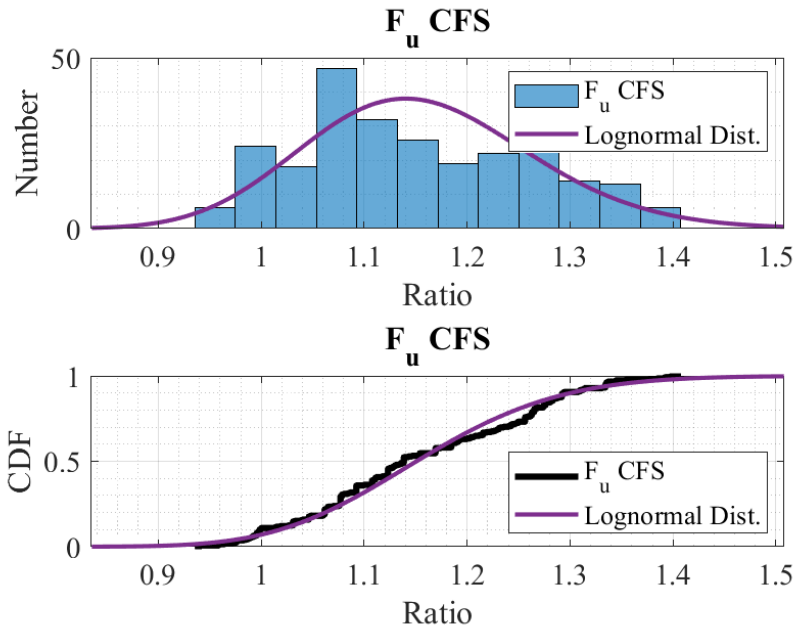

Figure 2.2: Ultimate stress distribution for CFS sections

2.1.2 Hot Rolled Steel Material Data

Figure 2.3 shows the distribution of 389 HRS tensile test data for yield strength. Compared to CFS material, the mean and the dispersion are smaller, and the Burr distribution was determined as the best fit for the collected data. The histogram and the best fit distribution for ultimate stress data is provided in Figure 2.4.

2.2. Cross-Sectional Properties

Hot-rolled steel (HRS) and cold-formed steel (CFS) angle and channel sections were randomly selected to generate cross-sectional imperfection data. SJI member companies collected cross-sectional measurements in varying quantities for the specified section types (HRS angle, CFS

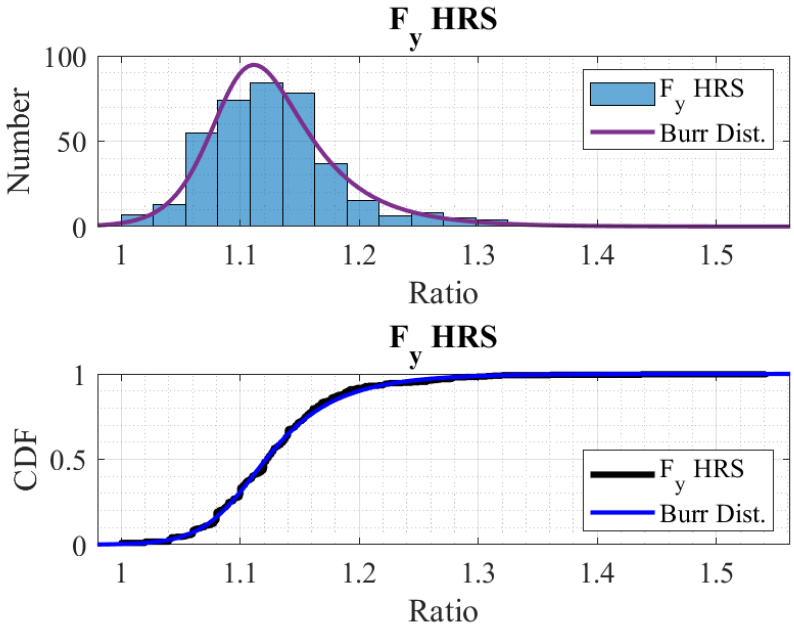

Figure 2.3: Yield stress distribution for HRS sections

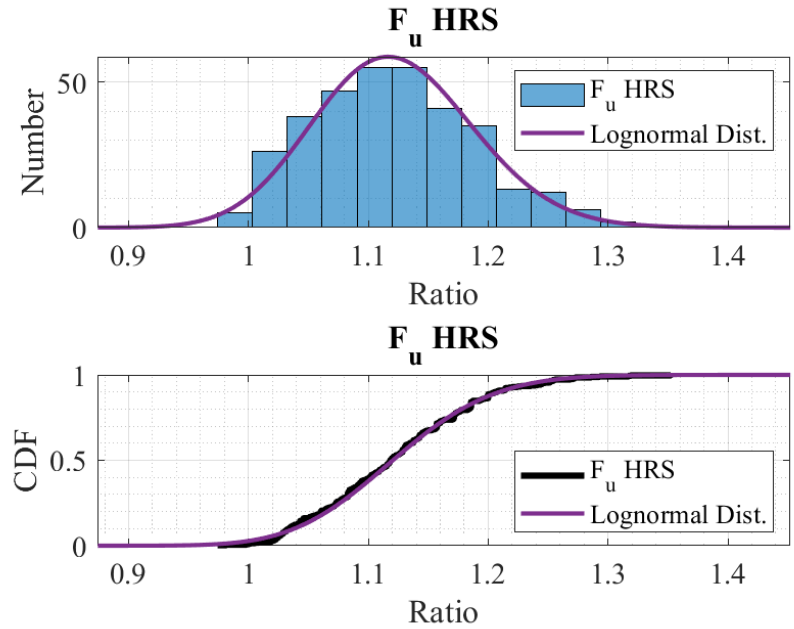

Figure 2.4: Ultimate stress distribution for HRS sections

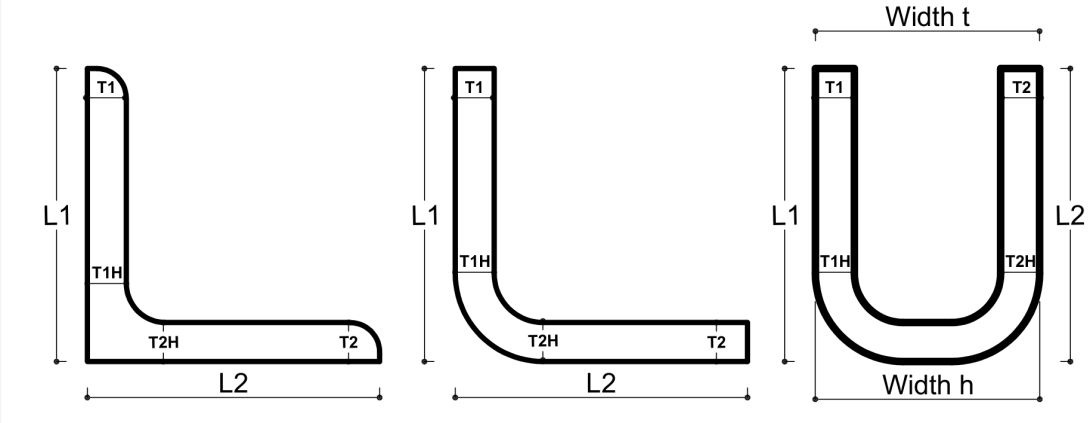

Figure 2.5: Left: HRS angle section, Middle: CFS angle section, Right:CFS channel section

angle, and CFS channel), as illustrated in Figure 2.5.

For angle sections, there are four thickness measurements per section which are from both heel (T1H and T2H) and toe (T1 and T2) ends of each leg, along with two leg length measurements (L1 and L2). For channel sections, toe and heel widths were measured (Width t and Width h, respectively), whereas for angle sections, the forming angle between legs was recorded to evaluate forming performance and accurately model the sections. To eliminate sectional differences, the same normalization method is used for cross-sectional imperfections, with lengths and thicknesses normalized by their nominal values.

2.2.1 HRS Angle Section Data

HRS sections are expected to have high consistency in cross-sectional dimensions due to the manufacturing methods. This high consistency creates additional challenges for distribution fitting due to very small margins or high repetitions in the data. An example to this is the forming angle between legs of HRS angle sections predominantly includes data between 89.5 to 90.5, with the majority of measurements being 90 degrees. Consequently, it was not feasible to generate a distribution fitting for that specific data.

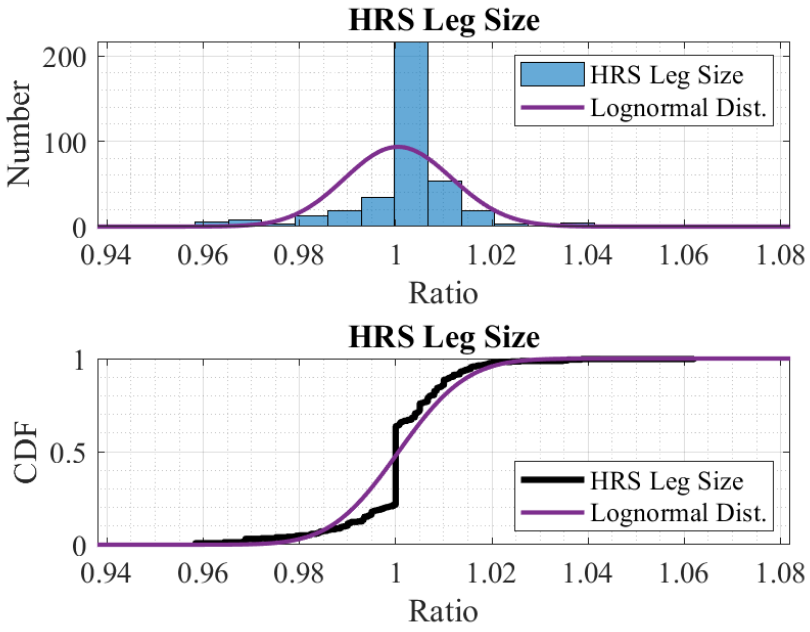

Figure 2.6: Distributions for HRS angle leg size

Another challenging dataset is the HRS angle leg sizes. While the variations are slightly larger than those observed in the forming angles, a significant portion of the data has a ratio of 1, creating a distinct peak at this value, as illustrated in Figure 2.6. Despite the challenges, the lognormal distribution was determined to be the best representation of the data.

The HRS thickness data, on the other hand, shows a clear distribution and a high concentration around the ratio of 1, as expected. Although using high degree functions in distribution fitting can lead to overfitting problem, this study relies on actual data collected from joist plants, making such functions applicable for a more accurate fit. In this case, the Stable distribution was selected as the best fit for HRS thickness data as shown in Figure 2.7.

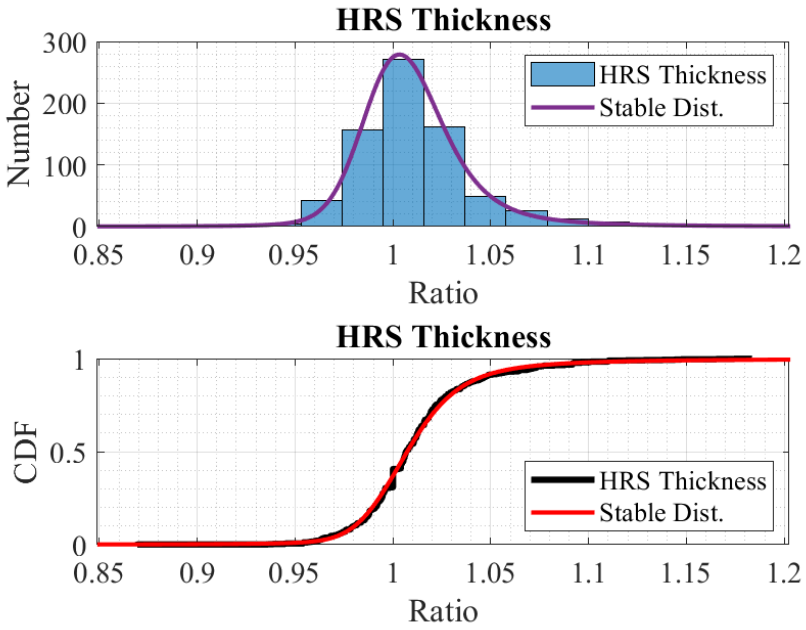

Figure 2.7: Distributions for HRS angle leg thickness values

2.2.2 CFS Angle and Channel Section Data

Measurements were completed for both CFS channel and angle sections in SJI manufacturing plants. Given that the forming of both section types are made by steel sheets, the thickness and leg size data showed similar distributions. Therefore, rather than applying separate distributions for thickness and leg size inputs, the data for each dimension was combined into two groups: CFS leg sizes and CFS thicknesses. The same distributions were used for both channel and angle sections. Both leg size and thickness histograms and fitted distributions are given in Figures 2.8 and 2.9.

CFS angle forming angle data shows similarity to HRS angle section forming angle data, making distribution fitting unfeasible. However, forming of CFS channel sections were included in analyses by including different width values for toe and heel ends of channels. Different distributions were applied to heel and toe widths, and channel cross-sections were generated based on these distributions at each step of the analysis.

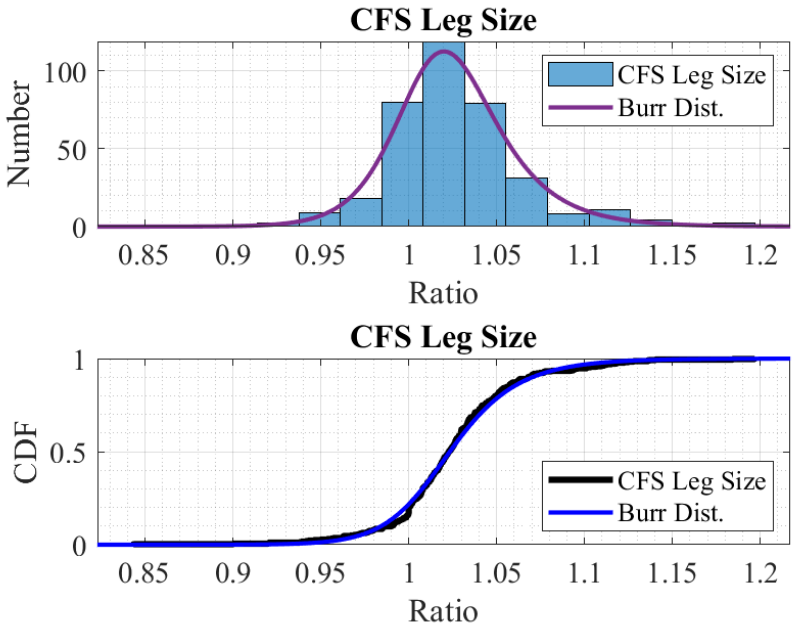

Figure 2.8: Distributions for CFS angle leg size

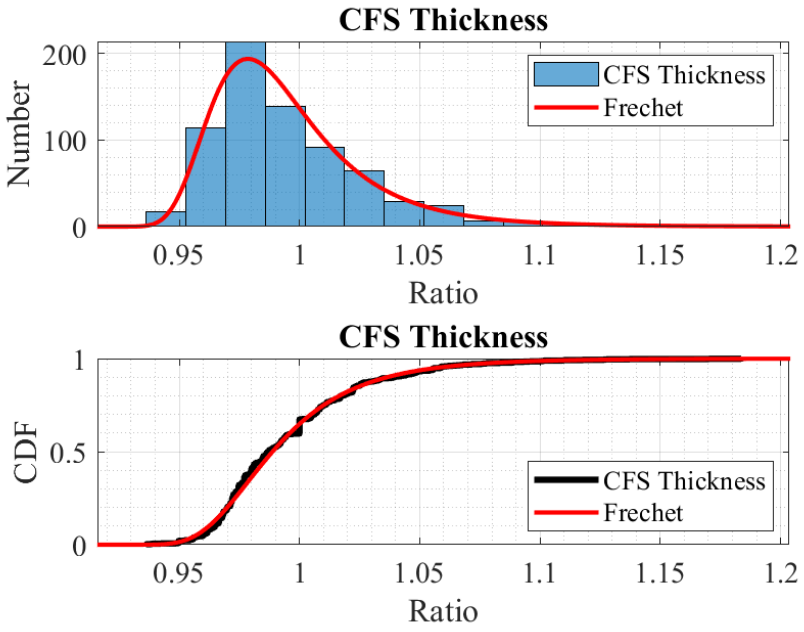

Figure 2.9: Distributions for CFS angle leg thickness values

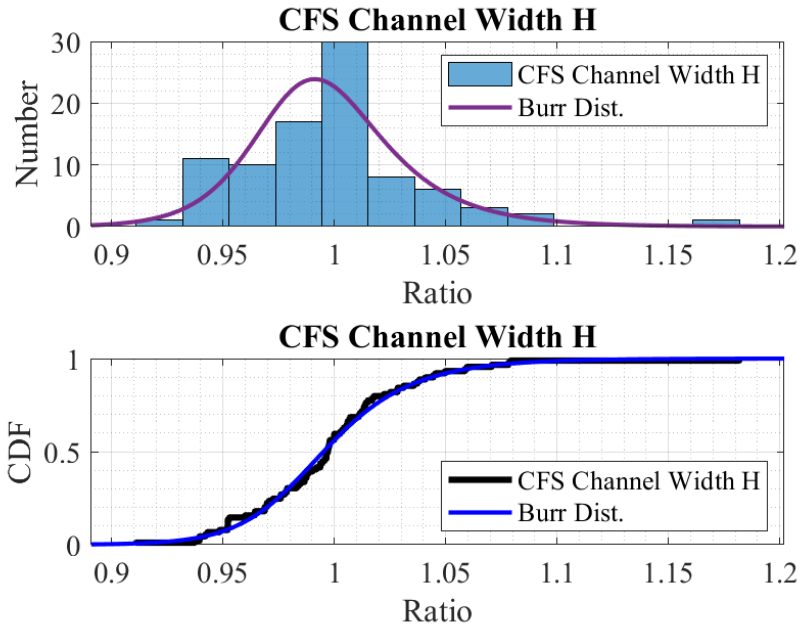

Figure 2.10: Distributions for CFS channel section heel width data

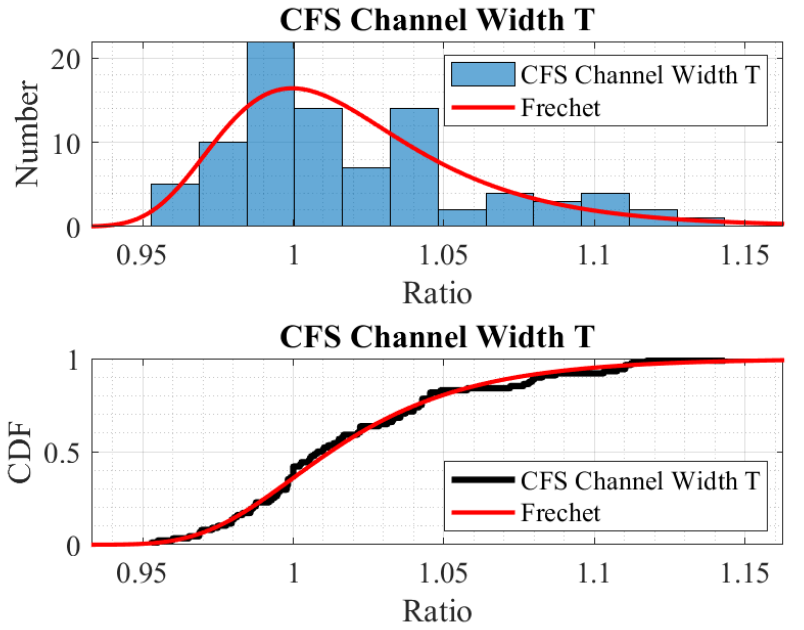

Figure 2.11: Distributions for CFS channel section toe width data

2.3. Weld Lengths

Another selected variable for random inputs is web weld lengths. The first six webs were considered, and weld lengths were measured from both sides of joists and both ends of the webs (top and bottom chord ends). Locations and names of the selected webs are shown in Figure 2.12. A filtration was applied to data to eliminate misentered inputs. The limits for this filtration was defined as 0.5 to 4 in ratios.

Weld lengths differentiates at every joist designs and at every web member. Ratio of measured weld lengths to the nominal weld length were used to eliminate these differences between different joist designs. After analyzing each web separately and generating their respective distributions, similar web weld length data were grouped together, reducing the total number of categories from six to three. The final groupings are as follows:

- W webs group (Combined data from W3, W4 and W5 web weld length data),
- W2 webs group (only the data includes the first webs),
- Vertical webs group (D2 and V1 webs).

The Frechet distribution was determined to be the best fit for each of these groups. More details, including distribution parameters and visualizations, are provided in this section.

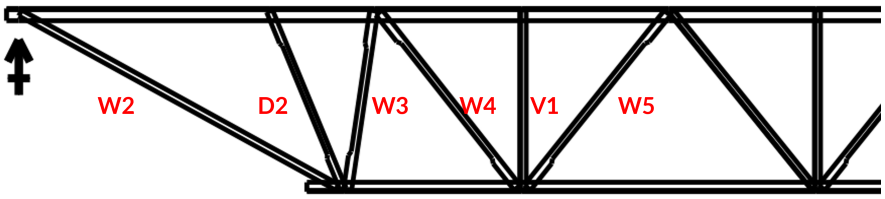

Figure 2.12: Webs that are used to measure the weld length at both ends and both sides of webs

2.3.1 W Webs Welds

This weld length data is a combined data coming from three different webs; W3, W4 and W5 webs. While the distribution fitting provides a single representation of these weld lengths, separately generated ratios were applied to each web in the analyses, ensuring independent random values for each case (uncorrelated).

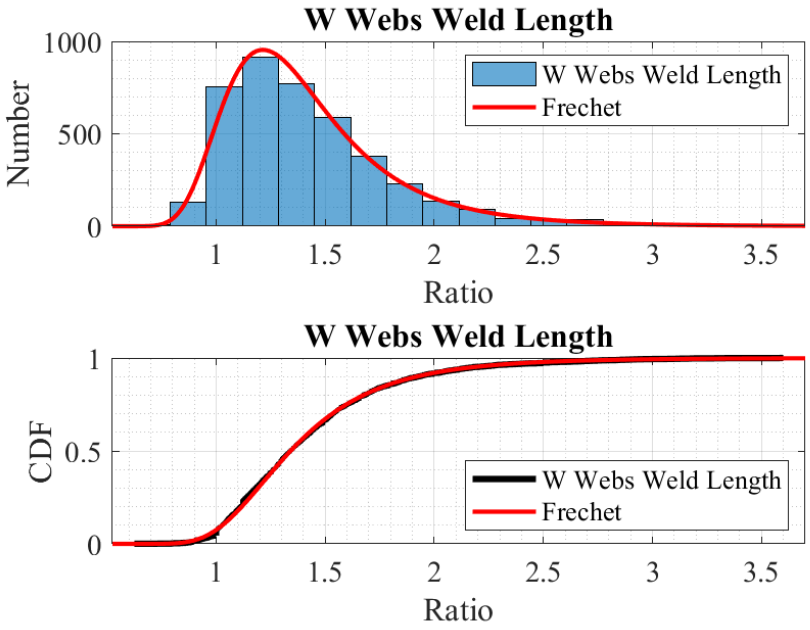

Figure 2.13: Distributions for W webs weld length data

2.3.2 W2 Webs Welds

The first web weld length data was analyzed separately from other web groups due to its distinct distribution and the importance of the first web given that one of the failure mode specifically focused on this member. The range is similar to the vertical web group but it is considerably larger than the W webs group.

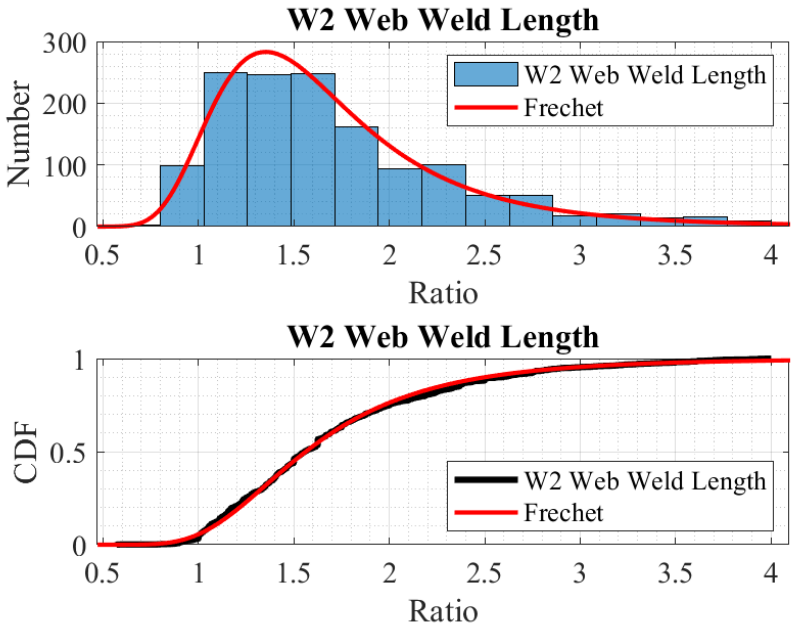

Figure 2.14: Distributions for W2 web weld length data

2.3.3 Vertical Webs Welds

The vertical webs group is the combination of weld length data from D2 and V1 webs. This group has the widest range among all web categories and has the highest mean ratio value. Its variability is greater compared to the W and W2 web groups, requiring a distinct distribution fitting for accurate representation in the analyses.

2.4. Material Models

In previous studies, it has been shown that CFS and HRS sections exhibit different material behaviors. Since nonlinear second-order analysis was used in this study, the nonlinear behavior of these sections were explicitly defined in ABAQUS. Models were generated based on the given

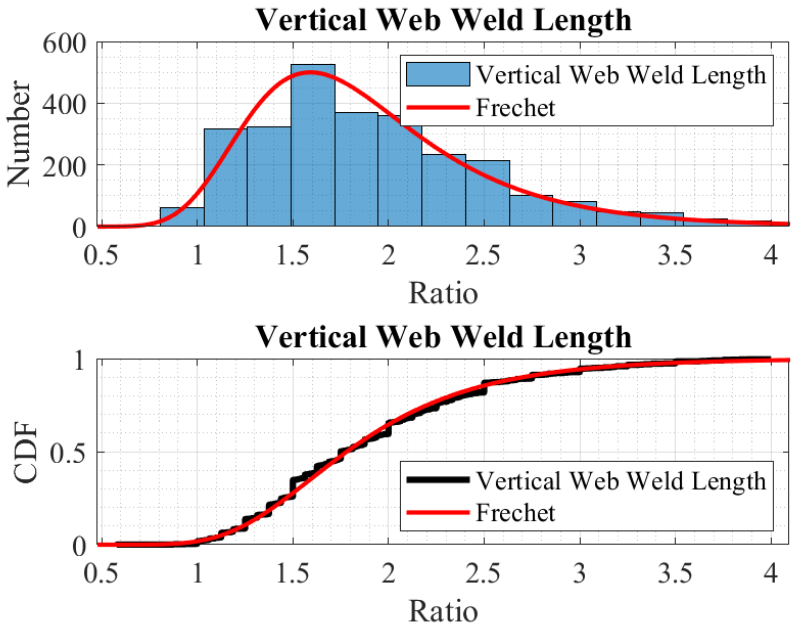

Figure 2.15: Distributions for vertical webs weld length data

Table 2.2: Distribution types and calculated parameters of collected data

Collected Data	**Distribution Type**	**Location / Mean (μ)**	**Scale / St. Dev. (σ)**	**Shape 1**	**Shape 2**	**# of Data**
HRS Yield Stress	Burr	-	1.098	52.059	0.497	389
CFS Yield Stress	Frechet	1.181	0.095	0.011	-	265
HRS Ult. Stress	Lognormal	0.114	0.059	-	-	389
CFS Ult. Stress	Lognormal	0.140	0.096	-	-	265
HRS Leg Size	Lognormal	0.0006	0.011	-	-	377
HRS Thickness	Stable	1.584	0.675	0.016	1.005	740
CFS Leg Size	Burr	-	1.015	60.029	0.711	365
CFS Thickness	Frechet	0.980	0.023	0.089	-	717
CFS Ch. Heel W.	Burr	-	0.985	58.576	0.675	89
CFS Ch. Toe W.	Frechet	1.0008	0.031	0.038	-	88
W Webs WL	Frechet	1.241	0.267	0.106	-	4163
W2 Webs WL	Frechet	1.407	0.414	0.141	-	1380
Vert. Webs WL	Frechet	1.613	0.458	0.048	-	2725

Abbreviations: Ult: Ultimate, WL: Weld Length, W: Width

Table 2.3: Theoretical mean and standard deviation values derived from the fitted probability distributions

Collected Data	Distribution Type	Mean	Standard Deviation	Number of Data
HRS Yield Stress	Burr Dist.	1.129	0.173	389
CFS Yield Stress	Frechet Dist.	1.237	0.124	265
HRS Ultimate Stress	Lognormal Dist.	1.122	0.067	389
CFS Ultimate Stress	Lognormal Dist.	1.156	0.111	265
HRS Leg Size	Lognormal Dist.	1.001	0.011	377
HRS Thickness	Stable Dist.	1.005	-	740
CFS Leg Size	Burr Dist.	1.015	0.142	365
CFS Thickness	Frechet Dist.	0.980	0.033	717
CFS Ch. Heel Width	Burr Dist.	0.985	0.141	89
CFS Ch. Toe Width	Frechet Dist.	1.020	0.042	88
W Webs Weld Length	Frechet Dist.	1.427	0.402	4163
W2 Webs Weld Length	Frechet Dist.	1.712	0.666	1380
Vert. Webs Weld Length	Frechet Dist.	1.900	0.629	2725

Table 2.4: Minimum and maximum ratios for collected data

Collected Data	Minimum Ratio	Maximum Ratio
HRS Yield Stress	1.000	1.542
CFS Yield Stress	1.023	1.594
HRS Ultimate Stress	0.974	1.352
CFS Ultimate Stress	0.935	1.408
HRS Leg Size	0.958	1.062
HRS Thickness	0.869	1.184
CFS Leg Size	0.844	1.197
CFS Thickness	0.936	1.184
CFS Ch. Heel Width	0.911	1.182
CFS Ch. Toe Width	0.953	1.143
W Webs Weld Length	0.625	3.600
W2 Webs Weld Length	0.571	4.000
Vert. Webs Weld Length	0.578	4.000

formulations in literature for preferred material models and updated by using randomly generated yield and ultimate stresses at every analysis. Consequently, each analysis featured different material

models for each chord and each web member according to the section type. It should also be noted that the members with same sections have the same material properties in each model (they are correlated) since that the same sections are most likely be coming from the same batch.

The nominal modulus of elasticity values were set as 29,000 ksi for HRS materials ([7]) and 29,500 ksi for CFS materials [6]. Additionally, since ABAQUS uses true stress - true strain behavior, the created material models were also converted to the true stress - true strain values before starting the analysis.

Material models allow modifying the F_y and F_u values along with the E value. These models then calculate the strains and the predictive model curvatures according to the formulas that were created by using the experimental background used in these studies.

2.4.1 Cold Formed Steel Material Model

The material model for CFS sections was taken from study of Gardner, et al. [1] and a plot for 50 ksi material with E=29,500 is given in Figure 2.16.

2.4.2 Hot Rolled Steel Material Model

HRS sections material models is different than the CFS section materials as mentioned before. The biggest difference is that this model has a clear yield plateau before the strain hardening starts. This model was taken from study of Yun, et al. [2] and a plot for 50 ksi material with E=29,000 is given in Figure 2.17.

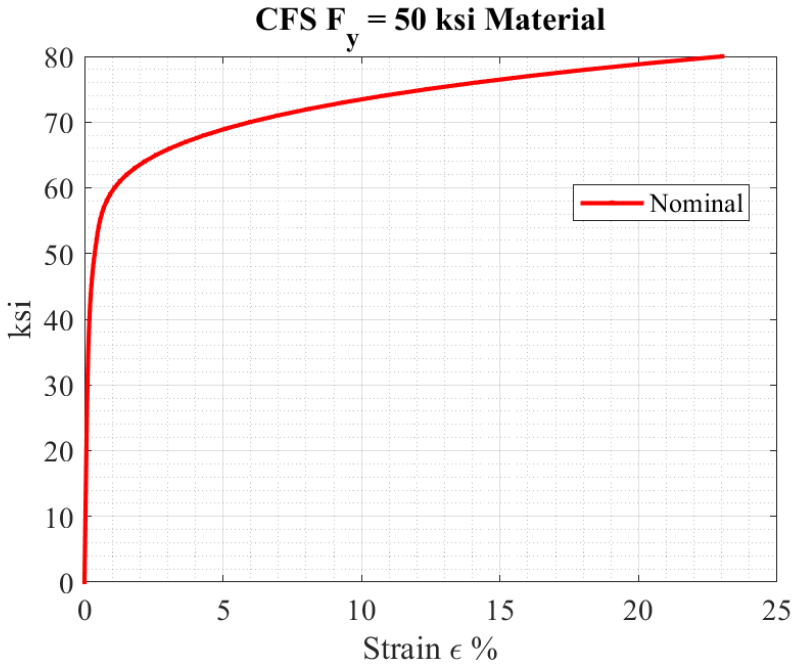

Figure 2.16: CFS Material Models (Gardner, et al. [1]))

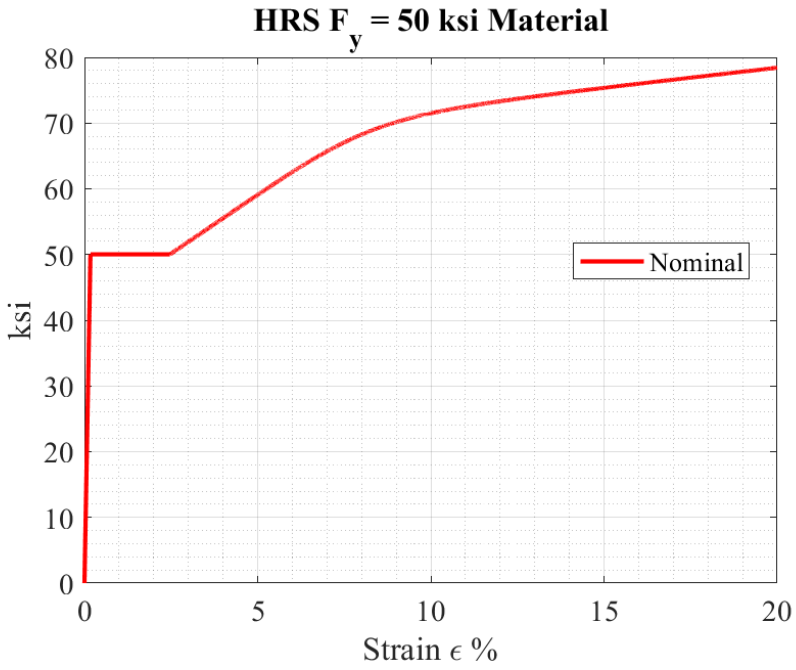

Figure 2.17: HRS Material Models (Yun, et al. [2])

3. Joist Models and Failure Modes

Two different joist designs, both with a 50 ft span and 30-inch deep, were used in this study. Each design corresponds to a different section type: hot-rolled steel (HRS) and cold-formed steel (CFS). These core designs were specifically selected and developed by the SJI Research Committee to ensure they represent current industry practices and were subsequently provided for use in this research; the design-sheets for these models are provided in the Appendix B.3. These core designs were further modified to have three different failure modes, leading to variations in ultimate load capacities in each designs and failure modes.

3.1. Joist Models with HRS Sections

A generic shape of first joist design (Joist I) is provided in Figure 3.1. The Joist I has rod sections as first webs, and uses crimped angle sections for web members. These angle web members are crimped 6 inches from their ends to fit between the chord angles.

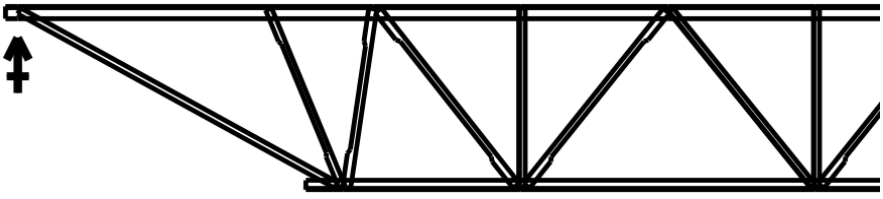

Figure 3.1: Joist with HRS sections (Joist I)

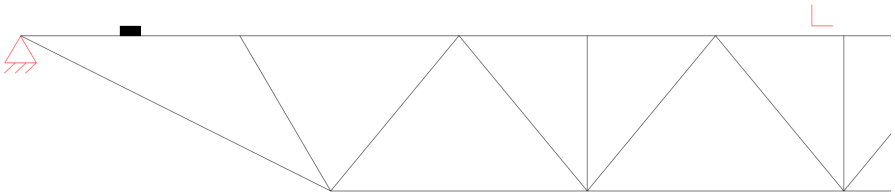

Figure 3.2: Joist with CFS sections (Joist II)

3.2. Joist Models with CFS Sections

Joist with CFS sections (Joist II) uses channel sections for all webs and uses CFS angles for chord members (Figure 3.2).

3.3. Failure Modes

Three primary failure modes were selected for further investigation for each joist design:

- Bottom Chord Yielding Failure
- First Web Yielding Failure
- Compression Web (W3 Member) Buckling Failure

Additionally, a serviceability limit state was considered based on the $L/60$ deflection limit, based on discussions with SJI research committee representatives. Although the International Building Code (IBC, [8]) typically defines the serviceability limit as $L/120$ for similar structural members, the SJI representatives recommended adopting twice this deflection ($L/60$) as the threshold for these analyses to better capture the ultimate behavior and extensive deformation capacity of the joist systems. Given the 600-inch span length, a 10-inch deflection limit was applied to all models.

3.3.1 Bottom Chord Yielding Failure

Yielding first initiates in the bottom chord, specifically around the midspan of the joist. As the load and deflection increase, this yielding spreads from the midspan toward the ends of the bottom chord. This increase in tension stresses also causes higher stress levels and yielding in the first web members. Due to the ductility of steel, this process results in significantly larger maximum deflections compared to other failure modes. Consequently, this is the failure mode that most frequently reaches the 10-inch deflection limit.

3.3.2 First Web Yielding Failure

In the second yielding failure mode, first web members with weaker cross-sections experience high yielding, specifically at both ends where rotational forces develop due to the deflected shape of the joist. As the first webs yield due to the deflected shape, high stresses are also induced in the bottom chord.

An important outcome of weakened first webs is the reduced rotational stiffness of the modified webs, which increases the likelihood of top chord buckling at the end panels. This failure mode is the second most frequent mode that can reach to 10 inches of deflection limit since there is a high stresses on both bottom chord and first webs.

3.3.3 First Compression Web (W3 Member) Buckling Failure

W3 web members are the first compression webs under gravity loads. As the load and deflection increase, bending and high-stress regions start to form at the ends of the W3 members due to their weakness. As the deflected shape progresses, these end rotations also cause additional stress at the ends of the W2 end webs. However, the bending in W3 results in failure due to buckling before the yielding reaches to the failure in W2 members or midspan deflections reach the $L/60$

limit. Because of this relatively early buckling, the overall deflections are smaller for this failure mode compared to others. Since compression buckling is the primary failure mode, imperfections or notional loads have a high impact on the accuracy of the analysis results.

Both implementing initial imperfections or notional loads to the system increase the analysis accuracy. Both methods can be affected by the material properties and cross-sectional properties. Since the initial imperfection method requires additional analysis to determine and utilize in the ABAQUS models, to increase the efficiency, this model includes notional loads on the midpoint of W3 web members. These notional loads were calculated using Eq. 3.1:

$$\text{Notional Load} = N = 0.002 F_y A \tag{3.1}$$

where F_y is the yield stress of W3 web material, and A is the area of W3 web section. Since F_y and A change at each random realization, the notional loads were updated accordingly to maintain consistency with the assigned input values.

4. Finite Element Models

All failure mode designs for both Joist I and Joist II models were first modeled with shell elements and solid elements (rod and filler sections) as this is the most accurate analysis type. Next, new finite element models were created using beam elements as they have significantly reduced run time compared to shell element models. Nonlinear second-order RIKS analyses were completed in ABAQUS. Loads, lateral and end supports, connections, and material models are presented in this chapter for the FE models.

Most of the modeling procedures used in developing the Abaqus shell-element models were adapted from previously validated studies with proven consistency (Sippel, Ziemian, and Blum [9], Rahnavard et al. [10], Adany and Schafer [11], Kapoor, Bogh and Peterman, [12] and Sippel, Ziemian, and Blum [13]). The methods for representing welded connections, end supports, and lateral restraints were primarily derived from earlier work (Sippel, Ziemian, and Blum [9]), with project-specific modifications developed in coordination with the SJI Research Committee. Crimped sections and filler components were also replicated following the approaches reported in previous studies. Material modeling was enhanced by replacing earlier simplified assumptions with more detailed nonlinear material definitions. For shell elements, the S4R element—widely recommended and used in the literature (Rahnavard et al. [10], Adany and Schafer [11], and Kapoor, Bogh and Peterman, [12])—was adopted, and mesh sizes were selected following guidance from prior research (Sippel, Ziemian, and Blum [13]), with additional refinement applied to compression members to ensure accurate representation of localized buckling behavior.

Shell models were verified by comparing the load-deflection results of FE models and

designs sheets provided by SJI at the service load levels. After the verification at the service load levels, the design loads were applied to the system with RIKS analysis to obtain the actual capacity of the designed joists for the following steps in the project.

Given that the reliability study requires high number of analyses, running shell elements would require excessive amount of time to run all possible design combinations. Therefore, beam element finite element models were used for the reliability study. Same material models, loads, and lateral and end supports were used in both models. The connections, however, were modeled with a different method for the beam FEM compared to the shell FE models.

Beam element models are not able to include the change in the weld length effectively. Therefore, rather than using rigid connection at the web end - chord connections, rotational springs with specific stiffness values for web groups were assigned to web ends. The method for spring stiffness calculations for varying weld lengths is explained this section. After the models were created, beam element FE models were verified by comparing the load-deflection results at service level with SJI design sheets and at design load level with shell element FE model results.

4.1. Shell Element Models

Shell element FE models were created first due to their accurate and realistic results. Detailed 3D models were created for each failure mode design. Previously mentioned material models were used, welded connections were modeled according to the given length in the provided design sheets with the given loads on top chords, and the supports were applied as in the actual joists.

HRS angle web members were crimped starting from 6 inches at the ends and these crimpings were also modeled in shell element models in ABAQUS with a transition region from regular angle to crimped angle sections, as illustrated in Figure 4.1.

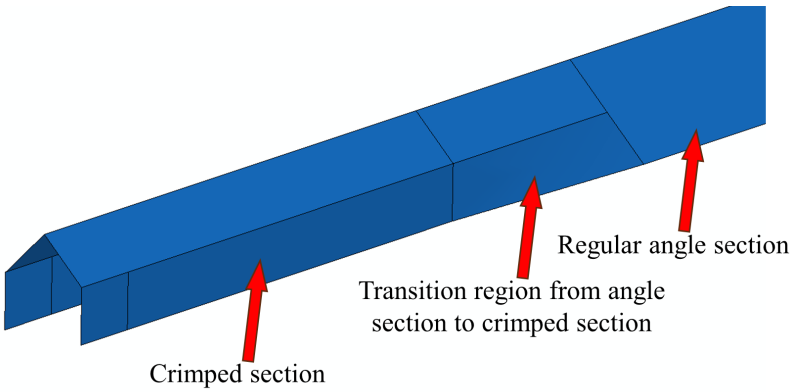

Figure 4.1: HRS angle web crimped at 6 inches at the ends

4.1.1 Connections

There were two types of connections used in shell element FE models for these two different weld types (bevel and fillet). The first connection type is surface to surface tie connection which was used in bevel welds (connections between solid element welds and chords). An example from rod end for this type of connections is shown in Figure 4.2. Additional weld elements with a different weld material with a yield stress of 75 ksi was used in this connection type. The second type connection is the welded connection between shell element webs and shell element chord members which was done by using only the edges of the web members to represent the fillet welds, presented in Figure 4.3.

4.1.2 Loading

Loads were applied as uniformly distributed surface loads to the top chord angles. Since [13] demonstrated the significant effects of torsional stiffness on top chord members in joist elements, the inner sides of the top chord angles were specifically chosen for load application. This approach was preferred to prevent generating additional torsional forces on the top chord angles. Figure 4.4 shows the loading configuration on the top chords.

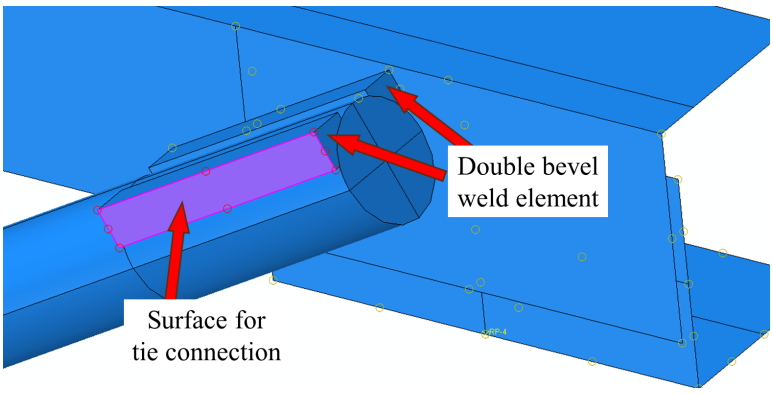

Figure 4.2: Surface to surface tie connection

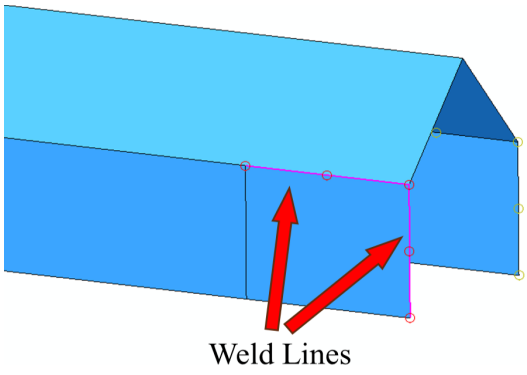

Figure 4.3: Weld lines tie connection for open section web ends

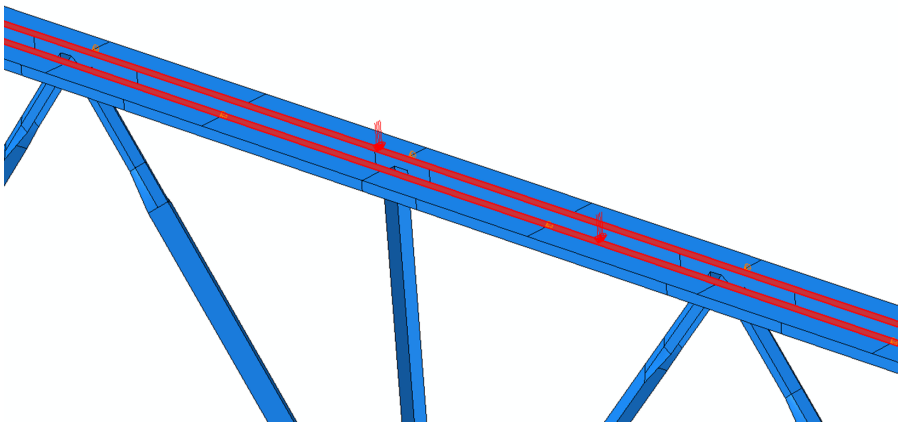

Figure 4.4: Uniformly distributed loads on top chord members

4.1.3 End and Lateral Supports

End supports were modeled in the same way with simply supported beams, a pinned connection on one end and a roller connection on the other end. However, the supports were not directly applied to the top chord angles but to seats angles. Seats were added to both ends and connected to the top chord angles on both sides to transfer the forces to the supports from top chords.

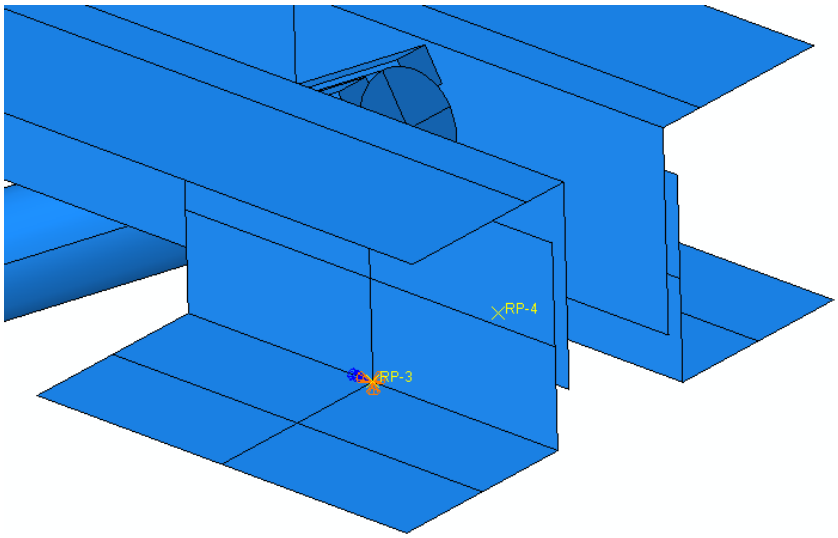

Figure 4.5: Seats and end supports of joist ends

Lateral supports were applied to the joist models in the same way with actual joists on both chords. Bottom chords were laterally supported at every panel point. Additional angle members were connected to the bottom chord members and the supports were applied to these members. Figure 4.6 includes an example to this lateral support type with the additional angle support member. A different method was used for top chord lateral supports. The supports were applied to the top chord angles directly alternating at every 12 inches to represent the connection between chord angles and deck on top, as the deck provides lateral restraint to the top chord.

In addition to lateral supports, fillers were used to prevent buckling of top chord members in steel joists, and were also included in FE models. The same sections with solid rod members were

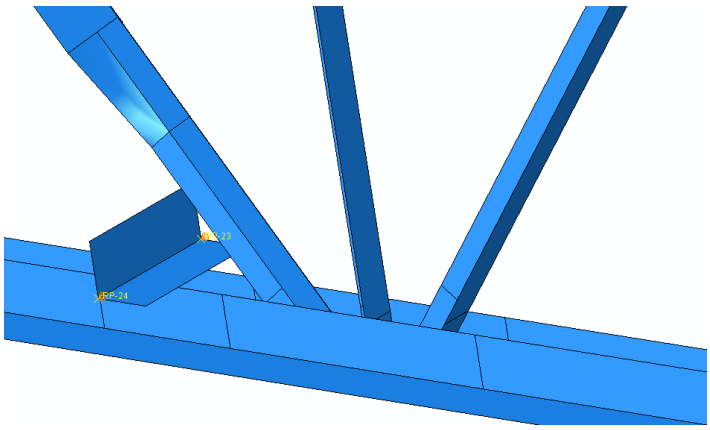

Figure 4.6: Lateral supports (orange arrows) at every panel point at bottom chords

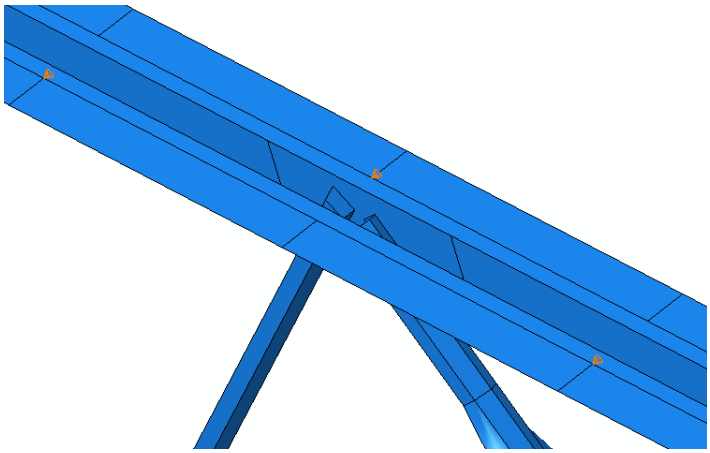

Figure 4.7: Alternating lateral supports (orange arrows) at every 12 inches on top chords

placed in the designated locations and welded connections were modeled.

4.1.4 Validation of Shell Element Models

Two different validation processes were completed to verify the shell element FE models. In the first validation, the shell element finite element (FE) model results were compared to the Steel Joist Institute (SJI) calculated displacements under serviceability loads. The reference values in Table 4.2 were provided by SJI designs; following the completion of the FE models, the vertical deflections under serviceability loads were compared against these reference values. The minimal percentage

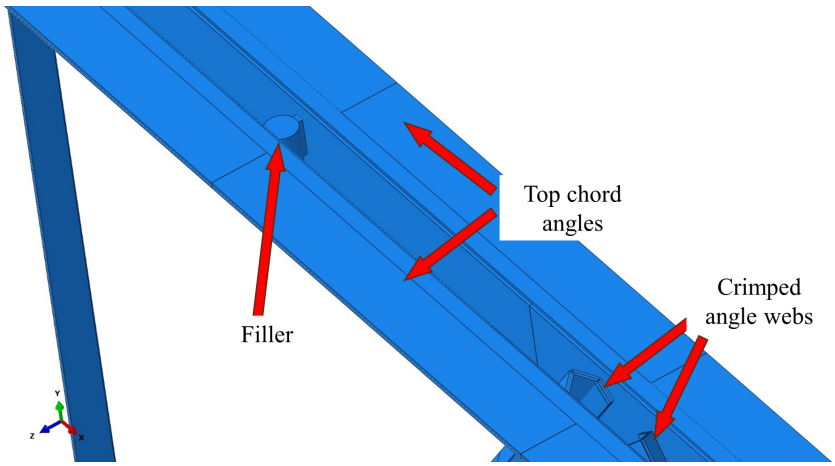

Figure 4.8: Filler and weld elements for connection with top chord angles

differences indicate that the FE models achieved high accuracy in predicting displacements within the serviceability range.

The second validation phase involved comparing the FE results with experimental data from two different joist models (24" and 30" depth) reported by Yost et al. [3]. While the study provides fundamental dimensions for the joist geometry, certain secondary parameters, such as specific weld lengths, web orientations, precise lateral support locations, and end support details, were not explicitly detailed in the original publication. Furthermore, material property documentation was primarily focused on the tested middle web members, which exhibited a yield strength of 57 ksi (exceeding the nominal 50 ksi specification). However, detailed stress-strain data or elasticity properties for the chords and other web members remained undefined.

To address these missing parameters, a series of engineering assumptions were made regarding support conditions and member orientations to reconstruct the models as faithfully as possible. Despite these inherent modeling challenges, the FE analyses demonstrated strong correlation with the experimental results. Figures 4.9 and 4.10 illustrate the failure modes, characterized by the buckling of W3 web members - a behavior consistent with the experimental observations. Moreover, the load-midspan deflection plots in Figures 4.11 and 4.12 reveal an excellent agreement in joist

Table 4.1: Comparison of deflection results under serviceability loads for design sheets and shell element FE models

Joist Type	Failure mode	Shell Element FEM (in)	Designsheets (in)	Difference (%)
Joist I	BC	1.685	1.670	0.9
	FW	1.642	1.600	2.6
	W3	1.640	1.600	2.5
Joist II	BC	1.636	1.60	2.2
	FW	1.600	1.600	0
	W3	1.631	1.600	1.9

Modes: BC: bottom chord failure, FW: first web failure, W3: web buckling failure

stiffness. The FE models accurately captured the failure occurring shortly after the linear elastic stage, mirroring the trends seen in the three experiments conducted by Yost et al. [3].

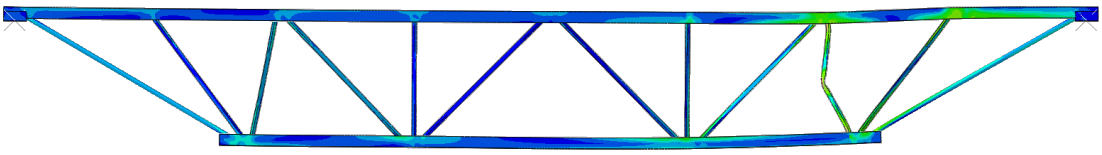

Figure 4.9: Buckled W3 web member in shell element FE models for joist with 24" depth

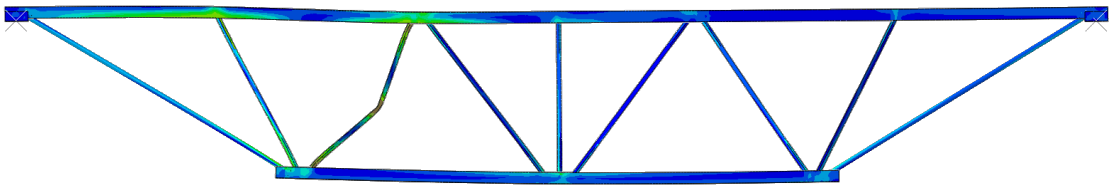

Figure 4.10: Buckled W3 web member in shell element FE models for joist with 30" depth

Following the verification process, the shell element FE models were analyzed under full loading conditions, leading to the identification of three failure modes: bottom chord yielding failure, first web yielding failure, and first compression web buckling failure. The results of these shell element FE models are presented in Figures 4.13 to 4.15, corresponding to each failure mode, respectively. The figures show the Von Mises stress distributions across the joist members. The red colored areas

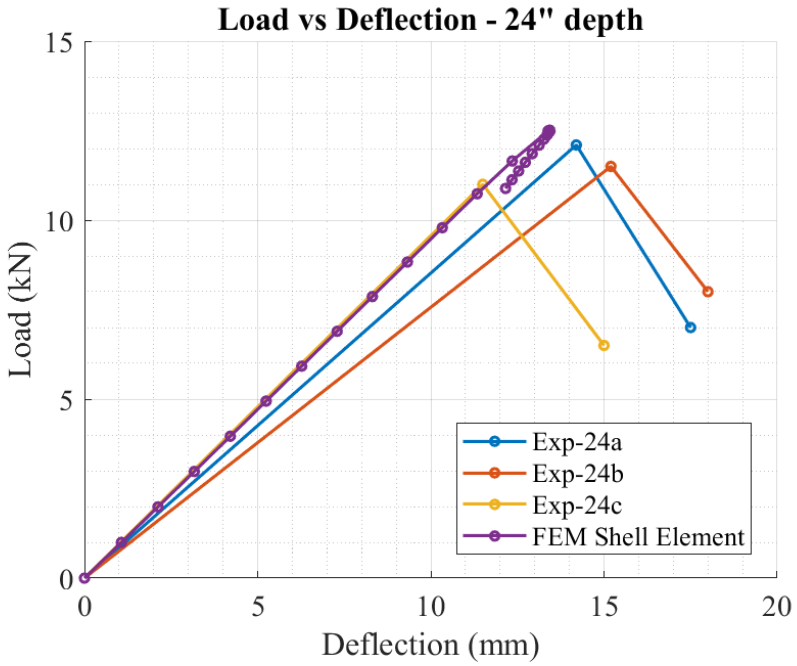

Figure 4.11: Comparison of experiments and shell element FE models for joist with 24" depth

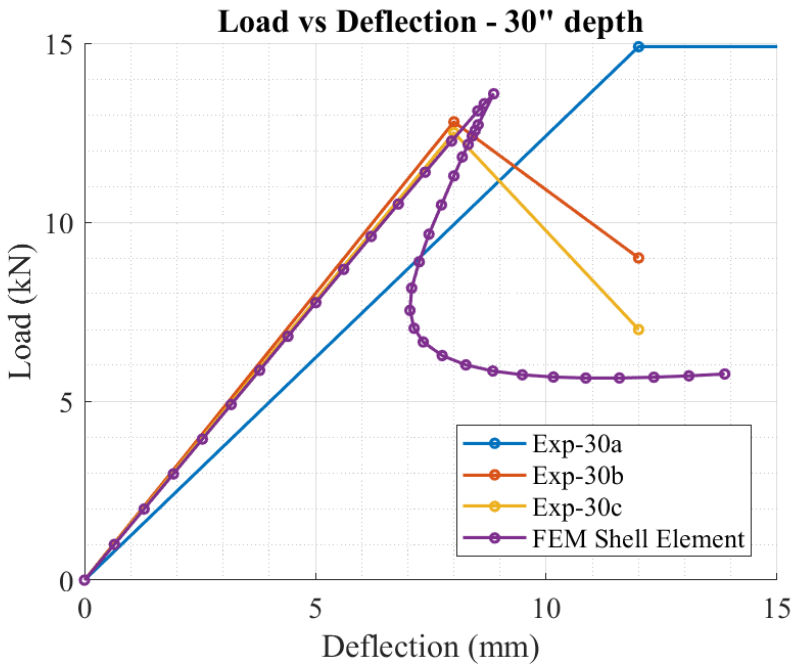

Figure 4.12: Comparison of experiments and shell element FE models for joist with 30" depth

Table 4.2: Comparison of load and midspan deflection results of experiments [3] and shell element FE models

Experiment [3]			FEM Shell	Difference (%)
Joist Type	Load (kN)	Avg. Load (kN)	Load (kN)	
24a	12.1			
24b	11.5	11.53	12.5	8.48
24c	11.0			
30a	14.9			
30b	12.8	13.40	13.6	1.49
30c	12.5			
Joist Type	Deflection (mm)	Average Deflection (mm)	Deflection (mm)	Difference (%)
24a	14.2			
24b	15.2	13.63	13.43	1.46
24c	11.5			
30a	12			
30b	8	9.33	8.86	5.05
30c	8			

represent the high stress regions whereas the blue colored regions are having the least stresses in the analysis.

4.2. Models for Calculation of Weld Length Effects (Moment-Rotation Values)

Beam element FE models are not able to reflect the welded end connection effects as accurately as the results from shell element FE. Assuming fixed or pin end for the web connections affects the behavior of not only web members but also chord members. Different combinations of chord strengths and web strengths might lead to buckling in chord or web members. An example to this is shown in a previous study of Cicek, Sputo, and Blum [14].

Given that this study includes web compression buckling failure as one of the main failure modes, the end conditions of web members are critically important. Therefore, rotational springs

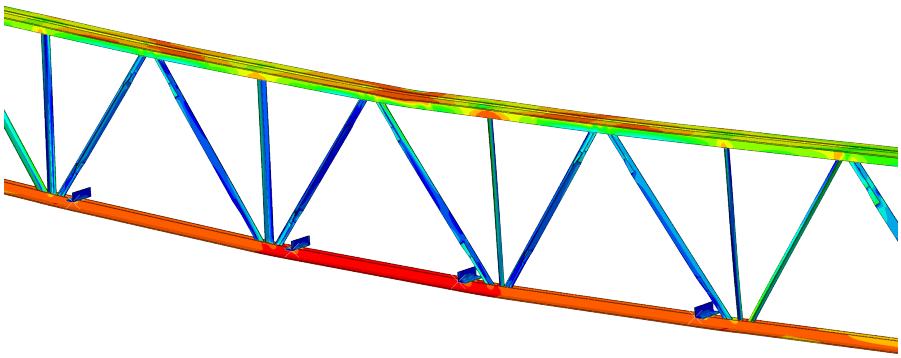

Figure 4.13: Bottom chord tension yielding failure mode shell element FE result

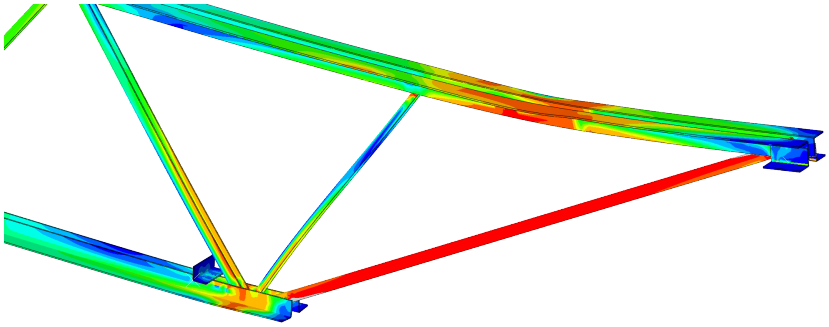

Figure 4.14: First web tension yielding failure mode shell element FE result

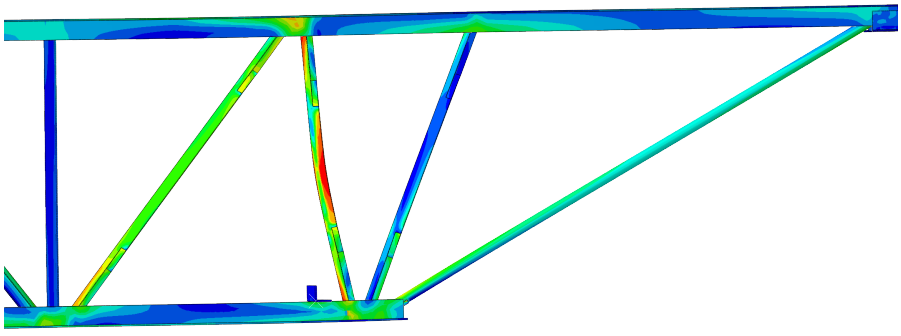

Figure 4.15: First compression web buckling failure mode shell element FE result

were assigned to web member ends and the rotational stiffness values of these springs were calculated by modifying the shell element FE models previously created in this study.

This modified models only include the bottom chord and part of the webs from each groups and updated with different web weld length ratio that were captured in statistical analysis on collected weld length data. For each web group, the minimum, mean and maximum weld length ratios were applied to the modified shell element FE model. The main criteria was obtaining the same moment at each web in each model with the same load. According to the rotation of the webs under these same moment values, moment-rotations of web groups for each weld length ratio were obtained, and the rotational stiffness values were calculated by using these results.

Figure 4.16 shows part of the modified Joist II model and loading, and Figure 4.17 shows the deflected shape of selected web members. Calculated moment-rotation curves of each weld groups with minimum, mean, and maximum weld length ratio levels are given in Figures A.1 through A.6 in Appendix Section A for both HRS crimped angle and CFS channel sections.

The boundaries for rotational stiffness values were calculated from moment-rotation curves by using minimum and maximum weld lengths. A linear formulation was defined between weld length ratio input and the rotational stiffness values for each weld group and section type. The effect of change in weld length was applied to the simulation beam element model with the change in rotational stiffness values instead of updating the weld lengths inside the model, and the defined formula was used at each weld length groups to calculate this rotational stiffness value. To evaluate the sensitivity of the model to these connections, additional analyses were performed using conventional "pin-pin" and "fix-fix" end conditions for the web members. As expected, the structural response of the models with assigned rotational springs fell consistently between these two idealized boundaries, providing a more realistic and advanced representation of the actual semi-rigid behavior of the welded joints.

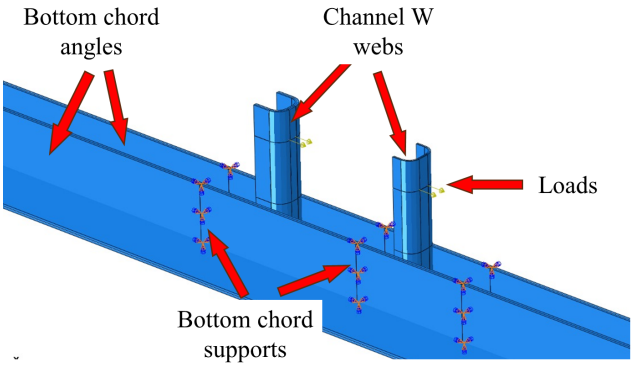

Figure 4.16: Loading of shell element FE model for moment-rotation analysis for Joist II W webs

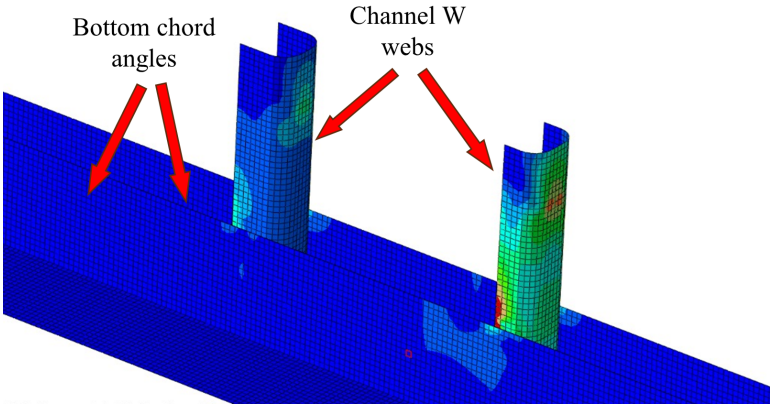

Figure 4.17: Shell element FE model result of moment-rotation analysis for Joist II W webs

4.3. Beam Element Models

Beam element FE models were preferred in this study for reliability analyses. The main reason for this is to reduce the time and storage cost of the whole study. Despite the lesser details in models than the shell element models, beam element FE models proved to be effective and showed that it can accurately predict the results. The same material models, load values, and input variables were used with necessary changes mainly in connections and supports. An important modification was applied to the W3 web buckling failure mode beam element models and explained in this chapter.

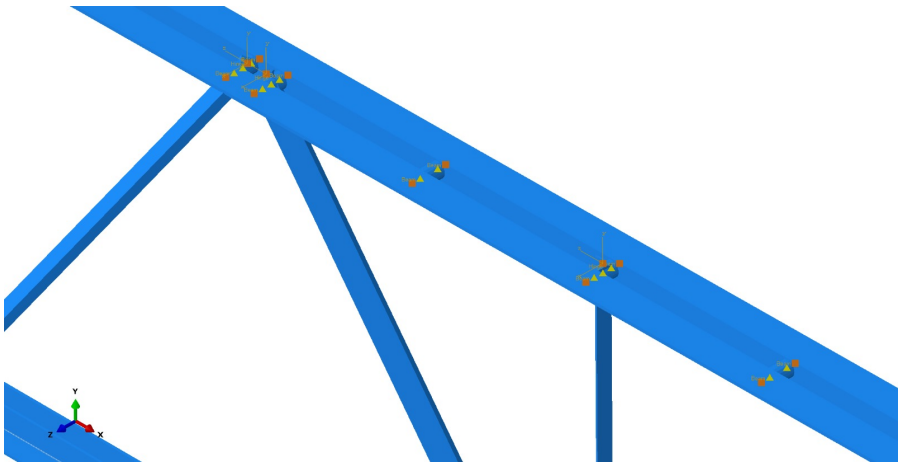

Figure 4.18: Rigid links between web-chord connection locations and filler locations

4.3.1 Web Connections

Chord angles were connected to each other with a rigid link in between chord angles at web end locations to create the same rigidity at web-chord connections. These rigid links were also used as filler members in filler locations. For the web-chord connections, web ends connected to the midpoint of these rigid links and the rotational springs (as detailed in Section 4.2) were assigned to the connection point.

4.3.2 Loading

Same ultimate load values were applied to the beam element FE models. The load were applied as surface loads in shell element models but for beam elements, uniformly distributed line loads were applied to the center of gravity of both top chord angles to prevent additional torsional forces.

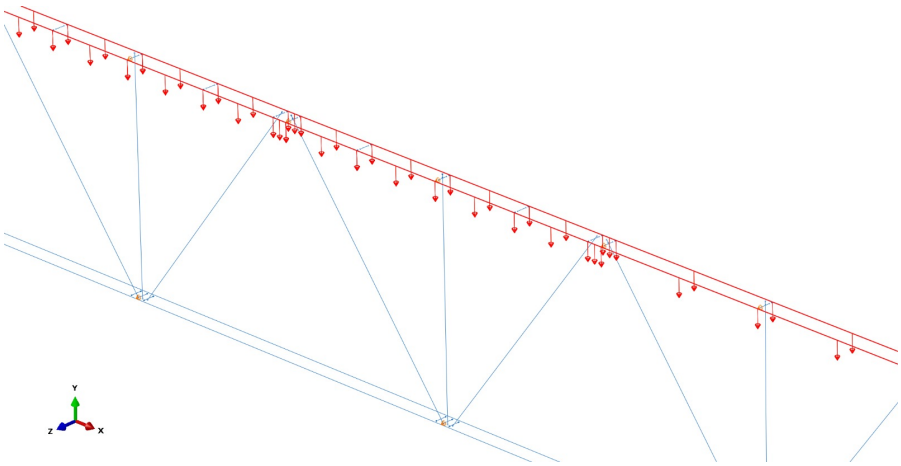

Figure 4.19: Uniformly distributed loads

4.3.3 Buckling failure models modification

A significant modification in the buckling failure mode of the beam element models involves the reduction of yield strength in the W3 web materials. While the shell element models clearly exhibited W3 web buckling failure, the beam element models did not capture this behavior and instead predicted approximately 12–15% higher load capacities compared to the shell element models. Several studies ([15], [16], [17], [18]) suggest that reducing the capacity of members in beam element models can increase the accuracy between the shell and beam element models. Two types of stiffness reduction was suggested in these studies, member stiffness reduction or system stiffness reduction by changing the tangent stiffness. Since the main focus of this study is to be able to capture the realistic capacity of the given designs, system stiffness reduction method is not the most feasible method, therefore, stiffness reduction of a single member method was selected. In this study, it was found that reducing only the yield strength of W3 web members, rather than changing the stiffness, increased the accuracy between the shell and beam element models, both in terms of load capacity and failure mode.

For Joist I, a reduction factor of 0.8 was adopted, as suggested in Section C2.3(a) of Chapter

C in AISC 360-22 [19]. For Joist II, an initial reduction factor of 0.9 provided the best results for singular web element models. The Figure 4.20 illustrates comparison of load-deflection responses between the beam and shell element models for a single W3 web member under compression, utilizing both angle and channel sections. With the applied reduction factors for yield strength, the accuracy of the predicted buckling loads between the beam and shell element models was significantly improved.

Following multiple analyses with randomly assigned variables, it was observed that the resultant Load Proportionality Factor (LPF) values in the beam element models were higher than expected. In the context of the nonlinear Riks analysis used in this study, the LPF acts as a dimensionless scaling multiplier for the applied load, which in this case, represents the specified load capacity for the joist design. Therefore, an LPF value indicates the ratio of the simulated failure load to the nominal design strength. To further investigate this difference, 300 random beam element models were selected and identical 300 shell element models were generated and analyzed. These simulations indicated that a reduction factor of 0.85 provided a higher degree of accuracy for cold-formed steel (CFS) systems. Consequently, the previously adopted 0.9 reduction factor was revised to 0.85, after which the full stochastic analyses were completed.

4.3.4 Validation of Beam Element Models

After the mentioned modifications were completed, the beam element models for six designed joists were analyzed with second order nonlinear analyses and the load-deflection (vertical deflection at mid-span) results were completed with the corresponding shell element models. Figures 4.21 to 4.23 show the outcome of each failure mode after the modified beam element FE models were analyzed.

Model comparisons were completed for joists designed with both nominal and mean values. Joists that were modeled with nominal value inputs were used in sensitivity analyses and joists that were modeled with mean value inputs were used to ensure the accuracy of the joists with full statistical

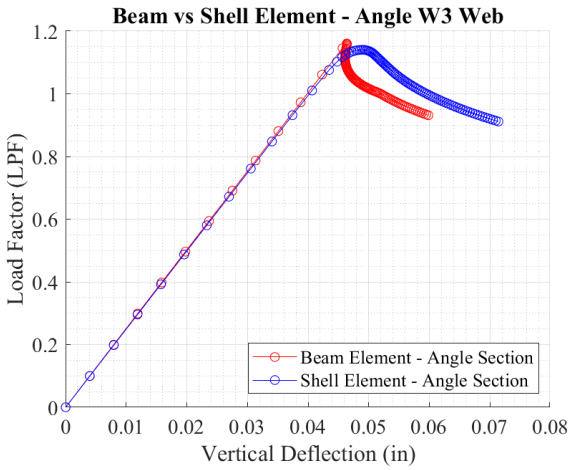

(a) Angle section W3 web

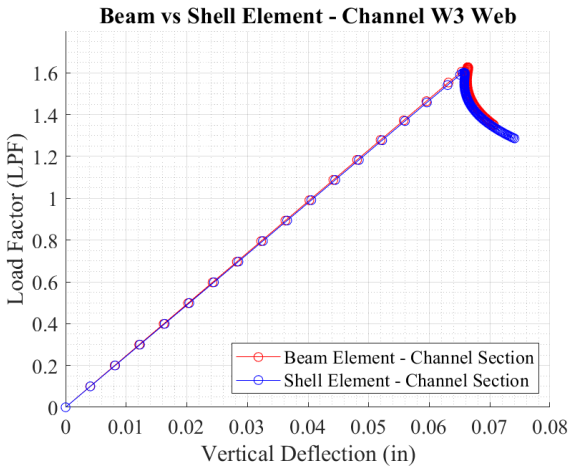

(b) Channel section W3 web

Figure 4.20: Shell vs beam element model load-deflection comparison with angle (a) and channel (b) sections for W3 web member

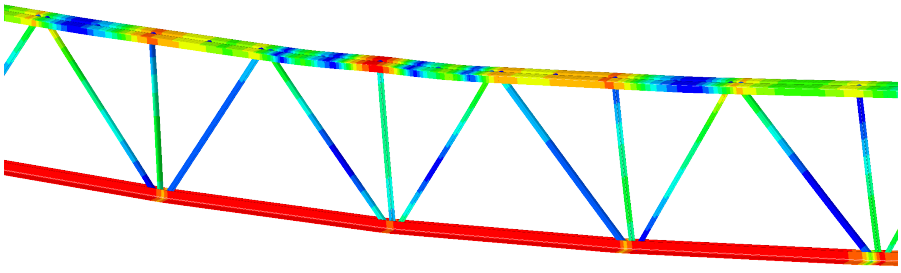

Figure 4.21: Bottom chord tension yielding failure mode beam element FE result

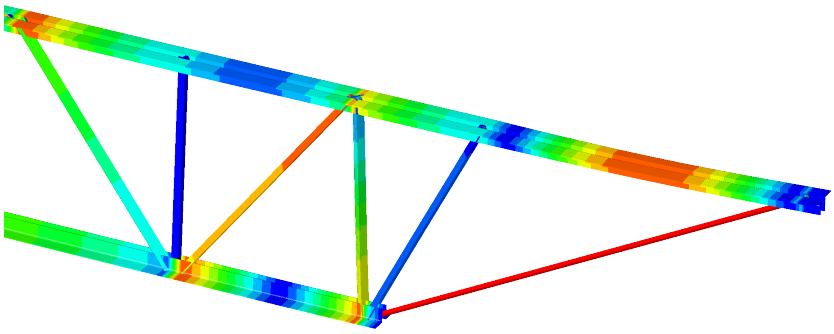

Figure 4.22: First web tension yielding failure mode beam element FE result

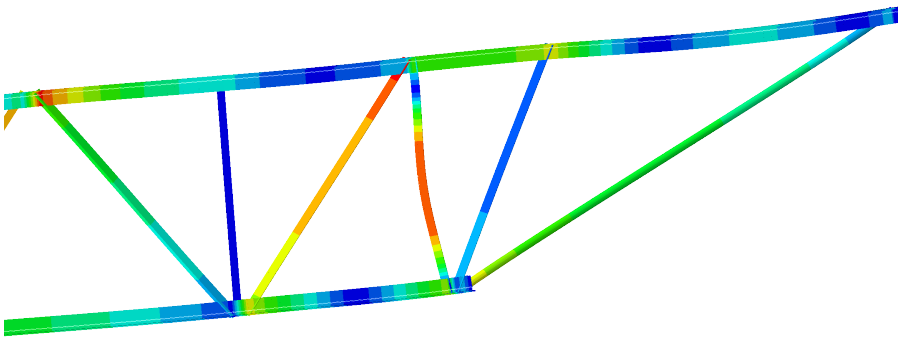

Figure 4.23: First compression web buckling failure mode beam element FE result

inputs. Table 4.3 and Table 4.4 shows the deflection comparison between shell and beam element models for nominal and mean value designed joists, respectively. Figures 4.24, 4.25, and 4.26 show the load-deflection curves of full joist analyses of six different models for both nominal and mean value designed joists.

Table 4.3: Comparison of vertical deflection at mid-span results under ultimate loads (load factor 1) for shell element and beam element FE models with nominal design values

Failure mode	Shell Element FEM (in)	Beam Element FEM (in)	Difference (%)
Joist I BC	4.272	4.279	0.16
Joist I FW	4.266	4.310	1.03
Joist I W3	2.701	2.707	0.22
Joist II BC	3.903	3.928	0.64
Joist II FW	3.219	3.241	0.68
Joist II W3	3.071	3.072	0.03

Modes: BC: bottom chord failure, FW: first web failure, W3: web buckling failure

Table 4.4: Comparison of vertical deflection at mid-span results under ultimate loads (load factor 1) for shell element and beam element FE models with mean design values

Failure mode	Shell Element FEM (in)	Beam Element FEM (in)	Difference (%)
Joist I BC	4.029	4.015	0.035
Joist I FW	4.243	4.296	1.249
Joist I W3	2.691	2.701	0.372
Joist II BC	3.928	3.944	0.407
Joist II FW	3.237	3.265	0.865
Joist II W3	3.079	3.085	0.195

Modes: BC: bottom chord failure, FW: first web failure, W3: web buckling failure

The comparisons indicate a high degree of accuracy between the shell and beam element FE models for both nominal and mean-value-designed joists. The strong agreement in overall stiffness of the joists is clear in the linear behavior phrase of the joists and this extends to the nonlinear behavior range of the analyzed joist models. As a result of this, the generated beam element FE models provide

652 a reliable basis for conducting the reliability analyses.

653 4.4. Second Order Nonlinear Analyses Results

654 After the validation of both shell and beam element FE models were completed, full analyses
655 with ultimate loads were completed and maximum load capacity of the models were obtained. Non-
656 linearity was integrated by both material and geometric properties in this study. Material nonlinearity
657 was included using the material models previously given (Section 2.4), whereas the geometric non-
658 linearity was simulated by performing second-order analyses, and also including initial imperfection
659 in the designs predicting W3 buckling failure modes. Tables 4.5 and 4.6 include the maximum load
660 factors (LPF) obtained from each models for nominal and mean value designed systems. Additional
661 to the given tables, Figures 4.24, 4.25, and 4.26 present the behavior of each failure modes of each
662 joist for nominal and mean value shell and beam FE models.

Table 4.5: Maximum LPF reached under ultimate loads for shell element and beam element FE models with nominal design values

Failure mode	Shell Element FEM (LPF)	Beam Element FEM (LPF)	Difference (%)
Joist I BC	1.096	1.109	1.19
Joist I FW	1.100	1.106	0.55
Joist I W3	1.290	1.323	2.56
Joist II BC	1.414	1.416	0.14
Joist II FW	1.579	1.560	1.20
Joist II W3	1.364	1.313	3.74

Modes: BC: bottom chord failure, FW: first web failure, W3: web buckling failure

663 The failure criterion for conventional member-based linear design is defined as the point at
664 which a member reaches its yield stress. However, for nonlinear systems, this is not always the case.
665 Nonlinear systems can sustain higher loads even after multiple members have yielded due to load

Table 4.6: Maximum LPF reached under ultimate loads for shell element and beam element FE models with mean design values

Failure mode	Shell Element FEM (LPF)	Beam Element FEM (LPF)	Difference (%)
Joist I BC	1.227	1.241	1.14
Joist I FW	1.234	1.236	0.16
Joist I W3	1.407	1.419	0.85
Joist II BC	1.580	1.586	0.38
Joist II FW	1.716	1.706	0.58
Joist II W3	1.462	1.430	2.19

Modes: BC: bottom chord failure, FW: first web failure, W3: web buckling failure

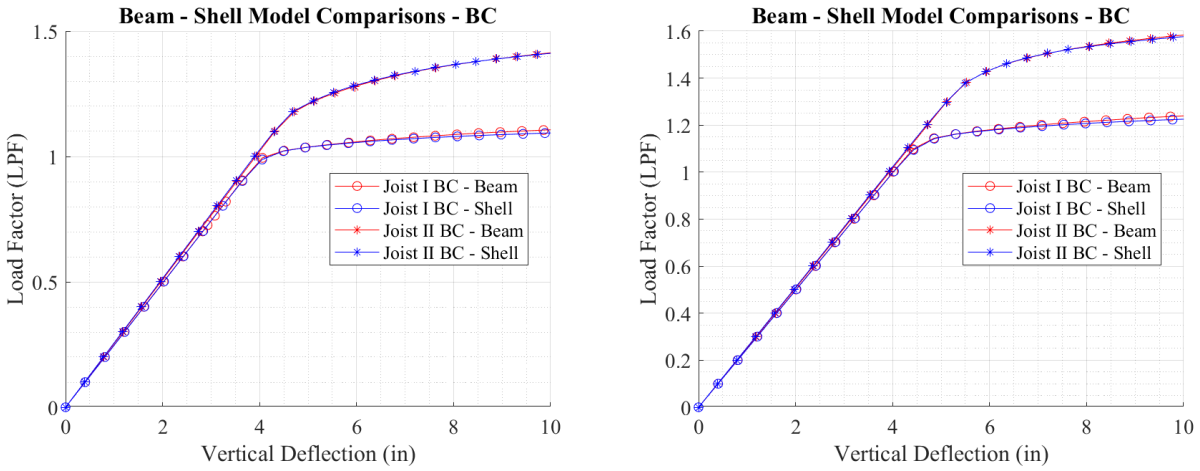

(a) Nominal value design

(b) Mean value design

Figure 4.24: Shell vs beam element model load-deflection comparison with nominal (a) and mean (b) values for BC failure mode

redistribution, provided that linear buckling does not occur in any member.

In the second-order nonlinear analyses of the modeled systems, none of the anticipated failure modes occurred under a load factor of 1. Second-order nonlinear Riks analysis provides the absolute highest load factor that the system can reach regardless of the failure mode. As a result, the analyses continued until one of the following conditions was met:

- A tension member (or multiple members) attained their ultimate stress levels or excessive strains

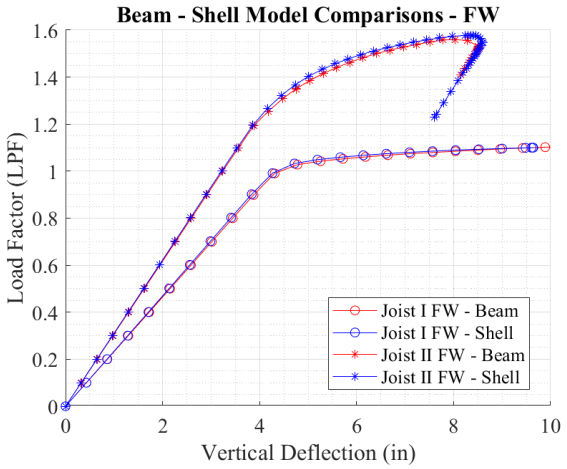

(a) Nominal value design

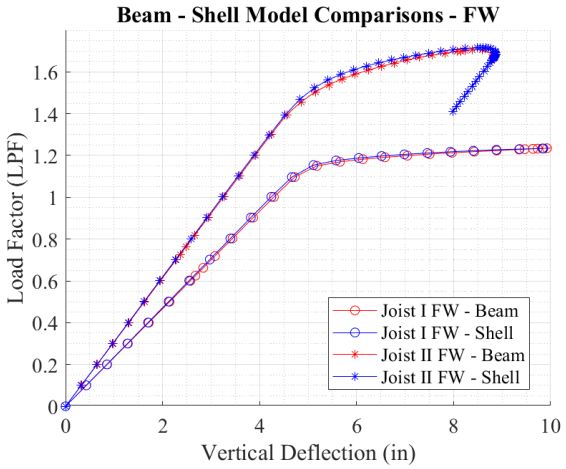

(b) Mean value design

Figure 4.25: Shell vs beam element model load-deflection comparison with nominal (a) and mean (b) values for FW failure mode

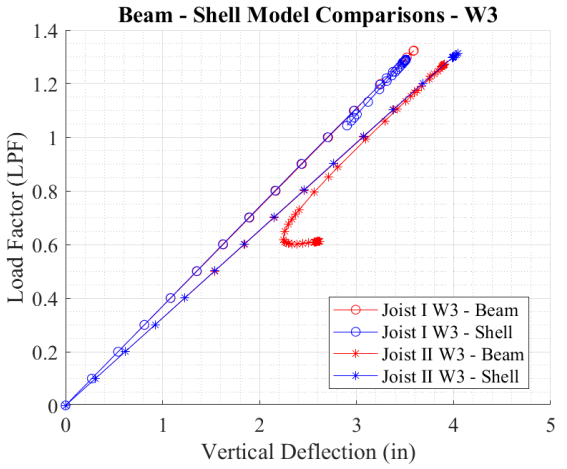

(a) Nominal value design

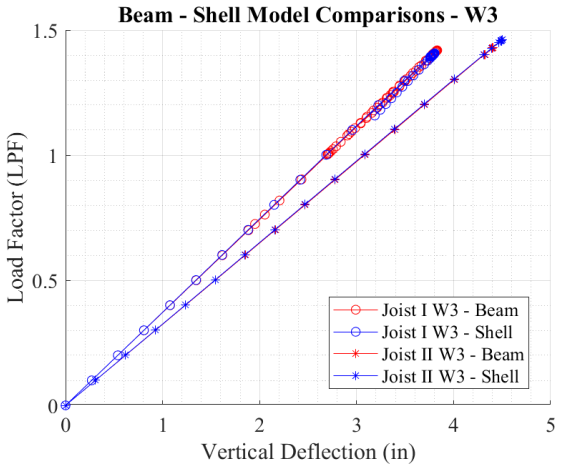

(b) Mean value design

Figure 4.26: Shell vs beam element model load-deflection comparison with nominal (a) and mean (b) values for W3 failure mode

(serviceability limit mentioned in Section 3.3)

- A compression member underwent compression buckling.

The obtained failure modes and anticipated failure modes are presented along with ultimate design loads in Table 4.7.

Table 4.7: Comparison of failure modes in design sheets and shell element FE models results under ultimate loads

Joist Model	Ultimate Load (plf)	Designsheets anticipated failure mode	Shell Element FEM failure mode
Joist I	340	BC	BC
	367	FW	BC
	254	W3	W3
Joist II	337	BC	BC
	284	FW	FW
	271	W3	W3

Modes: BC: bottom chord failure, FW: first web failure, W3: web buckling failure

5. Random Value Generation and Sensitivity Study

5.1. Latin Hypercube Sampling

Latin Hypercube Sampling (LHS) was preferred in this reliability study as an efficient alternative of Monte Carlo simulations. LHS was chosen to increase the computational efficiency and accuracy of the analysis, given the complexity and the number of the systems under consideration. The study focuses on three primary variables for two different systems with different failure modes, hence a robust sampling method was needed to adequately obtain the variability and combinations within the complex data. LHS method was proven to reduce the necessary number of sampling, hence the total number of analyses, and still acquire high performance. This efficiency is highly critical and beneficial for accurate probabilistic assessments. As a result, LHS method was adopted for the random sampling through this study.

While generating random samples for the simulations, truncation was applied to the probability distributions to enhance the physical accuracy of the models. The truncation limits were established by considering the range of the collected data while ensuring that the sampled values remained within realistic boundaries; specifically, extreme values that are theoretically possible in a standard distribution but practically impossible in manufacturing were discarded. In defining these truncated bounds, the limits for hot-rolled sections were determined based on ASTM A6/A6M specifications [20], while the limits for cold-formed sections were set in accordance with the AISI S240-20 [21] standard. This approach ensures that the stochastic variables not only reflect the variability of the collected data but also strictly adhere to the mandatory thickness and dimensional tolerances defined

by structural codes.

Due to the section type and size variety in a single joist, multiple random sets for same inputs such as yield stresses, leg thicknesses, were generated for repeatedly at each simulation. All these generated set of random values then verified with their own distribution parameters to ensure the consistency in input statistics. Example distributions of these random variables are provided in this section.

5.1.1 Material Properties

Different sections are manufactured from different batches in a manufactured joist. This means that in a single joist there might be several different steel material properties among different members. To include this complexity in the reliability study, every different section was assigned its own material model created with a different set of random values. Following the recommendations of the SJI Research Committee, a correlation was maintained between the material properties of identical sections within a single joist, while distinct sections were treated independently. Predefined distributions and distribution parameters were used to create different number of material sets for each design and these were embedded into batch analysis code scripts.

Figures 5.1 and 5.2 show the histograms of generated random numbers and fitted distributions.

5.1.2 Cross-sectional Imperfections

Both HRS and CFS sections might have cross-sectional imperfections due to manufacturing processes. The collected data shows that the variety of cross-sectional imperfections are higher in CFS sections than HRS sections. According to the calculated statistics, random numbers for different sections were created at each simulation. Assigning different set of random values for different type

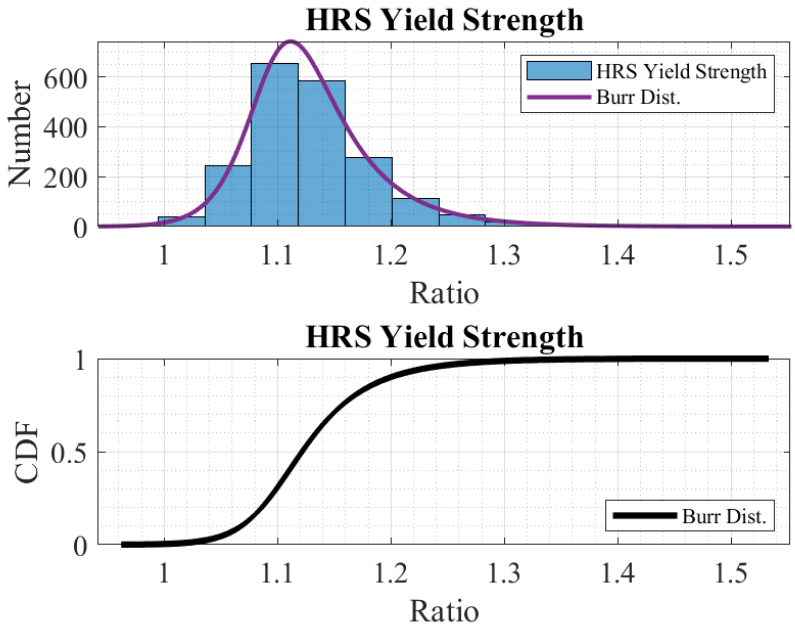

Figure 5.1: Histogram and statistical parameters of generated random HRS yield stress values

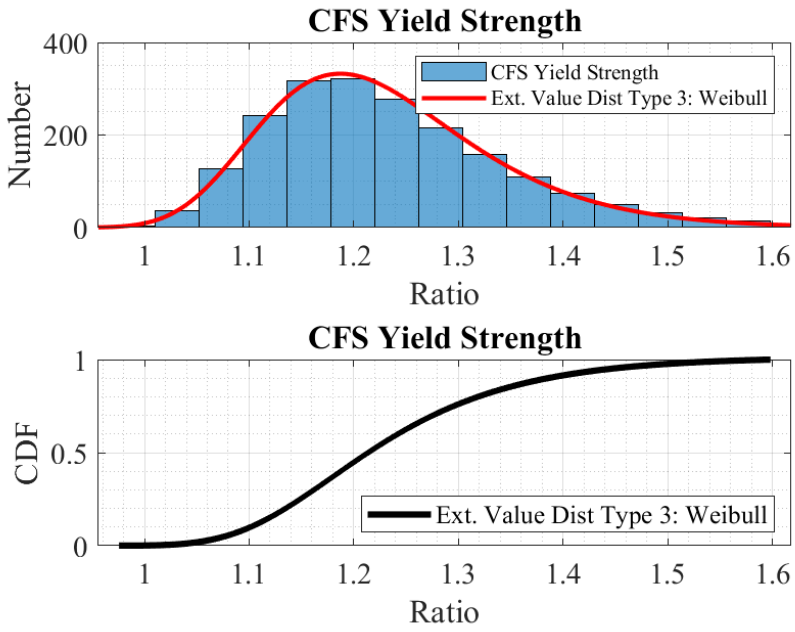

Figure 5.2: Histogram and statistical parameters of generated random CFS yield stress values

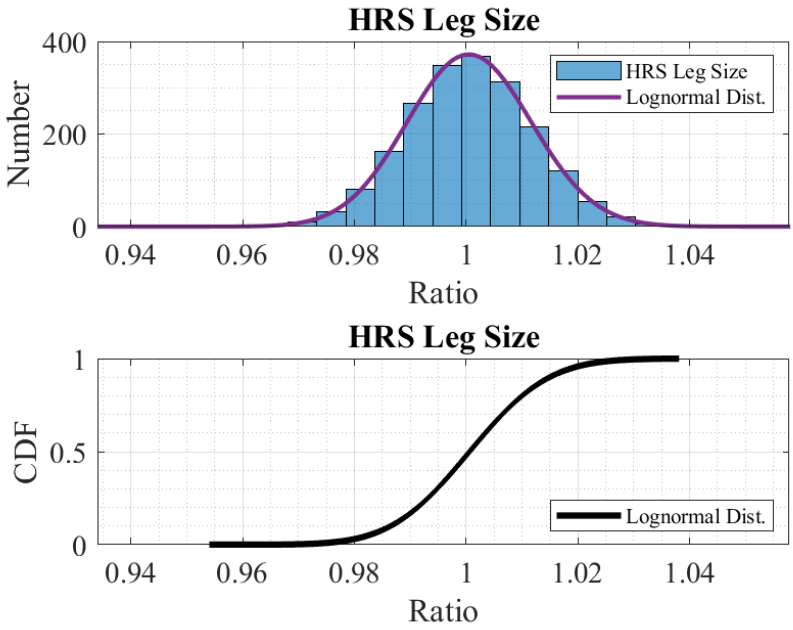

Figure 5.3: Histogram and statistical parameters of generated random HRS leg size values

of cross-sectional dimensions created the variability that the actual joist systems might have. Figures from 5.3 to 5.8 show the generated random numbers and fitted distributions for the cross-sectional imperfections input variables.

5.1.3 Weld Length

As detailed in Section 2.3, the weld length data were separated into three groups and statistical parameters were calculated for these groups. According to the random values, rotational springs were assigned with calculated rotational stiffness and the weld length effect was included in the joist design. Figures 5.9, 5.10 and 5.11 show the histograms of generated data and the fitted distributions.

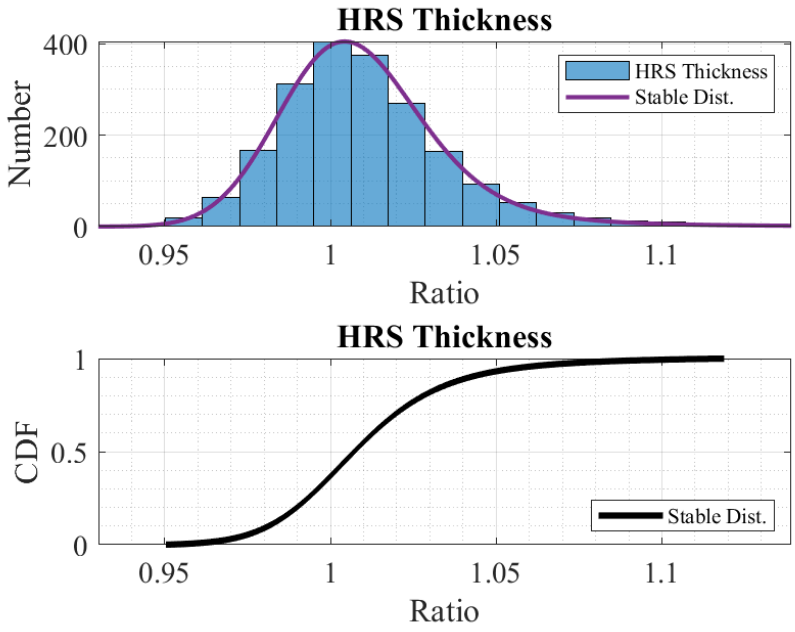

Figure 5.4: Histogram and statistical parameters of generated random HRS thickness values

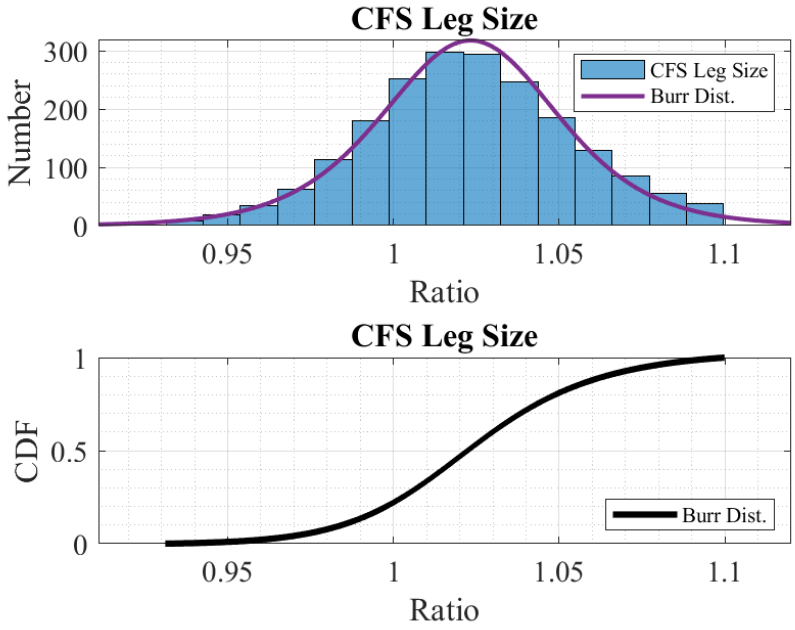

Figure 5.5: Histogram and statistical parameters of generated random CFS leg size values

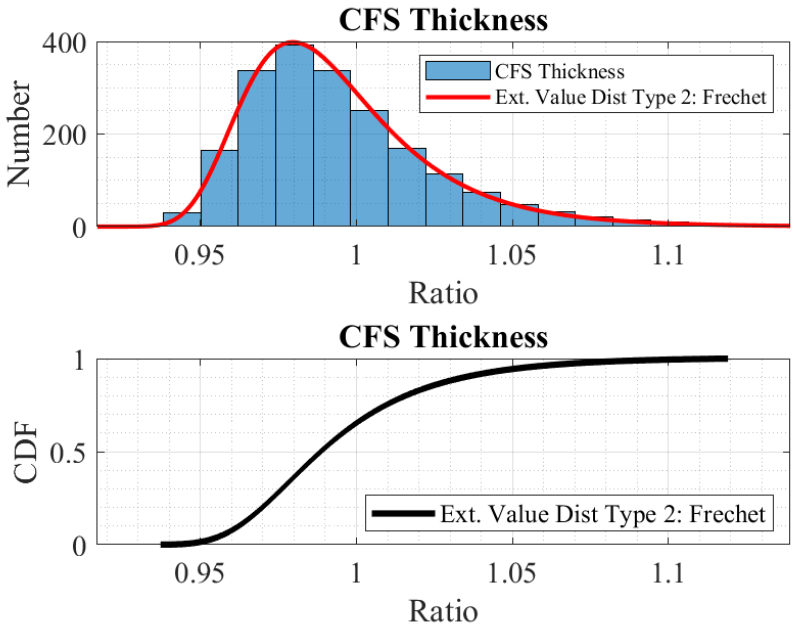

Figure 5.6: Histogram and statistical parameters of generated random CFS thickness values

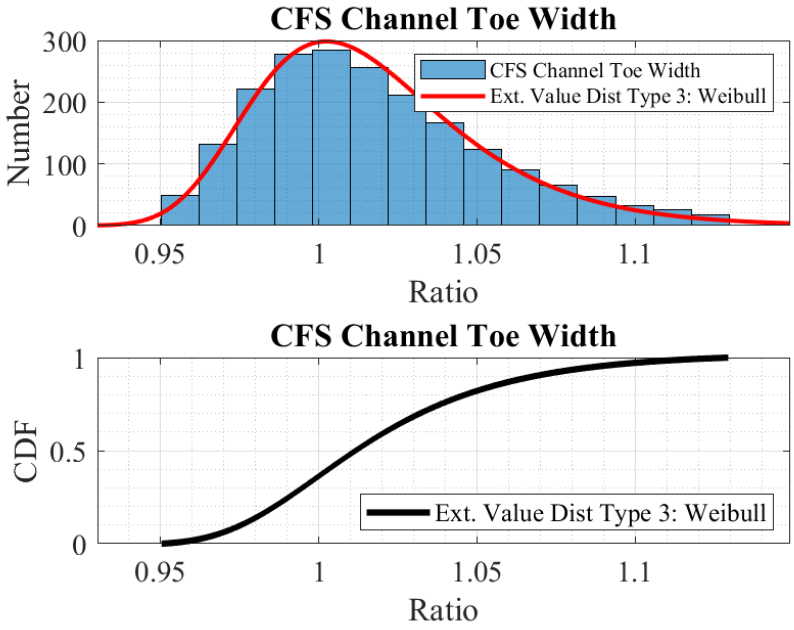

Figure 5.7: Histogram and statistical parameters of generated random CFS channel toe width values

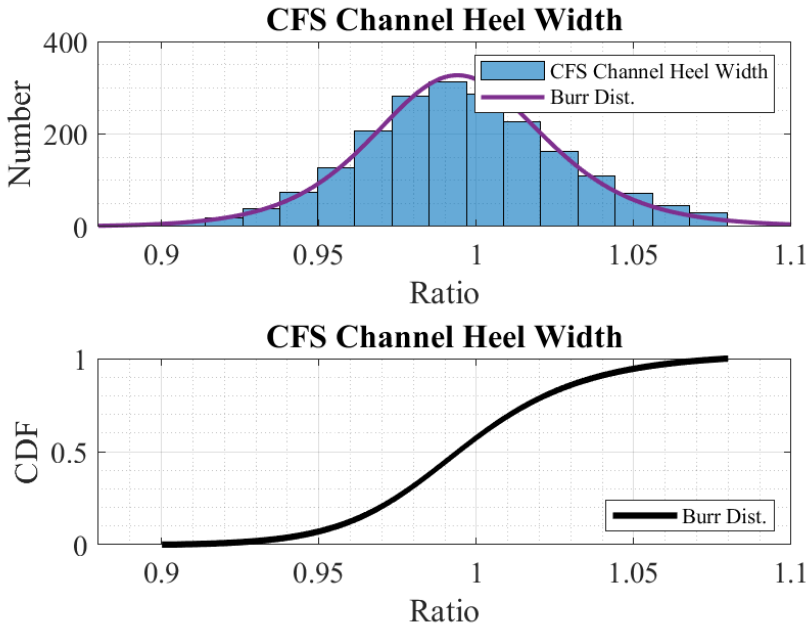

Figure 5.8: Histogram and statistical parameters of generated random CFS channel heel width values

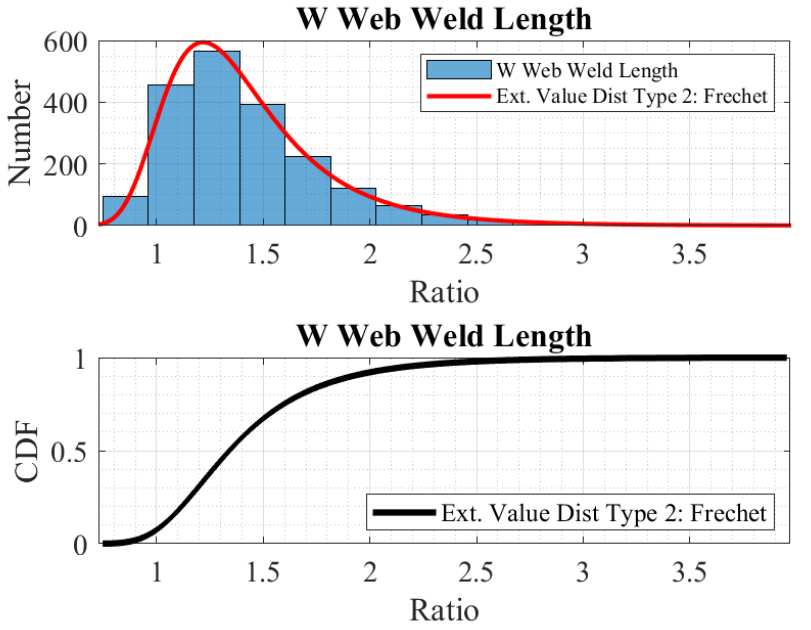

Figure 5.9: Histogram and statistical parameters of generated random W webs weld lengths values

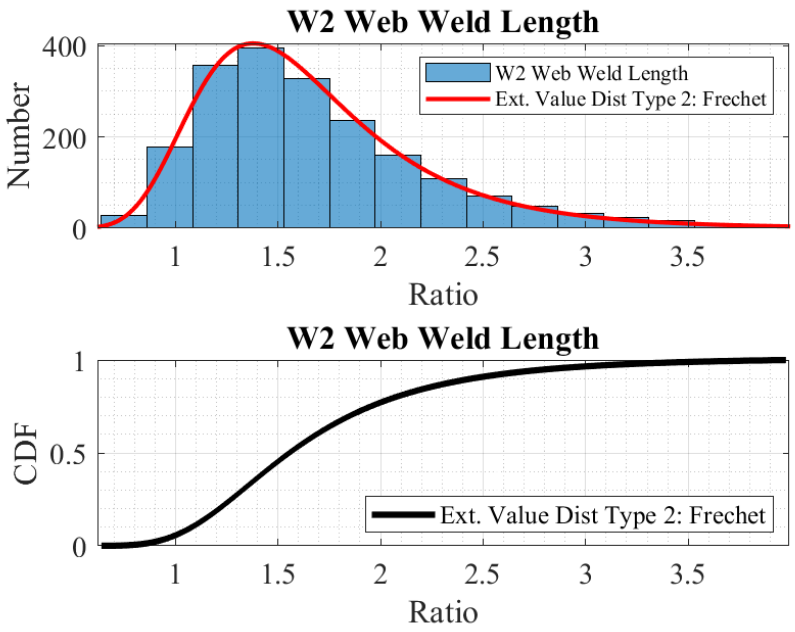

Figure 5.10: Histogram and statistical parameters of generated random W2 webs weld lengths values

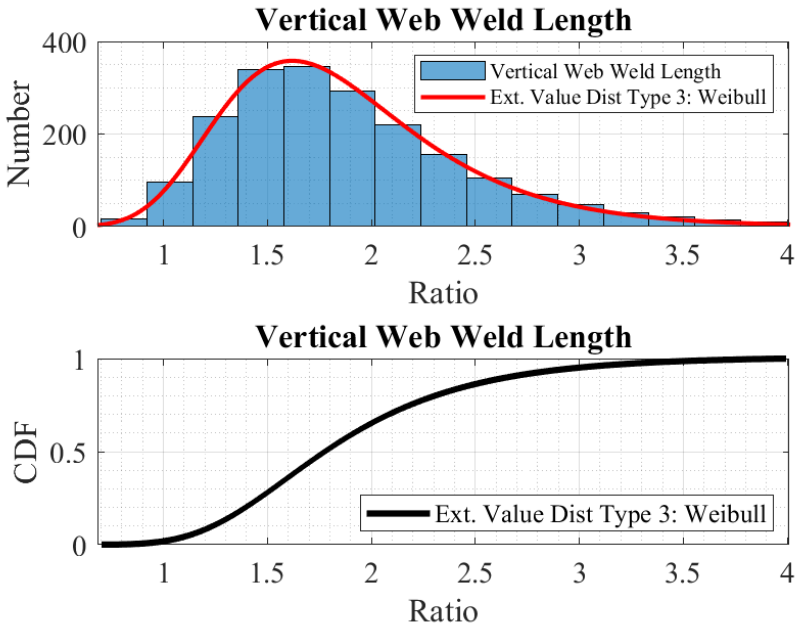

Figure 5.11: Histogram and statistical parameters of generated random vertical webs weld lengths values

5.2. Sensitivity Study and Sensitivity Results

Sensitivity study is a useful method to measure the impact of a single variable or a group of variables on a system behavior. By systematically changing the selected variables, it is possible to determine the influence of each variables by investigating the system responses.

In this study, sensitivity analyses were completed for all three variables for all failure modes of both joists. It was first completed using nominal design values for all variables in each joist design, to obtain the effect of each variable on a nominal system. The second sensitivity study was completed on joist systems modeled using mean values of collected data. Using these means for all variables simulated similar conditions closer to realistic joists. This dual approach provides understanding the effects of each selected variable on both ideal systems and on more realistic systems. The details and results of this sensitivity study, presented below and also provided with figures in the appendix, can be found in Cicek, Sputo, and Blum [22].

Table 5.1 and 5.2 present the mean load factors of each model calculated from the sensitivity analyses for each parameter for nominal and mean value systems, respectively. 1000 runs were completed for each parameter for each joist design. Although the number of analysis was primarily determined by stabilization of mean value of LPF results at each analysis, it was aimed to have at least 1000 analyses results to ensure the accuracy in distribution fitting. Also, to enhance the reliability of the outcomes, prematurely terminated analyses, such as LPF results with 0.3, were discarded from distribution fitting process. The figures of mean LPF value vs number of analysis for each failure mode are given in Appendix Section B.

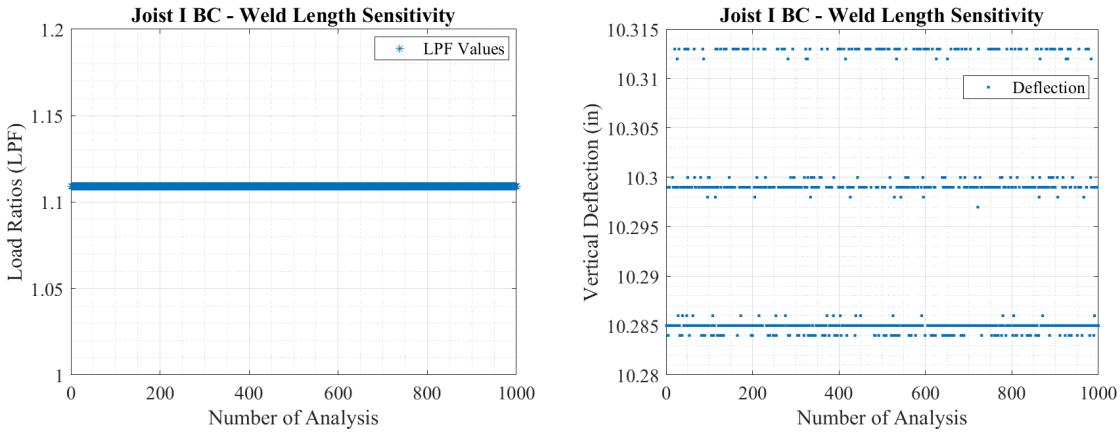

(a) LPF values at each analysis

(b) Deflection results of each analysis

Figure 5.12: Joist I BC weld length sensitivity analyses results

5.2.1 Weld Length Sensitivity

Earlier in this study, it was found that adding springs to web ends influences the behavior of the joist and increase the accuracy. Despite accounting the effect of weld lengths in models, the sensitivity analysis showed that variations in weld length have negligible impact on the load capacity of joists. For all 1,000 analyses conducted for each model, the LPF values remained unchanged or significantly small changes were captured. This indicates that the given range of weld length variations coming from the collected data is not sufficient to influence the overall joist capacity significantly. Figure 5.12 show LPF values and deflection results for weld length sensitivity of Joist I BC design. Therefore, the weld length results were excluded from the results presented in this paper, as they do not contribute to the sensitivity findings.

5.2.2 Cross-sectional Imperfection Sensitivity

The mean LPF values calculated from the cross-sectional imperfection sensitivity analysis show no significant differences compared to the mean LPF values obtained from the beam element

FE models with nominal system parameters. However, despite similar mean LFP values to nominal system, the dispersion of results indicates that the cross-sectional imperfections can increase and decrease the capacity of the designed joist. The results presented in the figures in Appendix B show the reduced capacity can vary between 5% and 15% under certain conditions. These results indicates the importance of the manufacturing processes and the quality control in manufacturing plants.

5.2.3 Yield Strength Sensitivity

For both HRS and CFS joists, yield strength was found to be the most critical parameter, significantly affecting the mean LPF values and creating a bigger spread in the distribution. All joists exhibited higher mean LPF values than the the original models as shown in Table 5.1 and 5.2. This differences show a parallel behavior to the collected data since both HRS and CFS materials show higher mean yield strength values relative to nominal. Another important outcome of the sensitivity study is the differences between nominal LPF value and the mean LPF value are higher for Joist II than Joist I for the yield strength sensitivity analysis. This difference between the two joist types can also be explained by the collected data. The CFS material has a higher mean yield stress than HRS materials as it was shown in Table 2.2. Therefore, the CFS systems have a higher sensitivity to the yield strength value than HRS material systems and as a result the increase in the mean LPF values are higher.

5.2.4 Discussion

The first outcome of sensitivity study is that both beam and shell element FE models show that including the material nonlinearity and using the semi-rigid web end connections instead of pinned-end webs increases the overall load-carrying capacity of the joist designs. Additionally, the sensitivity analyses demonstrate that yield strength has the most significant influence on joist

performance, particularly for CFS designs, where higher mean yield strength values resulted in greater increases in LPF mean values compared to HRS designs, which can be explained by the collected data. Cross-sectional imperfections sensitivity showed that the changes in the cross-sectional properties caused reductions in joist capacity by up to 15% under specific conditions, emphasizing the need for quality control in manufacturing processes. Weld length variations, however, showed negligible impact on joist performance, indicating sufficient weld length in the data at hand. As a result, these findings highlight the importance of both material and geometric parameters in providing safe and efficient joist designs.

Table 5.1: Sensitivity analysis results for nominal systems

Failure Mode	**Distribution Type**	**Mean**	**Standard Deviation**
Joist I BC Yield Strength	Weibull Dist.	1.238	0.051
Joist I BC Sect. Impf.	Weibull Dist.	1.120	0.028
Joist I FW Yield Strength	Normal Dist.	1.210	0.035
Joist I FW Sect. Impf.	Normal Dist.	1.105	0.023
Joist I W3 Yield Strength	Weibull Dist.	1.411	0.033
Joist I W3 Sect. Impf.	Weibull Dist.	1.337	0.040
Joist II BC Yield Strength	Weibull Dist.	1.615	0.082
Joist II BC Sect. Impf.	Lognormal Dist.	1.378	0.044
Joist II FW Yield Strength	Weibull Dist.	1.756	0.081
Joist II FW Sect. Impf.	Weibull Dist.	1.554	0.053
Joist II W3 Yield Strength	Weibull Dist.	1.367	0.062
Joist II W3 Sect. Impf.	Normal Dist.	1.304	0.063

Modes: BC: bottom chord failure, FW: first web failure, W3: first web buckling failure

Table 5.2: Sensitivity analysis results for mean systems

Failure Mode	**Distribution Type**	**Mean**	**Standard Deviation**
Joist I BC Yield Strength	Weibull Dist.	1.245	0.052
Joist I BC Sect. Impf.	Weibull Dist.	1.223	0.031
Joist I FW Yield Strength	Normal Dist.	1.218	0.035
Joist I FW Sect. Impf.	Normal Dist.	1.206	0.026
Joist I W3 Yield Strength	Weibull Dist.	1.423	0.034
Joist I W3 Sect. Impf.	Weibull Dist.	1.410	0.041
Joist II BC Yield Strength	Weibull Dist.	1.653	0.082
Joist II BC Sect. Impf.	Lognormal Dist.	1.661	0.062
Joist II FW Yield Strength	Weibull Dist.	1.792	0.083
Joist II FW Sect. Impf.	Weibull Dist.	1.788	0.064
Joist II W3 Yield Strength	Weibull Dist.	1.446	0.072
Joist II W3 Sect. Impf.	Normal Dist.	1.451	0.080

Modes: BC: bottom chord failure, FW: first web failure, W3: first web buckling failure

6. Simulation and Analysis Results

In this section, full-scale simulations conducted using the beam element FE models, which are previously verified in earlier sections, are presented. These simulations are a crucial step in evaluating the joists performance under the variations in the randomness of the selected parameters (material properties, cross-sectional properties, weld lengths) and represents the foundation for the upcoming reliability analysis.

To ensure statistical robustness, the number of analysis should be adequate to fit a distribution with high accuracy so that it would represent the randomness in input variables on both ends of the spectrum. To determine the adequate number of simulations the same method for the sensitivity study was used. The mean LPF value of each analysis result was recorded and the changes were observed. It was found out that after 2500 analyses all of the LPF results reached a plateau indicating that further analyses would not significantly impact the accuracy of the calculated statistics.

Increasing the number of analysis both increases the accuracy of the distribution fitting and increasing the likelihood of having a higher number of simulations with near-extreme conditions. Therefore, even though the figures show that 2000 analyses would be adequate to obtain a stable mean LPF value, 5000 analyses were conducted for each joist for all failure modes.

As it was mentioned in sensitivity study section that during the simulations a small number of analyses terminated prematurely and these failed analyses were identified and filtered out to ensure the integrity of the dataset. The remaining valid analyses were used to calculate statistical parameters.

The outcomes of these simulations are summarized in Table 6.1 and Figures 6.1 through 6.6. For each model, fitted distribution and related mean and standard deviation of the load factor

(LPF) values were provided. Furthermore, plots showing the convergence of the mean LPF values as the number of analyses increases were provided to demonstrate the adequacy of the number of simulations. These results set the basis for the reliability and resistance factor evaluation, which will be detailed in the next section.

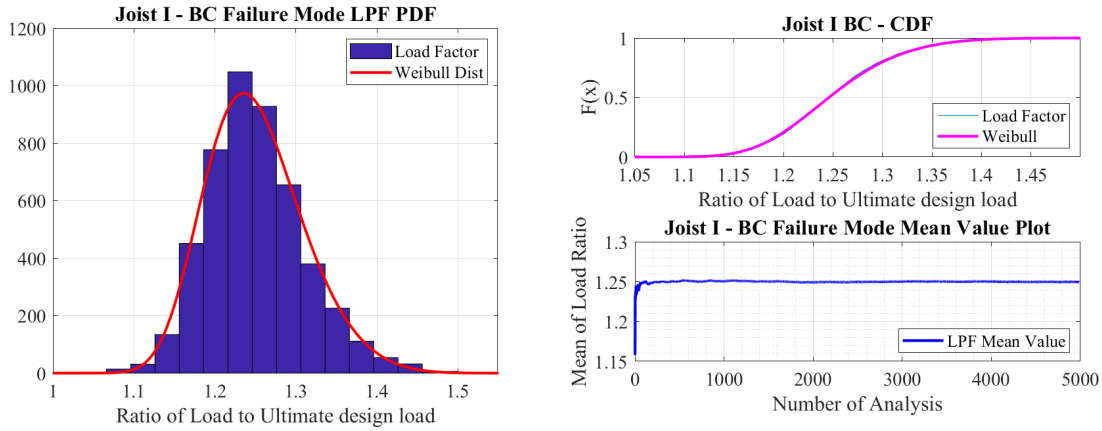

(a) Histogram of LPF and fitted distribution PDF (b) CDF and mean LPF value at each step

Figure 6.1: Joist I BC reliability analyses results and fitted distribution

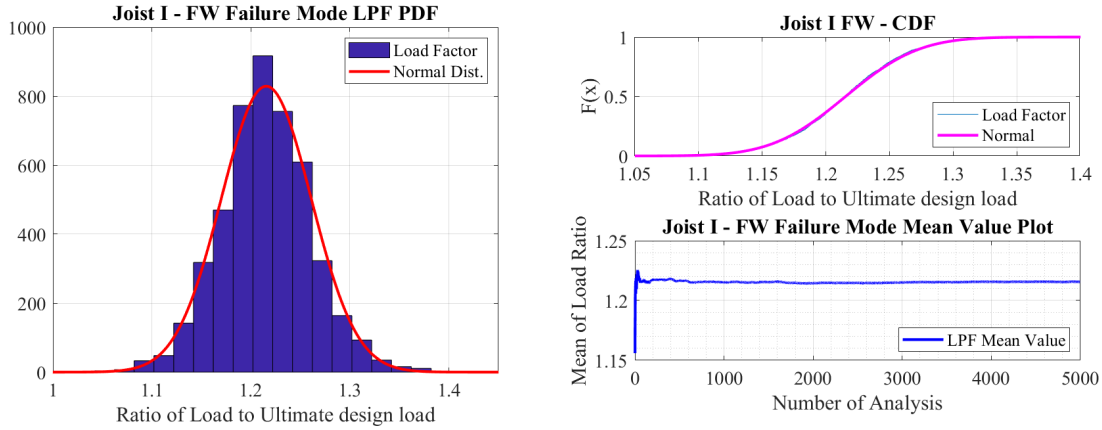

(a) Histogram of LPF and fitted distribution PDF (b) CDF and mean LPF value at each step

Figure 6.2: Joist I FW reliability analyses results and fitted distribution

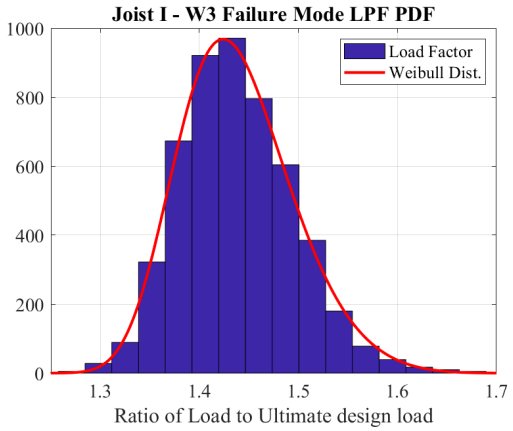

(a) Histogram of LPF and fitted distribution PDF

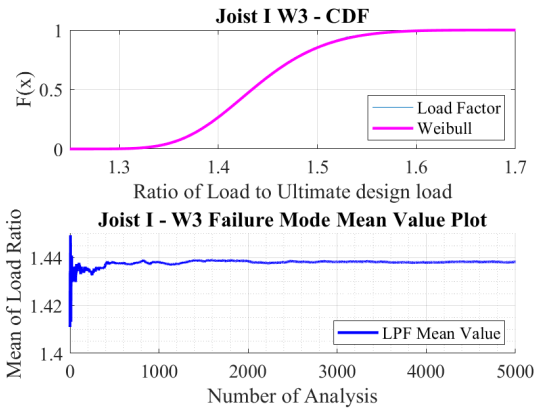

(b) CDF and mean LPF value at each step

Figure 6.3: Joist I W3 reliability analyses results and fitted distribution

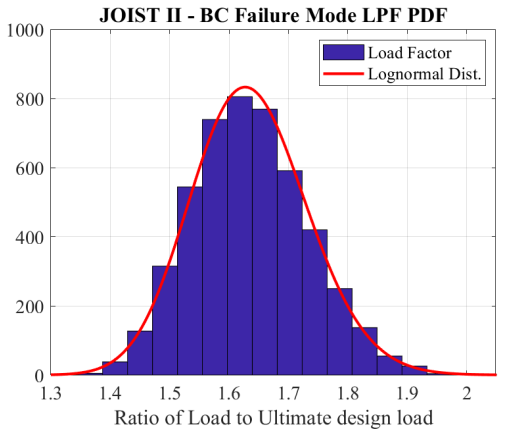

(a) Histogram of LPF and fitted distribution PDF

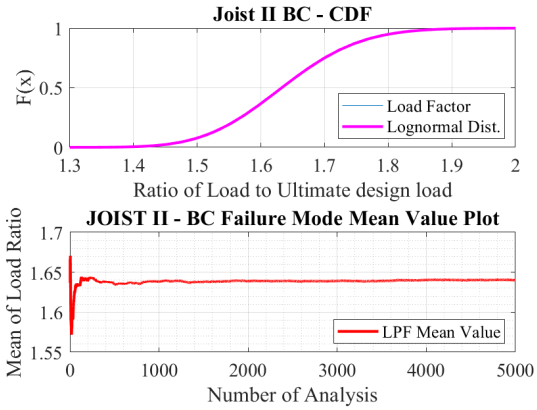

(b) CDF and mean LPF value at each step

Figure 6.4: Joist II BC reliability analyses results and fitted distribution

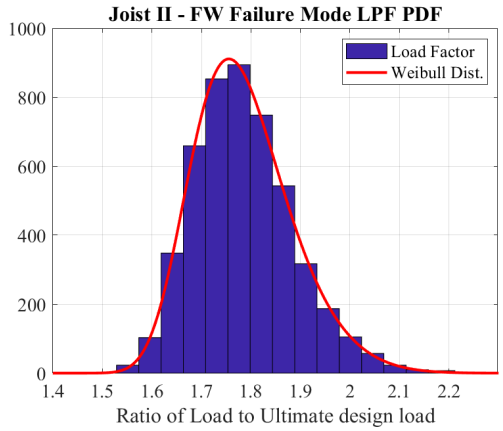

(a) Histogram of LPF and fitted distribution PDF

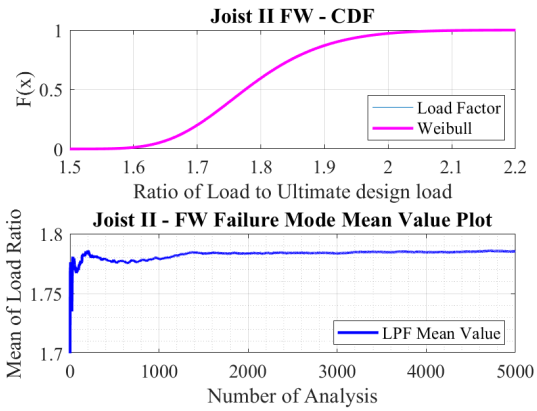

(b) CDF and mean LPF value at each step

Figure 6.5: Joist II FW reliability analyses results and fitted distribution

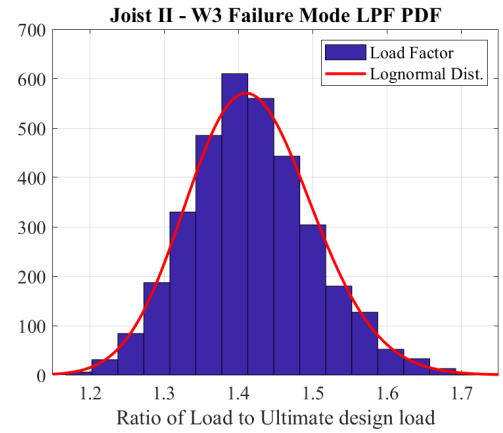

(a) Histogram of LPF and fitted distribution PDF

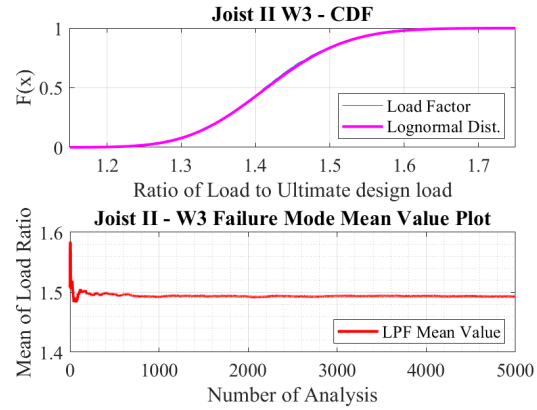

(b) CDF and mean LPF value at each step

Figure 6.6: Joist II W3 reliability analyses results and fitted distribution

Table 6.1: Full simulation analysis results (LPF)

Failure Mode	**Distribution Type**	**Location / Mean (μ)**	**Scale / St. Dev. (σ)**	**Shape (k)**
Joist I BC	Weibull Dist.	1.226	0.056	-0.156
Joist I FW	Normal Dist.	1.215	0.045	-
Joist I W3	Weibull Dist.	1.415	0.053	-0.157
Joist II BC	Lognormal Dist.	0.490	0.0597	-
Joist II FW	Weibull Dist.	1.744	0.0894	-0.125
Joist II W3	Lognormal Dist.	0.347	0.0598	-

Modes: BC: bottom chord failure, FW: first web failure, W3: first web buckling failure

Table 6.2: Theoretical mean and standard deviation values derived from the fitted probability distributions from full simulation analysis results (LPF)

Failure Mode	**Distribution Type**	**Location / Mean (μ)**	**Scale / St. Dev. (σ)**
Joist I BC	Weibull Dist.	1.251	0.061
Joist I FW	Normal Dist.	1.215	0.045
Joist I W3	Weibull Dist.	1.439	0.058
Joist II BC	Lognormal Dist.	1.636	0.098
Joist II FW	Weibull Dist.	1.785	0.100
Joist II W3	Lognormal Dist.	1.418	0.085

Modes: BC: bottom chord failure, FW: first web failure, W3: first web buckling failure

7. Structural Reliability Sample Framework

In structural engineering, reliability is defined as the probability that a structure or component will fulfill its intended function safely under specified conditions for a given duration. To evaluate this performance, a limit state function, also known as a performance function, is typically utilized to define the boundary between safe and unsafe regions. As discussed by Nowak, A. and Collins, K. [23], this relationship can be fundamentally expressed as:

$$g(R, Q) = R - Q \tag{7.1}$$

where R represents the resistance (capacity) and Q represents the load effect (demand). In this traditional safety margin framework, the structure is considered safe when $g \geq 0$, whereas the condition $g < 0$ signifies failure. Since both R and Q are continuous random variables characterized by their own probability density functions (PDFs), the safety of the system is governed by the probability of failure (P_f), expressed as:

$$P_f = P(R - Q < 0) = P(g < 0) \tag{7.2}$$

While structural reliability involves the interplay between demand and capacity, this project specifically focuses on the resistance (R) side of the reliability equation. The objective is to accurately characterize the variability in joist capacity resulting from uncertainties in material properties and geometric configurations. This emphasis on the resistance component is consistent with the reliability provisions of AISI S100 Chapter K ([6]), which provides a framework for establishing resistance

factors (ϕ) based on statistical data. Code committees could combine the results of this project on resistance variability with loading statistics and variability of their choosing.

To generate the necessary data for this resistance-focused evaluation, Latin Hypercube Sampling (LHS) with truncated distributions was employed. This method efficiently captures the variability of the input variables affecting resistance, while truncation ensures that the generated samples remain within physically realistic bounds based on collected data. By isolating and analyzing the stochastic nature of the joist capacity through high-fidelity FEA, the coefficients required for the AISI S100 reliability equations were calculated. Specifically, the data collected and analyzed in this study allow for a refined calibration of the resistance factors, ensuring that the target reliability index (β) is achieved when these joists are subjected to standard load combinations.

$$\phi = C_\phi (M_m F_m P_m) e^{-\beta_o \sqrt{V_M^2 + V_F^2 + C_P V_P^2 + V_Q^2}} \tag{7.3}$$

Resistance Factor (ϕ) for each system were calculated by using Equation 7.3. Explanations and formulations of each coefficient are given in AISI S100. The ϕ coefficient was calculated according to the distribution parameters of material and cross-sectional properties, and the calculated distribution parameters of LPF simulation results of each joist model.

Certain coefficients in the reliability equation are not derived from the collected data or the FEA results but are based on established load and reliability theories. The AISI Specification provides recommended values for C_ϕ, β_o, and V_Q, which are functions of the live-to-dead load ratio (α). These values are derived from the mean load intensities and the corresponding coefficients of variation established by Ellingwood [24]. While the Specification typically assumes a ratio of $\alpha = 5$, the SJI research committee representatives suggested using $\alpha = 3$ to better reflect realistic service conditions for steel joists.

Consequently, instead of using the default tabulated values from AISI, C_ϕ and V_Q were

recalculated using the corresponding equations provided in the Commentary to the Specification and here in Eqs. 7.4, 7.5 and 7.6 (more details can be found in paper of Meimand and Schafer [25]). This approach, following the probabilistic framework developed by Ellingwood [24], ensures that the derived resistance factor ϕ_{sys} accurately represents the behavior of the steel joist system under the combined uncertainties of material, fabrication, and loading effects. This provides a rational basis for the reliability calibration presented in Section 4.3.

$$C_\phi = \frac{\frac{1.2 + 1.6\alpha}{\alpha}}{\frac{1.05 + \alpha}{\alpha}} \tag{7.4}$$

$$\beta = \frac{\ln\left[\frac{M_m \cdot F_m \cdot P_m \cdot \Omega \cdot \left(\frac{1+\alpha}{\alpha}\right)}{\frac{1.05+\alpha}{\alpha}}\right]}{\sqrt{V_M^2 + V_F^2 + V_P^2 + V_Q^2}} \tag{7.5}$$

$$V_Q = \sqrt{\frac{\left(\frac{1.05}{\alpha}\right)^2 \cdot 0.1^2 + 0.25^2}{\frac{1.05+\alpha}{\alpha}}} \tag{7.6}$$

where $\alpha = \frac{L}{D}$

The coefficients related to the materials and sectional imperfections are also included in the formulation. Since the joists were designed using CFS and HRS materials separately, the M_m and V_M parameters resulted in different values for Joist I and Joist II. These values were determined based on the Coefficient of Variation (C.O.V) values obtained from the mean and standard deviation of the material data provided by SJI, which was previously discussed in Section 2.

Similarly, the coefficients F_m and V_F in the formula are related to the sectional property distribution parameters. For the cross-sectional properties, distribution parameters are available for

both thickness and leg sizes, based on the data and distributions previously analyzed in Section 2. To determine a single representative value for these coefficients, a sensitivity analysis was performed by separately varying only the thickness and only the leg size. This sensitivity analysis involved 1000 simulations for each parameter for both Joist I and Joist II. The results showed that thickness and leg size have nearly the same impact on the load-carrying capacity. Therefore, the mean and standard deviation values from both thickness and leg size were averaged (separately for CFS and HRS materials) and used as the final distribution parameters for the calculations in Eq. 7.3.

Coefficients P_m, V_P, and C_P are the inputs related to the analyses or test results of the study where:

- P_m represents the mean value of professional factor (P) for tested component (which is the mean LPF values),
- V_P denotes coefficient of variation of test results (C.O.V of obtained LPF distribution), with a minimum value of 0.065.
- C_P coefficient is given as the number of simulations/tests completed.

These input parameters are derived from the LPF distribution results of the 5000 reliability analyses per joist. The LPF is defined as the load ratio, which is calculated by dividing the maximum load obtained from the analysis by the nominal capacity of the joist determined by the SJI truss method.

Initially, the nominal strength was taken from SJI capacity calculations where the load factor was set to 1 (LPF = 1). However, as Table 4.5 shows, shell FE models show that the designed systems can actually achieve higher load capacities than the truss method predicts. Therefore, a new normalization was also applied to the P_m calculations. In this updated approach, the P_m values were normalized using the load factors obtained from the shell FE models (previously provided in Table 4.5) with all random variables at their nominal values, instead of using LPF = 1.

This method more accurately reflects the impact of the randomness of the input variables

since the shell model represents joist behavior more precisely than the design calculations. Since the nominal load factors from the shell FE models are higher than LPF = 1, this normalization resulted in lower P_m values, and therefore, lower resistance factors and reliability values compared to the initial method. The updated coefficient values and the calculated resistance factors with predefined target reliability values are presented in Tables 7.3 and 7.4, respectively.

Tables 7.1 and 7.3 present the values for each coefficient associated with each failure mode design. These tables utilize P_m and M_m values derived from the nominal distribution equivalent parameters provided in Table 6.2. The decision to use equivalent normal distribution parameters is primarily based on the operational characteristics of the First-Order Reliability Method (FORM), as the accuracy of FORM is significantly enhanced when input variables follow a Gaussian distribution. While FORM can accommodate non-normal distributions, the precision of the method tends to decrease as the input distributions deviate further from the normal shape.

A potential disadvantage of this transformation is the risk of losing accuracy if the equivalent normal distribution fails to capture the extreme tail behavior of the original best-fit distributions. However, a comparative analysis of the distributions used in this study indicates that both the best-fit and normal distribution fits cover the tail regions effectively, justifying the use of normal equivalents. Ultimately, while both approaches—using original non-normal distributions or their normal equivalents—are viable within the FORM framework, the choice depends on balancing computational accuracy with the specific characteristics of the data. Given the strong tail alignment observed in this study, the normal equivalent parameters were adopted to ensure higher reliability in the FORM results.

Based on these inputs, Resistance Factors (ϕ) were calculated for Target Reliability Indices (β_o) of 2.5, 2.6, 3.0, 3.25, and 3.5. These specific β_o values were selected based on the recommendations from the SJI research committee representatives and the corresponding standard reliability index levels specified in ASCE 7-16 [26]. The results are provided in Tables 7.2 and 7.4. Additionally,

these tables present the Reliability Index values for a constant Resistance Factor (ϕ) of 0.9.

Table 7.1: Coefficient values for each model (Nominal Capacity with SJI calculation)

	Joist I			Joist II		
Failure Mode	BC	FW	W3	BC	FW	W3
C_ϕ	1.48			1.48		
M_m	1.098			1.237		
F_m	1.003			0.977		
P_m	1.251	1.215	1.439	1.636	1.785	1.418
V_M	0.158			0.1		
V_F	0.011			0.123		
V_P (min = 0.065)	0.065	0.065	0.065	0.065	0.065	0.065
C_P	1	1	1	1	1	1
V_Q	0.19			0.19		

Modes: BC: bottom chord failure, FW: first web failure, W3: web buckling failure

Table 7.2: Resistance Factors with varying Target Reliability Index, β_o (Nominal capacity with SJI calculation)

	Resistance Factors										Reliability Index
	$\beta_o = 2.5$		$\beta_o = 2.6$		$\beta_o = 3$		$\beta_o = 3.25$		$\beta_o = 3.5$		$\phi = 0.9$
	ϕ	ϕ/0.9	ϕ	ϕ/0.9	ϕ	ϕ/0.9	ϕ	ϕ/0.9	ϕ	ϕ/0.9	β_o
Joist I BC	1.076	1.196	1.049	1.165	0.947	1.052	0.888	0.987	0.833	0.926	3.199
Joist I FW	1.046	1.162	1.020	1.133	0.921	1.023	0.864	0.960	0.810	0.900	3.088
Joist I W3	1.238	1.375	1.246	1.341	1.089	1.210	1.022	1.135	0.959	1.065	3.747
Joist II BC	1.543	1.715	1.504	1.671	1.358	1.509	1.274	1.415	1.195	1.328	4.608
Joist II FW	1.684	1.872	1.642	1.824	1.482	1.647	1.390	1.545	1.304	1.449	4.950
Joist II W3	1.338	1.486	1.303	1.449	1.117	1.308	1.104	1.226	1.036	1.151	4.049

Modes: BC: bottom chord failure, FW: first web failure, W3: web buckling failure

Table 7.3: Coefficient values for each model (Nominal Capacity with shell element models)

	Joist I			Joist II		
Failure Mode	BC	FW	W3	BC	FW	W3
C_ϕ	1.48			1.48		
M_m	1.098			1.237		
F_m	1.003			0.977		
P_m	1.140	1.105	1.115	1.160	1.131	1.096
V_M	0.158			0.1		
V_F	0.011			0.123		
V_P (min = 0.065)	0.065	0.065	0.065	0.065	0.065	0.0779
C_P	1	1	1	1	1	1
V_Q	0.19			0.19		

Modes: BC: bottom chord failure, FW: first web failure, W3: web buckling failure

Table 7.4: Resistance Factors with varying Target Reliability Index, β_o (Nominal capacity with shell element models)

	Resistance Factors										Reliability Index
	β_o = 2.5		β_o = 2.6		β_o = 3		β_o = 3.25		β_o = 3.5		ϕ = 0.9
	ϕ	ϕ/0.9	ϕ	ϕ/0.9	ϕ	ϕ/0.9	ϕ	ϕ/0.9	ϕ	ϕ/0.9	β_o
Joist I BC	0.981	1.090	0.957	1.063	0.864	0.960	0.811	0.901	0.760	0.845	2.840
Joist I FW	0.951	1.057	0.927	1.030	0.837	0.930	0.785	0.872	0.736	0.818	2.715
Joist I W3	0.959	1.066	0.935	1.039	0.844	0.938	0.792	0.880	0.743	0.826	2.750
Joist II BC	1.091	1.213	1.064	1.182	0.960	1.067	0.901	1.001	0.845	0.939	3.254
Joist II FW	1.067	1.185	1.040	1.155	0.939	1.043	0.881	0.978	0.826	0.918	3.164
Joist II W3	1.025	1.139	0.998	1.109	0.900	1.000	0.844	0.937	0.791	0.878	3.000

Modes: BC: bottom chord failure, FW: first web failure, W3: web buckling failure

8. Conclusion

This study provides a comprehensive evaluation of steel joist reliability through the integration of high-fidelity shell and beam finite element modeling with advanced stochastic analyses. By shifting the focus from traditional member-based assessments to a system-based resistance approach, this research accurately captures the complex interactions and failure mechanisms inherent in joist systems. The methodology successfully incorporates realistic variations in material properties, cross-sectional dimensions, and weld lengths, providing a more refined representation of actual structural capacity.

A central contribution of this work is the detailed investigation of the resistance (R) component of the reliability equation. By isolating the variability in joist capacity, the study underscores how material strength fluctuations and geometric imperfections—captured via Latin Hypercube Sampling—directly influence structural robustness. The research demonstrates that while the First-Order Reliability Method (FORM) is a versatile tool, its application using normal equivalent distribution parameters provides a stable and accurate framework for deriving design values, provided that tail behaviors are carefully aligned.

Furthermore, the results support the premise that current structural standards, which are primarily based on member reliability, tend to underestimate the inherent reliability of the entire system. As shown in Table 7.4, although these joists were originally designed for a target reliability index (β_o) of 2.5, the actual calculated indices using the AISI S100 Chapter K formulation and probabilistic analysis yields significantly higher values, often exceeding 3.0. This discrepancy confirms that the actual system reliability is higher than prescribed target values, suggesting that current member-based

939 design codes may lead to overly conservative or inefficient designs.

940 To bridge the gap between probabilistic research and engineering practice, the findings were
941 implemented within the AISI S100 Chapter K framework. By calculating system-level resistance
942 factors (ϕ) across a diverse range of target reliability indices (β_o), this study provides a practical
943 roadmap for the industry. These results illustrate how high-resolution resistance data can be seamlessly
944 translated into codified design parameters. Code committees can implement this study on the
945 variability in resistance with their own assumptions on the variability of loading demand. Ultimately,
946 the provided framework and calibrated factors offer a robust foundation for future design standards,
947 enabling more efficient, economical, and safer steel joist applications that better reflect true structural
948 performance.

A. Moment-Rotation Outcome of Varying Weld Length Ratios

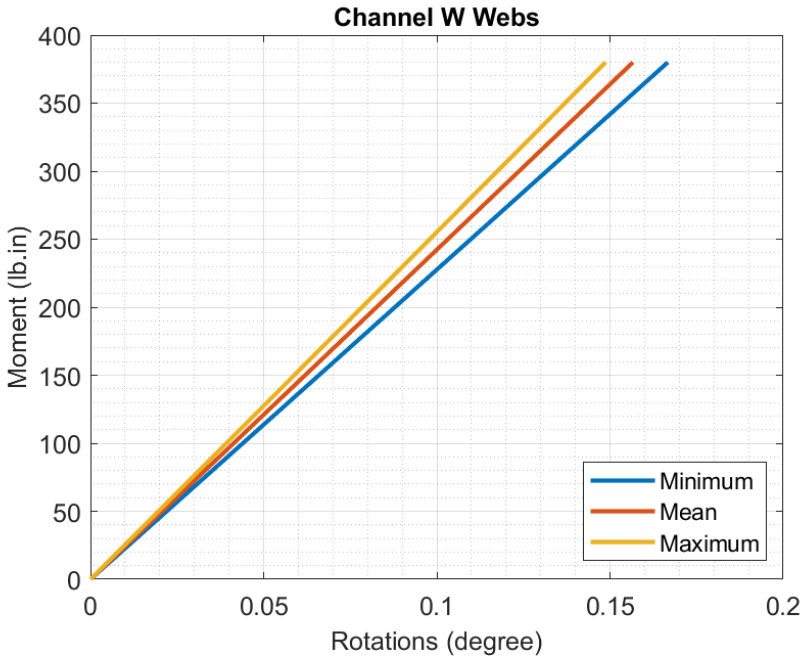

Figure A.1: Moment-rotation output for different ratio levels of weld length for channel W webs

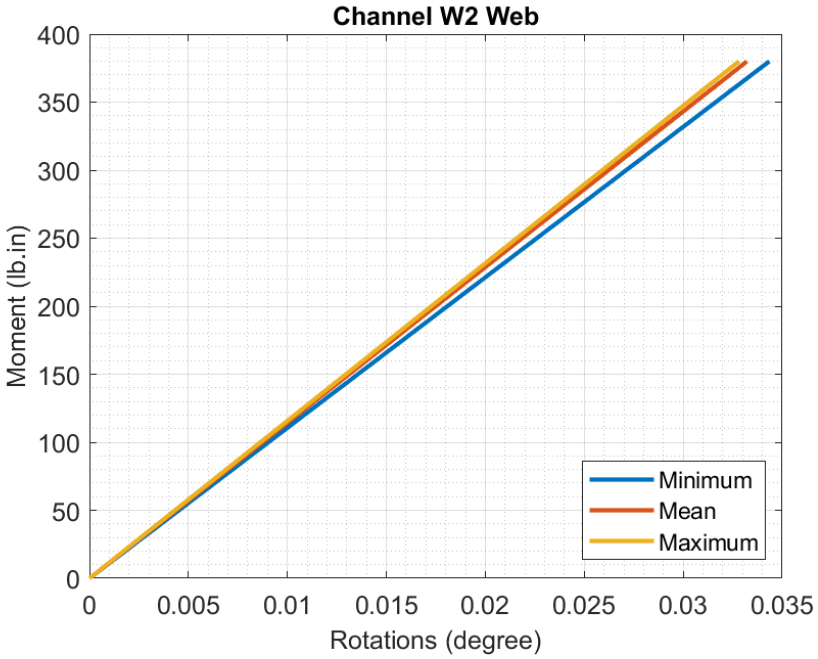

Figure A.2: Moment-rotation output for different ratio levels of weld length for channel W2 webs

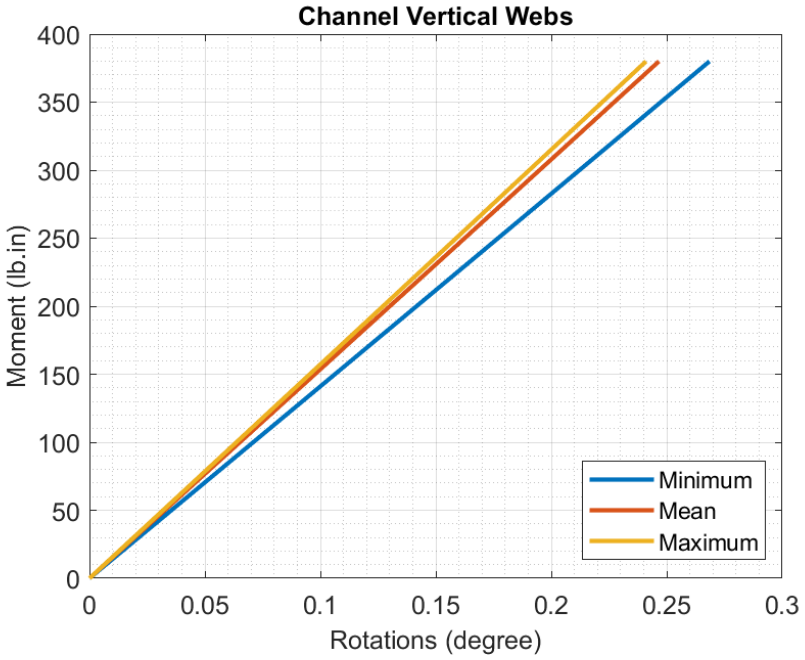

Figure A.3: Moment-rotation output for different ratio levels of weld length for channel vertical webs

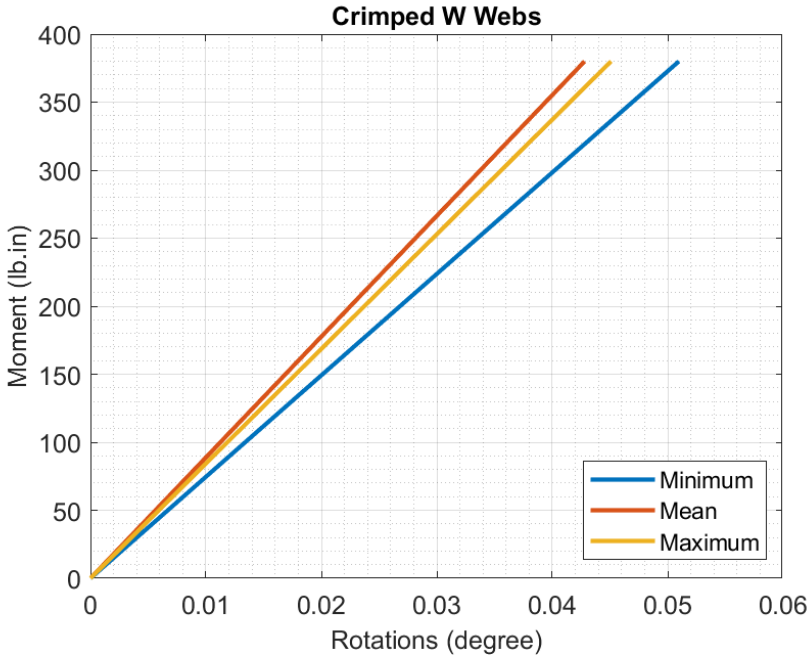

Figure A.4: Moment-rotation output for different ratio levels of weld length for crimped W webs

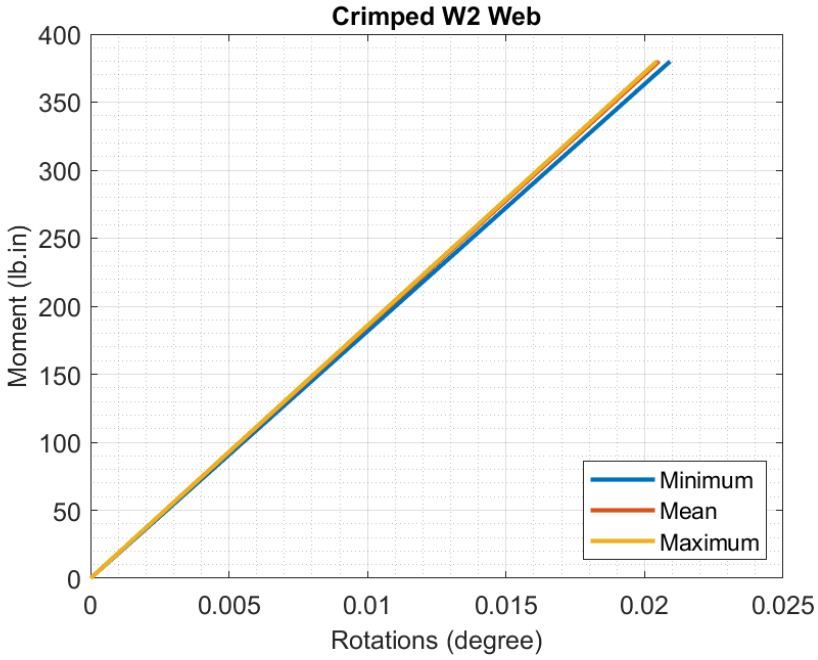

Figure A.5: Moment-rotation output for different ratio levels of weld length for crimped W2 webs

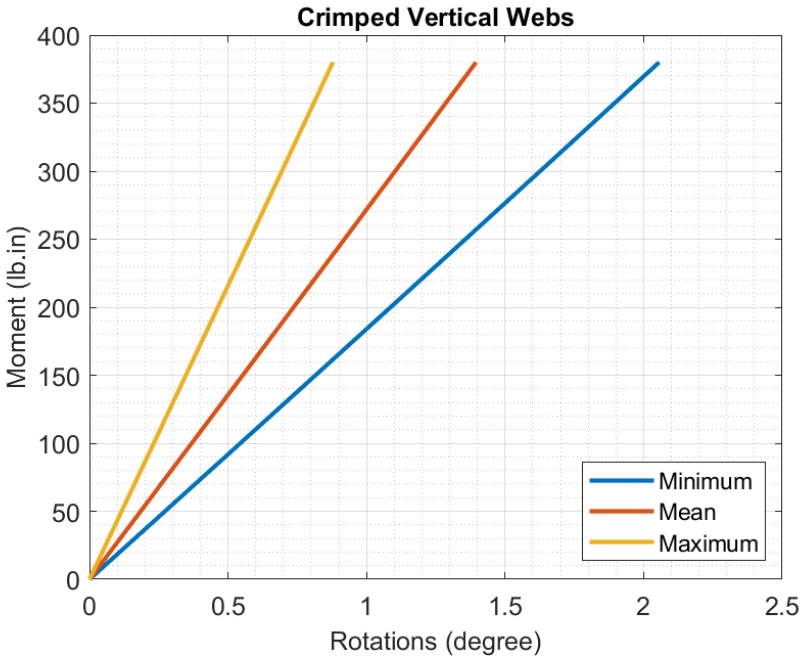

Figure A.6: Moment-rotation output for different ratio levels of weld length for crimped vertical webs

B. Sensitivity Study Result Figures

B.1. Nominal Value System Sensitivity Figures

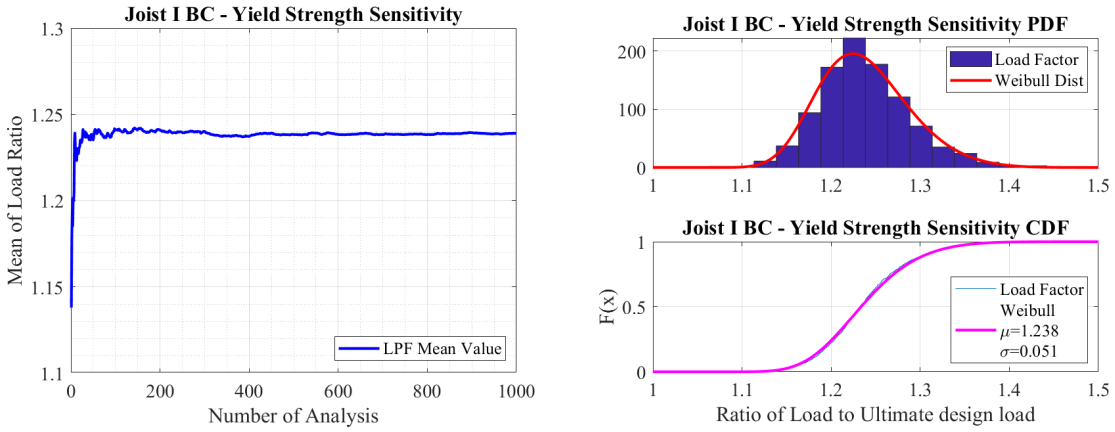

(a) Mean value of LPF at each step

(b) Fitted distribution type for LPF results

Figure B.1: Joist I BC yield strength sensitivity analyses results and fitted distribution

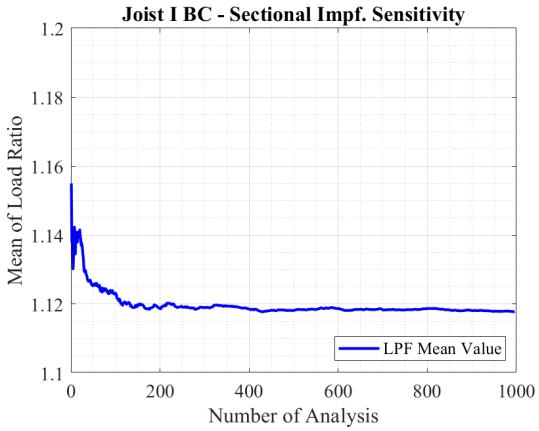

(a) Mean value of LPF at each step

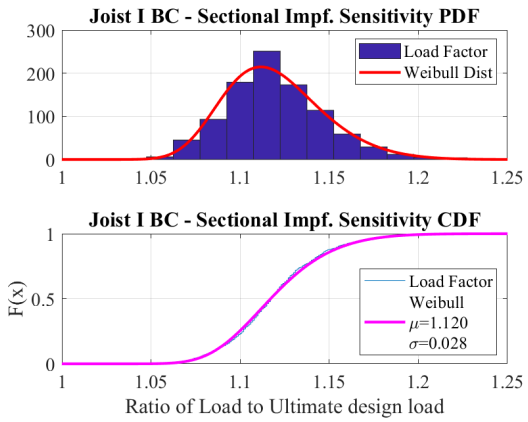

(b) Fitted distribution type for LPF results

Figure B.2: Joist I BC cross-sectional imperfection sensitivity analyses results and fitted distribution

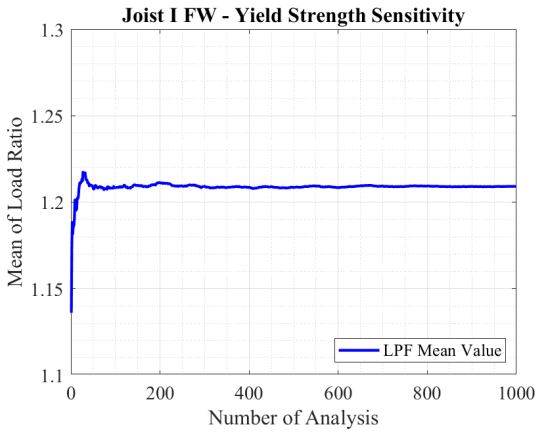

(a) Mean value of LPF at each step

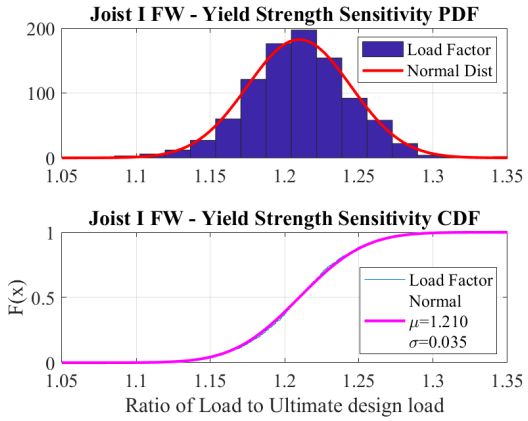

(b) Fitted distribution type for LPF results

Figure B.3: Joist I FW yield strength sensitivity analyses results and fitted distribution

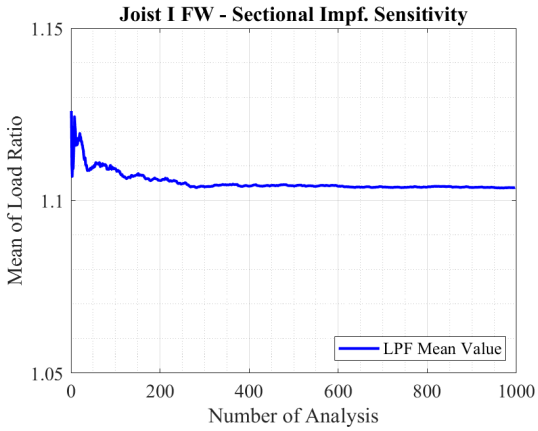

(a) Mean value of LPF at each step

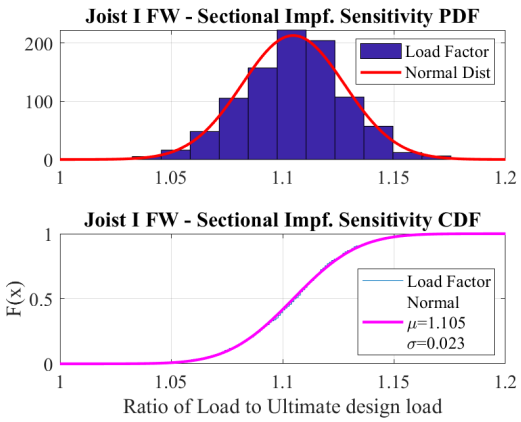

(b) Fitted distribution type for LPF results

Figure B.4: Joist I FW cross-sectional imperfection sensitivity analyses results and fitted distribution

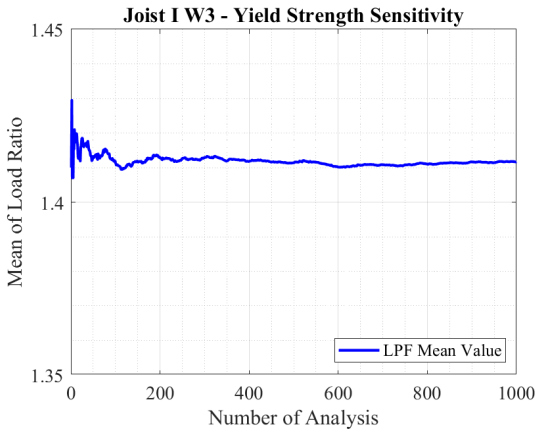

(a) Mean value of LPF at each step

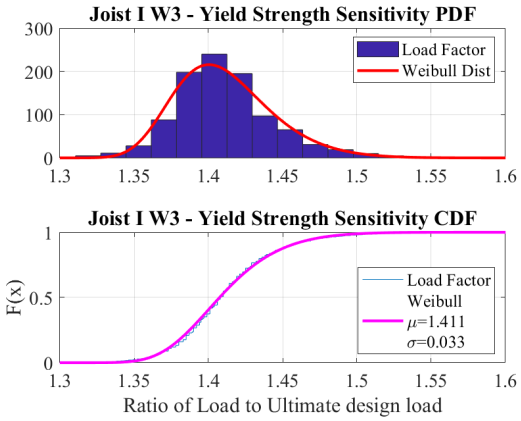

(b) Fitted distribution type for LPF results

Figure B.5: Joist I W3 yield strength sensitivity analyses results and fitted distribution

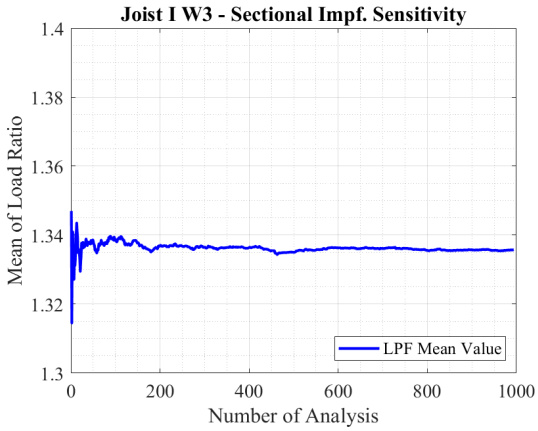

(a) Mean value of LPF at each step

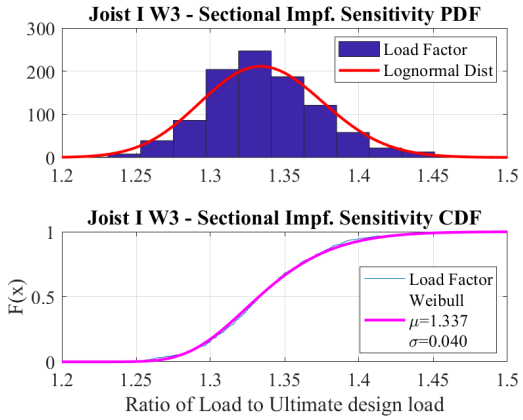

(b) Fitted distribution type for LPF results

Figure B.6: Joist I W3 cross-sectional imperfection sensitivity analyses results and fitted distribution

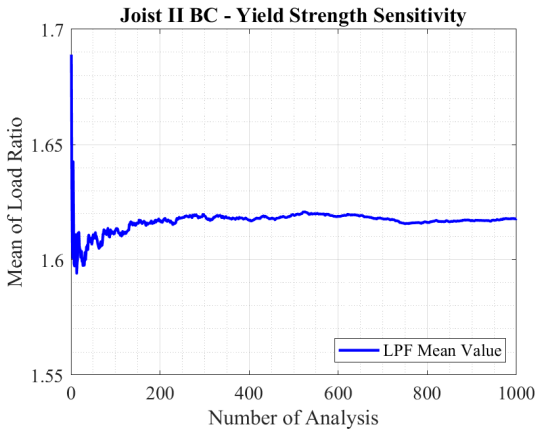

(a) Mean value of LPF at each step

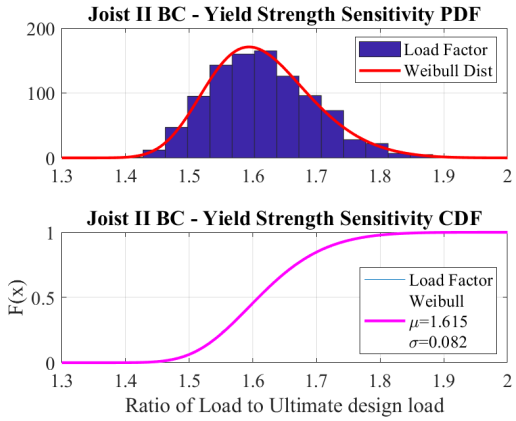

(b) Fitted distribution type for LPF results

Figure B.7: Joist II BC yield strength sensitivity analyses results and fitted distribution

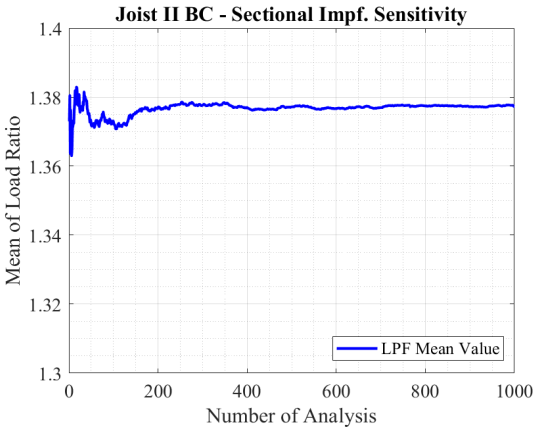

(a) Mean value of LPF at each step

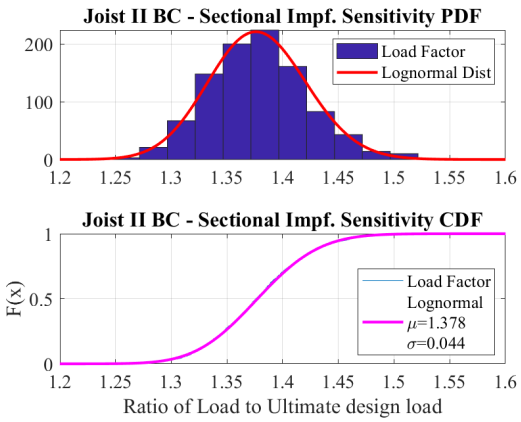

(b) Fitted distribution type for LPF results

Figure B.8: Joist II BC cross-sectional imperfection sensitivity analyses results and fitted distribution

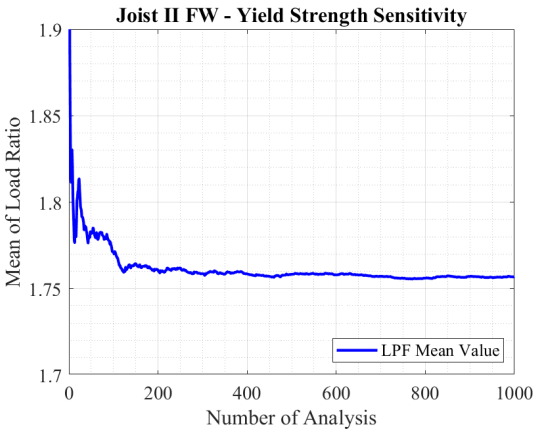

(a) Mean value of LPF at each step

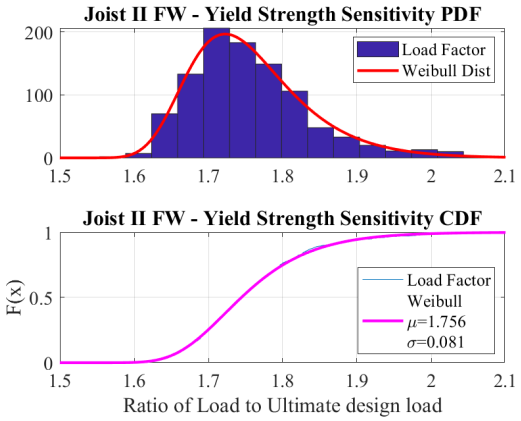

(b) Fitted distribution type for LPF results

Figure B.9: Joist II FW yield strength sensitivity analyses results and fitted distribution

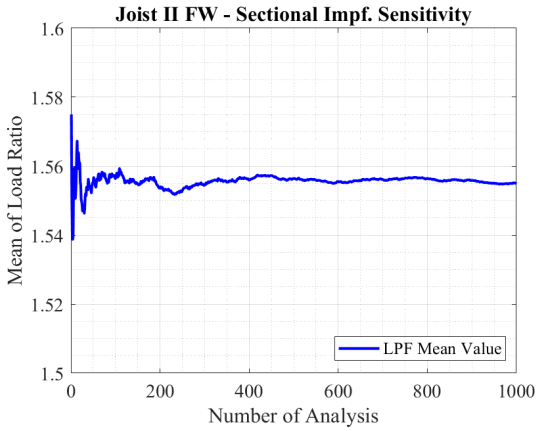

(a) Mean value of LPF at each step

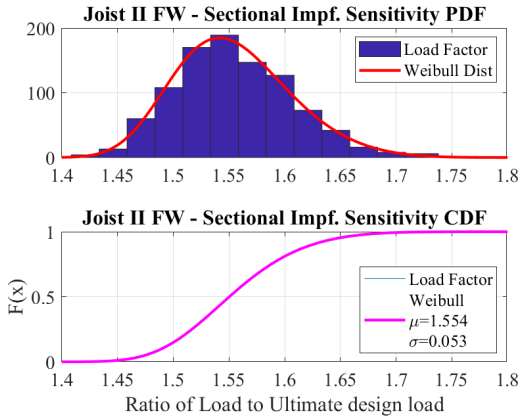

(b) Fitted distribution type for LPF results

Figure B.10: Joist II FW cross-sectional imperfection sensitivity analyses results and fitted distribution

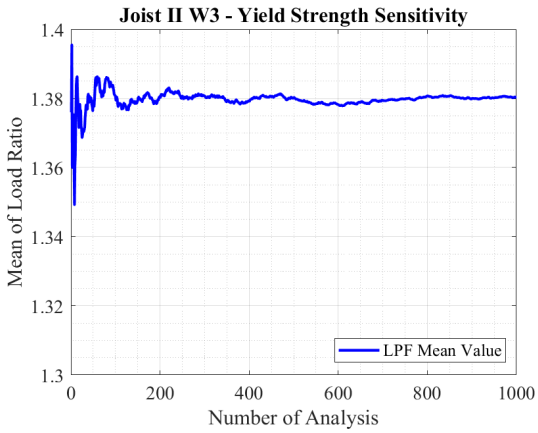

(a) Mean value of LPF at each step

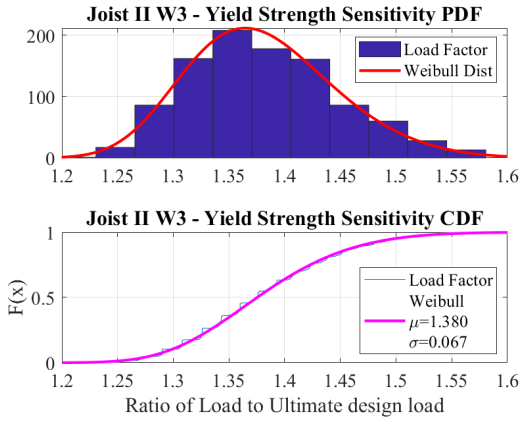

(b) Fitted distribution type for LPF results

Figure B.11: Joist II W3 yield strength sensitivity analyses results and fitted distribution

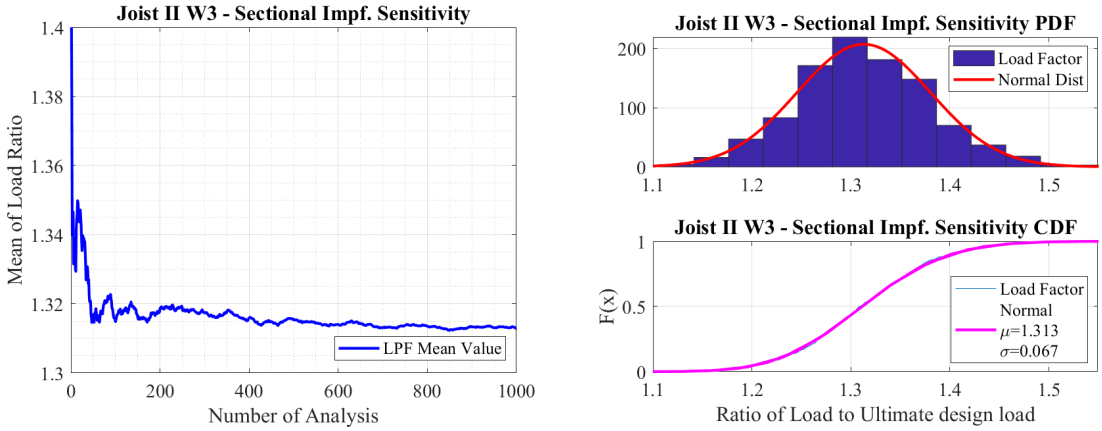

(a) Mean value of LPF at each step (b) Fitted distribution type for LPF results

Figure B.12: Joist II W3 cross-sectional imperfection sensitivity analyses results and fitted distribution

B.2. Mean Value System Sensitivity Figures

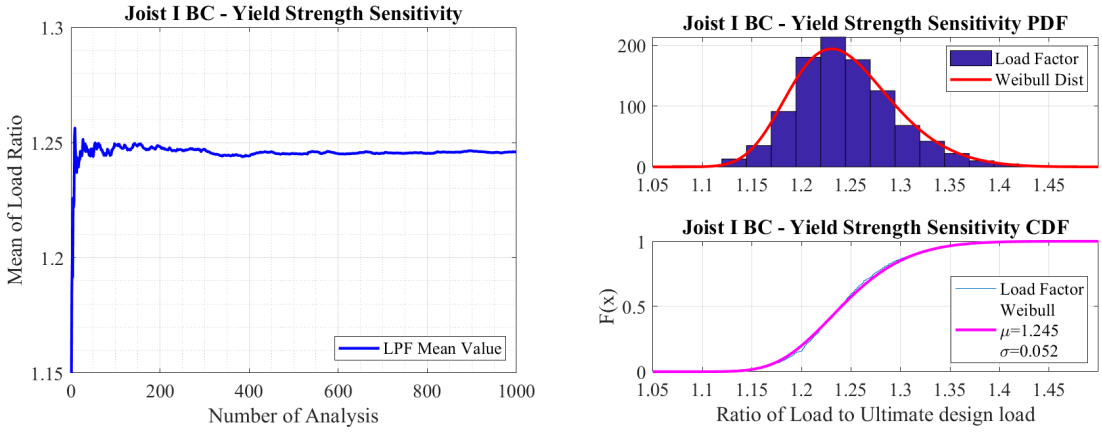

(a) Mean value of LPF at each step (b) Fitted distribution type for LPF results

Figure B.13: Joist I BC yield strength sensitivity analyses results and fitted distribution

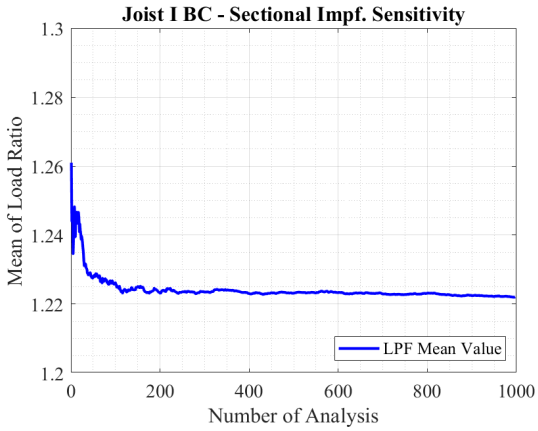

(a) Mean value of LPF at each step

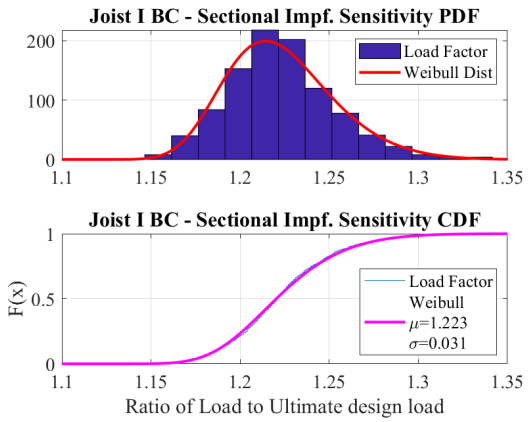

(b) Fitted distribution type for LPF results

Figure B.14: Joist I BC cross-sectional imperfection sensitivity analyses results and fitted distribution

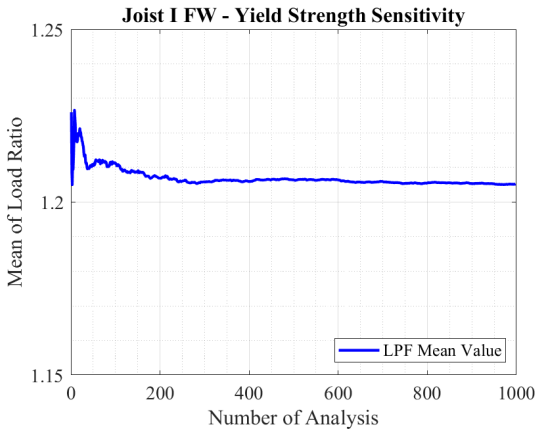

(a) Mean value of LPF at each step

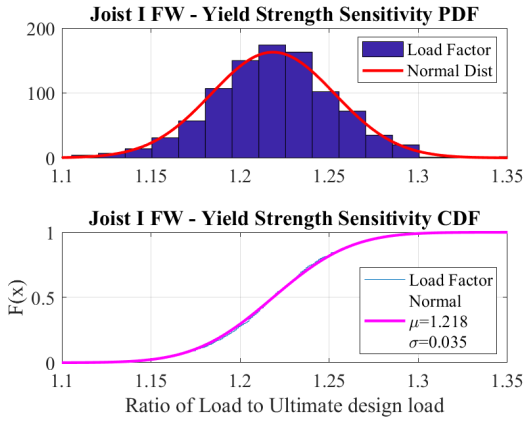

(b) Fitted distribution type for LPF results

Figure B.15: Joist I FW yield strength sensitivity analyses results and fitted distribution

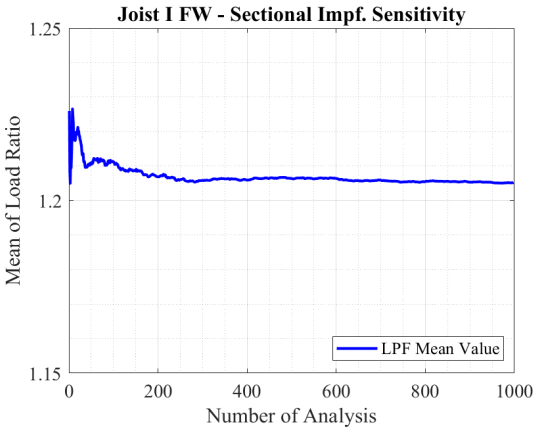

(a) Mean value of LPF at each step

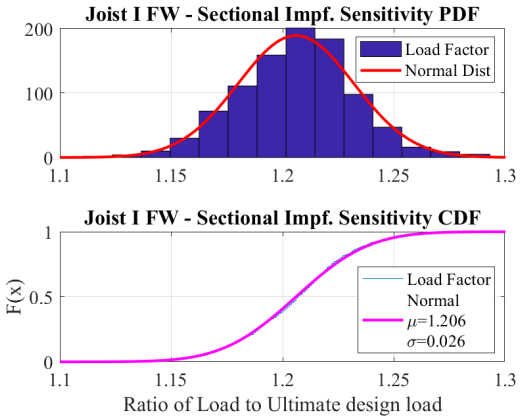

(b) Fitted distribution type for LPF results

Figure B.16: Joist I FW cross-sectional imperfection sensitivity analyses results and fitted distribution

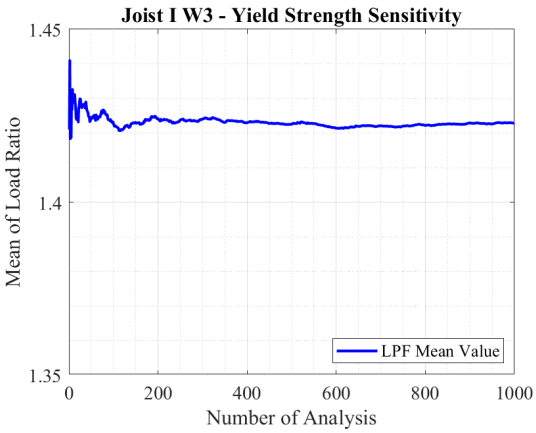

(a) Mean value of LPF at each step

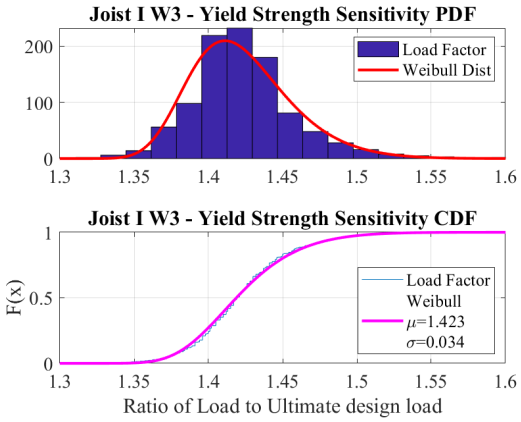

(b) Fitted distribution type for LPF results

Figure B.17: Joist I W3 yield strength sensitivity analyses results and fitted distribution

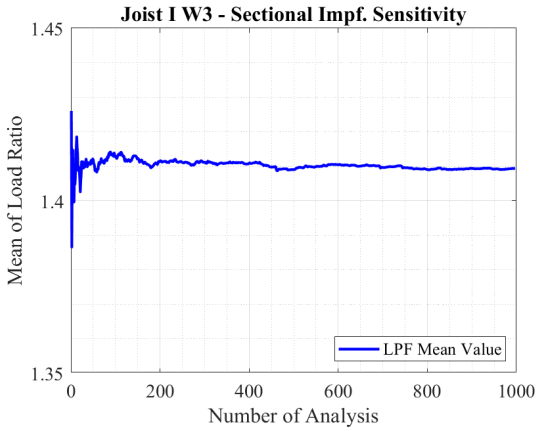

(a) Mean value of LPF at each step

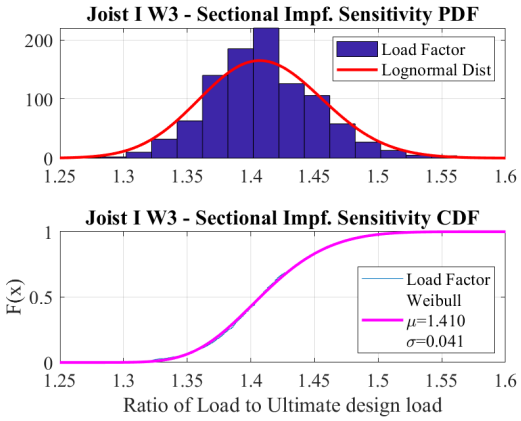

(b) Fitted distribution type for LPF results

Figure B.18: Joist I W3 cross-sectional imperfection sensitivity analyses results and fitted distribution

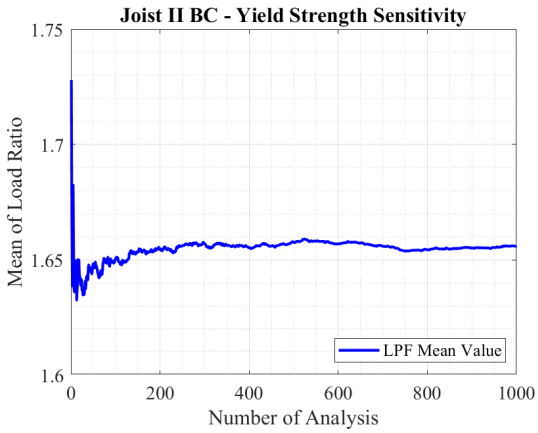

(a) Mean value of LPF at each step

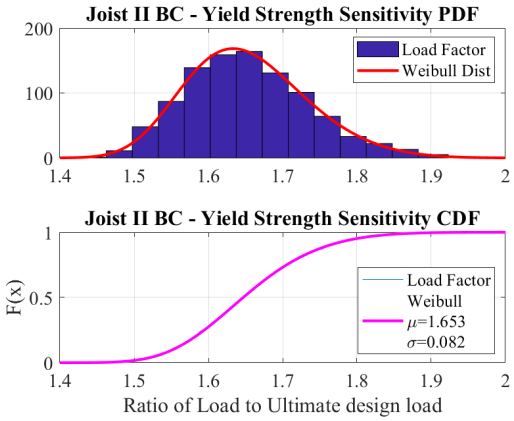

(b) Fitted distribution type for LPF results

Figure B.19: Joist II BC yield strength sensitivity analyses results and fitted distribution

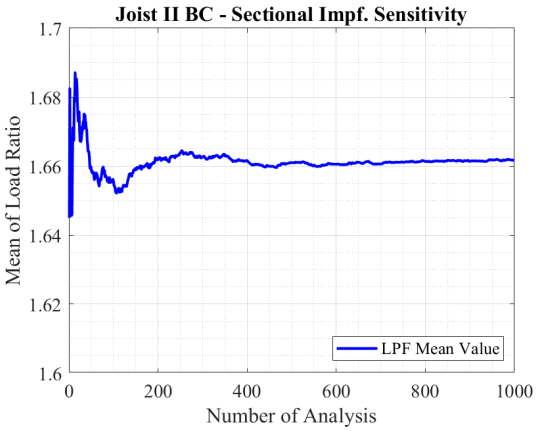

(a) Mean value of LPF at each step

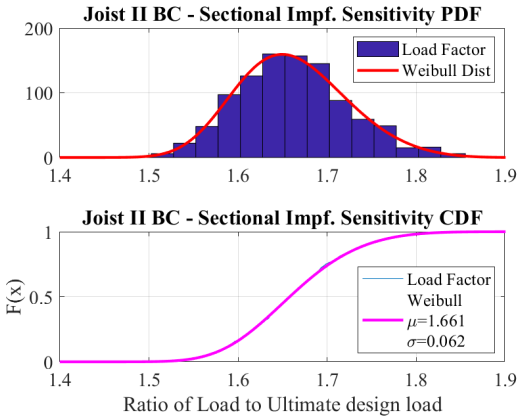

(b) Fitted distribution type for LPF results

Figure B.20: Joist II BC cross-sectional imperfection sensitivity analyses results and fitted distribution

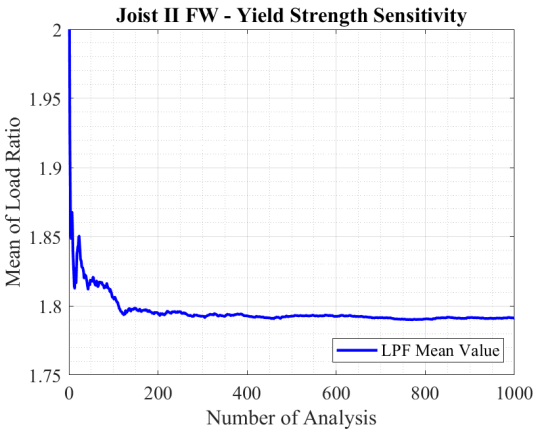

(a) Mean value of LPF at each step

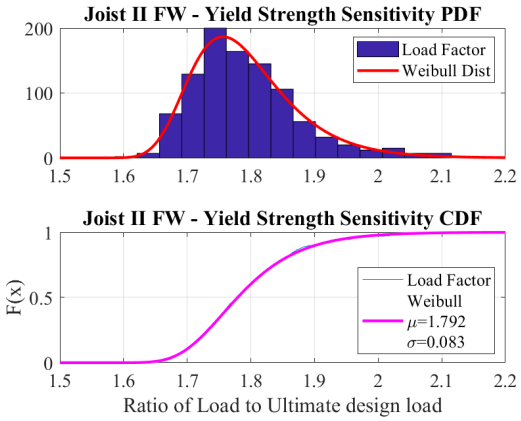

(b) Fitted distribution type for LPF results

Figure B.21: Joist II FW yield strength sensitivity analyses results and fitted distribution

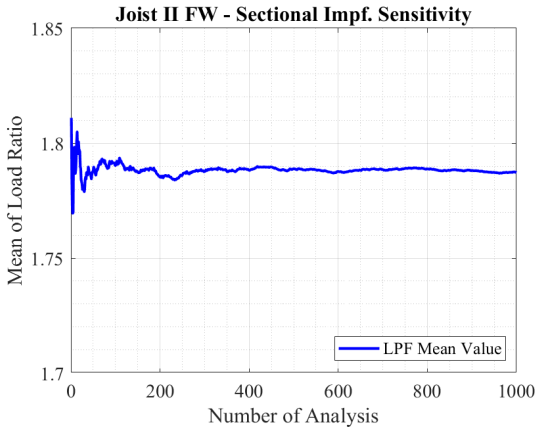

(a) Mean value of LPF at each step

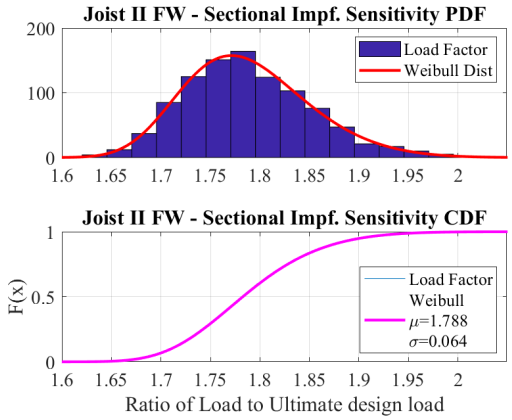

(b) Fitted distribution type for LPF results

Figure B.22: Joist II FW cross-sectional imperfection sensitivity analyses results and fitted distribution

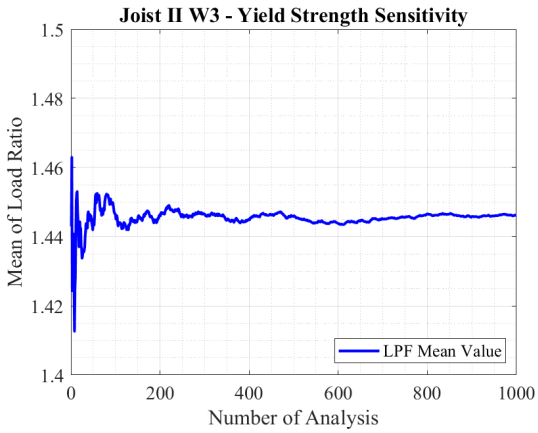

(a) Mean value of LPF at each step

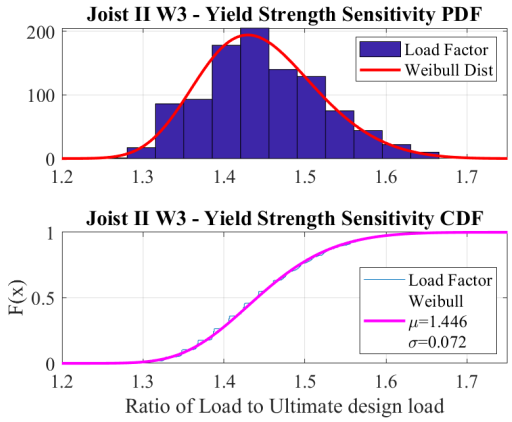

(b) Fitted distribution type for LPF results

Figure B.23: Joist II W3 yield strength sensitivity analyses results and fitted distribution

B.3. Design Sheets

STRESS ANALYSIS - PAGE 1

NEW MILLENNIUM BUILDING SYSTEMS

Job Number:	Job Name:	Date Run:
00-0-0576	SJI RESEARCH - SHOPORDERS	9/20/2022 4:31:17 PM

Location:	Joist Description:	Mark:
BUTLER, IN	Short Span Crimp 30K9	30K9BC

Geometry

Base Length:	Working Length:	Joist Depth:	Effective Depth:	BC Panel Length:	Shape:
50-0 954	49-8	30.00	28.90	10 @ 4-0	Parallel Chords

Variable	Left End	Right End
BC Panel	5-0	5-0
TC Panel	3-7	3-7
First Half	2-0	2-0
First Diag.	7-0	7-0
Depth	30.00	30.00

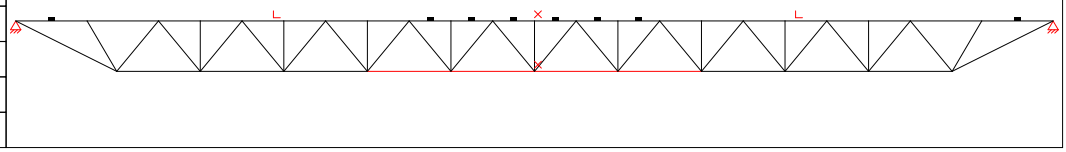

Loads, *** All loads are factored ***

Load Type	Category	Load1	Load2	Position	Direction	Loc/Begin	Sp/End	Reference
Uniform (plf)	LL	225.60	225.60	TC	+	0-0	50-0	L-BL
Uniform (plf)	DL	141.40	141.40	TC	+	0-0	50-0	L-BL

Stress Analysis Summary

Int. Panel TC:	Max Panel BC:	Reaction LE:	Reaction RE:	Minimum Shear:	Max TC Comp.:	Max BC Tension
24.00	48.00	9,113.83	9,113.83	2,278.46	46,980.63	46,675.91

Member	TC Tension	TC Compresion	BC Tension	BC Compresion	Web Tension	Web Comp.	Web Length	PP Dist.
W2	0.00	17,029.71	0.00	0.00	19,027.30	0.00	64.80	0-2
V1S	0.00	16,292.23	0.00	0.00	0.00	1,539.86	33.53	3-7
W3	0.00	16,292.23	22,297.86	0.00	0.00	9,624.51	37.57	5-0
W4	0.00	27,478.20	22,297.86	0.00	8,754.51	0.00	37.57	7-0
W5	0.00	27,478.20	32,049.08	0.00	0.00	7,913.33	37.57	9-0
W6	0.00	36,010.51	32,049.08	0.00	7,100.95	0.00	37.57	11-0
W7	0.00	36,010.51	39,362.49	0.00	0.00	6,317.39	37.57	13-0
W8	0.00	42,105.01	39,362.49	0.00	5,562.65	66.53	37.57	15-0
W9	0.00	42,105.01	44,238.10	0.00	561.96	4,836.72	37.57	17-0
W10	0.00	45,761.72	44,238.10	0.00	4,139.60	1,086.20	37.57	19-0
W11	0.00	45,761.72	46,675.91	0.00	1,639.25	3,471.29	37.57	21-0
W12	0.00	46,980.63	46,675.91	0.00	2,961.49	2,221.12	37.57	23-0
W12	0.00	46,980.63	46,675.90	0.00	2,961.49	2,221.12	37.57	25-0
W11	0.00	45,761.73	46,675.90	0.00	1,639.25	3,471.29	37.57	27-0
W10	0.00	45,761.73	44,238.10	0.00	4,139.60	1,086.20	37.57	29-0
W9	0.00	42,105.02	44,238.10	0.00	561.96	4,836.72	37.57	31-0
W8	0.00	42,105.02	39,362.49	0.00	5,562.65	66.53	37.57	33-0
W7	0.00	36,010.51	39,362.49	0.00	0.00	6,317.39	37.57	35-0
W6	0.00	36,010.51	32,049.08	0.00	7,100.95	0.00	37.57	37-0
W5	0.00	27,478.20	32,049.08	0.00	0.00	7,913.33	37.57	39-0
W4	0.00	27,478.20	22,297.86	0.00	8,754.51	0.00	37.57	41-0
W3	0.00	16,292.23	22,297.86	0.00	0.00	9,624.51	37.57	43-0
V1S	0.00	16,292.23	0.00	0.00	0.00	1,539.86	33.53	46-5
W2	0.00	17,029.71	0.00	0.00	19,027.30	0.00	64.80	45-0

Standard Verticals

Member	Position	Max Tension	Max Comp.	Length
V2	Interior	0.00	968.90	28.90

STRESS ANALYSIS - PAGE 2

NEW MILLENNIUM BUILDING SYSTEMS

Job Number:	Job Name:	Date Run:
00-0-0576	SJI RESEARCH - SHOPORDERS	9/20/2022 4:31:17 PM

Location:	Joist Description:	Mark:
BUTLER, IN	Short Span Crimp 30K9	30K9BC

Chord Properties

Chord	Area	Rx	Rz	Ryy	Y	Ix	Q	Material
TC	0.6209	0.6011	0.3559	1.2877	0.5763	0.2243	1.0000	A34A = 1.9380 x 0.176
BC	0.4776	0.5442	0.3206	1.2107	0.5190	0.1414	1.0000	A28A = 1.7500 x .150

Axial and Bending Analysis

K:	Fy:	Fb:	Mom of Inertia:	LL 360:	LL 240:	Max Bridg TC:	Max Bridg BC:
0.75	50,000.00	45,000.00	451.81	137.77	206.66	17-3 1/8	24-2 1/2

Top Chord Check	End Panel LE	First Panel LE	Interior Panel	First Panel RE	End Panel RE
Length	41.00	41.00	24.00	41.00	41.00
Bending Load	367.00	367.00	367.00	367.00	367.00
Axial Load	17,029.71	16,292.23	46,980.63	16,292.23	17,029.71
fa	13,713.73	13,119.85	37,832.69	13,119.85	13,713.73
Maximum K L/r	68.21	115.20	33.72	115.20	68.21
Fcr	35,582.52	18,914.09	46,011.85	18,914.09	35,582.52
Fa	32,024.27	17,022.68	41,410.67	17,022.68	32,024.27
F'e	61,521.02	61,521.02	319,187.78	61,521.02	61,521.02
Cm	0.9257	0.9289	0.9473	0.9289	0.9257
Panel Point Moment	5,709.10	5,709.10	1,468.00	5,709.10	5,709.10
Mid Panel Moment	3,809.25	2,137.33	734.00	2,137.33	3,809.25
Panel Point fb	17,329.66	17,329.66	4,456.03	17,329.66	17,329.66
Mid Panel fb	4,893.61	2,745.75	942.94	2,745.75	4,893.61
Fillers	1	0	6	0	1
Panel Point Stress	31,043.39	30,449.51	42,288.72	30,449.51	31,043.39
Mid Panel Stress	0.5472	0.8368	0.9339	0.8368	0.5472

Gap Between Chords: **1.1250**

Min Weld Len 2X: **0.5000**

Max Load Fillers TC: **50,503.57**

Max Load no Fillers TC: **45,528.86**

TC OAL/Ryy: **462.85**

BC OAL/Ryy: **492.29**

BC Stress: **1.09**

BC L/Rz: **149.7193**

TC Shear Stress: **17,991.50**

BC Shear Stress: **23,711.88**

Web Design

Member	Web Tension	Allow Tension	Web Comp	Allow Comp	Weld	Qty	Material
W2	19,027.30	19,451.71	0.00	5,599.71	5.69 x 0.150	1	C28AA = 1.125 x 1.347 x .150
W3	0.00	21,613.01	9,624.51	10,000.62	2.88 x 0.150	1	C28AA = 1.125 x 1.347 x .150
W4	8,754.51	11,808.24	0.00	5,630.10	3.74 x 0.105	1	C16AA = 1.125 x 0.943 x .105
W5	0.00	16,380.48	7,913.33	7,969.79	2.65 x 0.134	1	C22AA = 1.125 x 1.086 x .134
W6	7,100.95	8,420.89	0.00	2,408.84	3.54 x 0.090	1	C12AA = 1.125 x 0.715 x .090
W7	0.00	13,526.79	6,317.39	6,404.13	2.47 x 0.115	1	C18AA = 1.125 x 1.012 x .115
W8	5,562.65	7,177.20	66.53	2,000.43	3.26 x 0.077	1	C10AA = 1.125 x 0.700 x 0.07
W9	561.96	11,808.24	4,836.72	5,630.10	2.07 x 0.105	1	C16AA = 1.125 x 0.943 x .105
W10	4,139.60	7,177.20	1,086.20	2,000.43	2.42 x 0.077	1	C10AA = 1.125 x 0.700 x 0.07
W11	1,639.25	11,808.24	3,471.29	5,630.10	2.00 x 0.105	1	C16AA = 1.125 x 0.943 x .105
W12	2,961.49	8,420.89	2,221.12	2,408.84	2.00 x 0.090	1	C12AA = 1.125 x 0.715 x .090
W12	2,961.49	8,420.89	2,221.12	2,408.84	2.00 x 0.090	1	C12AA = 1.125 x 0.715 x .090
W11	1,639.25	11,808.24	3,471.29	5,630.10	2.00 x 0.105	1	C16AA = 1.125 x 0.943 x .105
W10	4,139.60	7,177.20	1,086.20	2,000.43	2.42 x 0.077	1	C10AA = 1.125 x 0.700 x 0.07
W9	561.96	11,808.24	4,836.72	5,630.10	2.07 x 0.105	1	C16AA = 1.125 x 0.943 x .105
W8	5,562.65	7,177.20	66.53	2,000.43	3.26 x 0.077	1	C10AA = 1.125 x 0.700 x 0.07
W7	0.00	13,526.79	6,317.39	6,404.13	2.47 x 0.115	1	C18AA = 1.125 x 1.012 x .115
W6	7,100.95	8,420.89	0.00	2,408.84	3.54 x 0.090	1	C12AA = 1.125 x 0.715 x .090
W5	0.00	16,380.48	7,913.33	7,969.79	2.65 x 0.134	1	C22AA = 1.125 x 1.086 x .134

* Continued on Next Page...

STRESS ANALYSIS - PAGE 2

NEW MILLENNIUM BUILDING SYSTEMS

Job Number:	Job Name:	Date Run:
00-0-0576	**SJI RESEARCH - SHOPORDERS**	**9/20/2022 4:31:17 PM**

Location:	Joist Description:	Mark:
BUTLER, IN	**Short Span Crimp 30K9**	**30K9BC**

Web Design, Continued...

Member	Web Tension	Allow Tension	Web Comp	Allow Comp	Weld	Qty	Material
W4	8,754.51	11,808.24	0.00	5,630.10	3.74 x 0.105	1	C16AA = 1.125 x 0.943 x .105
W3	0.00	21,613.01	9,624.51	10,000.62	2.88 x 0.150	1	C28AA = 1.125 x 1.347 x .150
W2	19,027.30	19,451.71	0.00	5,599.71	5.69 x 0.150	1	C28AA = 1.125 x 1.347 x .150
V1	0.00	7,177.20	1,539.86	2,511.00	2.00 x 0.077	1	C10AA = 1.125 x 0.700 x 0.07
V2	0.00	7,177.20	968.90	3,246.30	2.00 x 0.077	1	C10AA = 1.125 x 0.700 x 0.07

STRESS ANALYSIS - PAGE 3

NEW MILLENNIUM BUILDING SYSTEMS

Job Number:	Job Name:	Date Run:
00-0-0576	**SJI RESEARCH - SHOPORDERS**	**9/20/2022 4:31:17 PM**

Location:	Joist Description:	Mark:
BUTLER, IN	**Short Span Crimp 30K9**	**30K9BC**

TCX Design

957 TCX Left	
TCX Length	0-0
TCX Type	R
TCX Depth	2 1/2
BPL Length	0-4
Clear Bearing	0-4 1/4
BPL Material: 1714 = 1 3/4 x 1 3/4 x .143	

TCX Right	
TCX Length	0-0
TCX Type	R
TCX Depth	2 1/2
BPL Length	0-4
Clear Bearing	0-4 3/8
BPL Material: 1714 = 1 3/4 x 1 3/4 x .143	

Total Load	367.00
Reqd TL Def L/80	0.00
Live Load	225.60
Reqd LL Def L/120	0.00
Section Modulus	0.0000
Reqd SM	0.0000
Mom of Inertia	0.0000
Reqd MI	0.0000

Seat Type: Lapped

Total Load	367.00
Reqd TL Def L/80	0.00
Live Load	225.60
Reqd LL Def L/120	0.00
Section Modulus	0.0000
Reqd SM	0.0000
Mom of Inertia	0.0000
Reqd MI	0.0000

Seat Type: Lapped

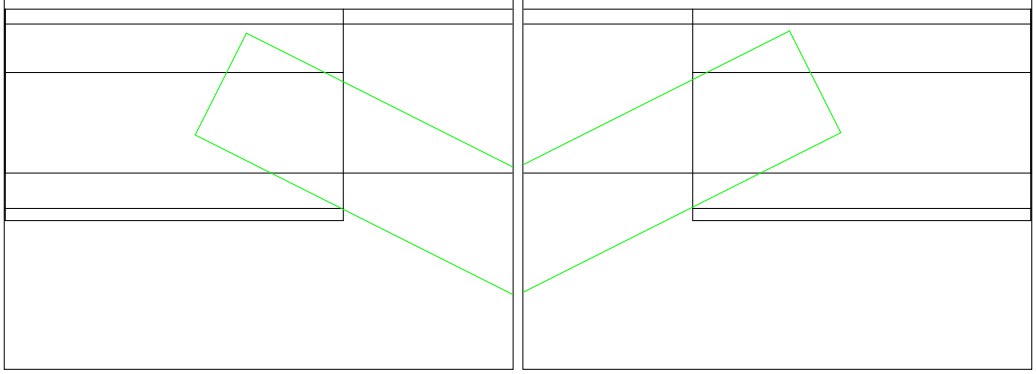

Load Combinations

Case 1a: DL
Case 1b: 1.4(DL)
Case 2a: LL
Case 2b: SL
Case 3a: 1.2(DL+CL)+1.6(TL+LL)
Case 3b: 1.2(DL+CL)+1.6(TL+SL)
Case 3c: 1.2(DL+CL)+1.6(TL+LL+FEM)
Case 3d: 1.2(DL+CL)+1.6(TL+SL+FEM)
Case 3e: DL+CL+TL+LL
Case 3f: DL+CL+TL+SL
Case 4a: 1.2(DL)+0.5(CL+LL)+1.6(WL+AX)+0.8(TL)
Case 4b: 1.2(DL)+0.5(CL+LL)+1.6(WL-AX)+0.8(TL)
Case 4c: 1.2(DL)+0.5(CL+LL)+1.6(WL+AX+IP)+0.8(TL)
Case 4d: 1.2(DL)+0.5(CL+LL)+1.6(WL-AX+IP)+0.8(TL)
Case 4e: 1.2(DL+CL)+1.6(WL+AX)+1.1(TL)+LL
Case 4f: 1.2(DL+CL)+1.6(WL-AX)+1.1(TL)+LL
Case 5a: 0.9(DL)+1.6(WL+AX)
Case 5b: 0.9(DL)+1.6(WL-AX)
Case 5c: 0.9(DL)+1.6(WL+AX+IP)
Case 5d: 0.9(DL)+1.6(WL-AX+IP)
Case 5e: 0.9(DL)+SM+AX
Case 5f: 0.9(DL)+SM-AX
Case 6a: 1.2(DL)+0.5(CL+SL)+1.6(WL+AX)+0.8(TL)
Case 6b: 1.2(DL)+0.5(CL+SL)+1.6(WL-AX)+0.8(TL)
Case 6c: 1.2(DL)+0.5(CL+SL)+1.6(WL+C+AX+IP)+0.8(TL
Case 6d: 1.2(DL)+0.5(CL+SL)+1.6(WL+C-AX+IP)+0.8(TL
Case 6e: 1.2(DL)+0.5(CL+SL)+1.6(WL+AX+IP)+0.8(TL)
Case 6f: 1.2(DL)+0.5(CL+SL)+1.6(WL-AX+IP)+0.8(TL)
Case 7a: 1.2(DL+CL)+0.8(WL+AX)+1.6(TL+LL)
Case 7b: 1.2(DL+CL)+0.8(WL-AX)+1.6(TL+LL)
Case 7c: 1.2(DL+CL)+0.8(WL+C+AX+IP)+1.6(TL+LL)
Case 7d: 1.2(DL+CL)+0.8(WL+C-AX+IP)+1.6(TL+LL)
Case 7e: 1.2(DL+CL)+0.8(WL+AX+IP)+1.6(TL+LL)
Case 7f: 1.2(DL+CL)+0.8(WL-AX+IP)+1.6(TL+LL)
Case 8a: 1.2(DL+CL)+0.8(WL+AX)+1.6(TL+SL)
Case 8b: 1.2(DL+CL)+0.8(WL-AX)+1.6(TL+SL)
Case 8c: 1.2(DL+CL)+0.8(WL+C+AX+IP)+1.6(TL+SL)
Case 8d: 1.2(DL+CL)+0.8(WL+C-AX+IP)+1.6(TL+SL)
Case 8e: 1.2(DL+CL)+0.8(WL+AX+IP)+1.6(TL+SL)
Case 8f: 1.2(DL+CL)+0.8(WL-AX+IP)+1.6(TL+SL)
Case 9a: 1.2(DL+CL)+0.7(LL)+0.9(TL)+SM+AX+FEM
Case 9b: 1.2(DL+CL)+0.7(LL)+0.9(TL)+SM-AX+FEM
Case 9c: 1.2(DL+CL)+0.7(SL)+0.9(TL)+SM+AX+FEM
Case 9d: 1.2(DL+CL)+0.7(SL)+0.9(TL)+SM-AX+FEM
Case 9e: 1.2(DL+CL)+LL+1.1(TL)+SM+AX+FEM
Case 9f: 1.2(DL+CL)+LL+1.1(TL)+SM-AX+FEM
Case 10a: 1.2(DL)+SM+AX
Case 10b: 1.2(DL)+SM-AX
Case 10c: 1.2(DL+CL)+SM+AX
Case 10d: 1.2(DL+CL)+SM-AX

STRESS ANALYSIS - PAGE 1

NEW MILLENNIUM BUILDING SYSTEMS

Job Number:	Job Name:	Date Run:
00-0-0576	SJI RESEARCH - SHOPORDERS	9/20/2022 4:34:44 PM

Location:	Joist Description:	Mark:
BUTLER, IN	Short Span Crimp 30K9	30K9W2

Geometry

Base Length:	Working Length:	Joist Depth:	Effective Depth:	BC Panel Length:	Shape:
50-0 958	49-8	30.00	28.89	10 @ 4-0	Parallel Chords

Variable	Left End	Right End
BC Panel	5-0	5-0
TC Panel	3-7	3-7
First Half	2-0	2-0
First Diag.	7-0	7-0
Depth	30.00	30.00

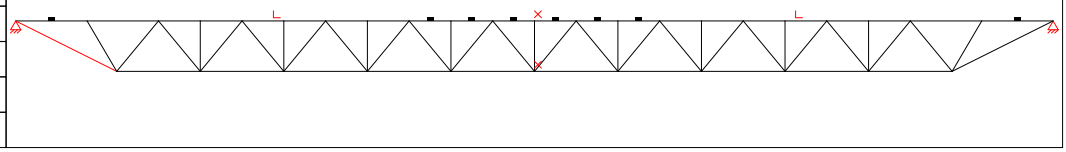

Loads, *** All loads are factored ***

Load Type	Category	Load1	Load2	Position	Direction	Loc/Begin	Sp/End	Reference
Uniform (plf)	LL	225.60	225.60	TC	+	0-0	50-0	L-BL
Uniform (plf)	DL	141.40	141.40	TC	+	0-0	50-0	L-BL

Stress Analysis Summary

Int. Panel TC:	Max Panel BC:	Reaction LE:	Reaction RE:	Minimum Shear:	Max TC Comp.:	Max BC Tension
24.00	48.00	9,113.83	9,113.83	2,278.46	47,010.39	46,705.48

Member	TC Tension	TC Compresion	BC Tension	BC Compresion	Web Tension	Web Comp.	Web Length	PP Dist.
W2	0.00	17,040.50	0.00	0.00	19,036.96	0.00	64.80	0-2
V1S	0.00	16,302.56	0.00	0.00	0.00	1,540.15	33.52	3-7
W3	0.00	16,302.56	22,311.99	0.00	0.00	9,627.00	37.56	5-0
W4	0.00	27,495.61	22,311.99	0.00	8,756.77	0.00	37.56	7-0
W5	0.00	27,495.61	32,069.38	0.00	0.00	7,915.37	37.56	9-0
W6	0.00	36,033.32	32,069.38	0.00	7,102.79	0.00	37.56	11-0
W7	0.00	36,033.32	39,387.43	0.00	0.00	6,319.03	37.56	13-0
W8	0.00	42,131.70	39,387.43	0.00	5,564.09	66.55	37.56	15-0
W9	0.00	42,131.70	44,266.13	0.00	562.10	4,837.97	37.56	17-0
W10	0.00	45,790.73	44,266.13	0.00	4,140.67	1,086.48	37.56	19-0
W11	0.00	45,790.73	46,705.48	0.00	1,639.67	3,472.19	37.56	21-0
W12	0.00	47,010.39	46,705.48	0.00	2,962.26	2,221.69	37.56	23-0
W12	0.00	47,010.39	46,705.48	0.00	2,962.26	2,221.69	37.56	25-0
W11	0.00	45,790.72	46,705.48	0.00	1,639.67	3,472.19	37.56	27-0
W10	0.00	45,790.72	44,266.13	0.00	4,140.67	1,086.48	37.56	29-0
W9	0.00	42,131.70	44,266.13	0.00	562.10	4,837.97	37.56	31-0
W8	0.00	42,131.70	39,387.43	0.00	5,564.09	66.55	37.56	33-0
W7	0.00	36,033.33	39,387.43	0.00	0.00	6,319.03	37.56	35-0
W6	0.00	36,033.33	32,069.39	0.00	7,102.79	0.00	37.56	37-0
W5	0.00	27,495.61	32,069.39	0.00	0.00	7,915.37	37.56	39-0
W4	0.00	27,495.61	22,311.99	0.00	8,756.77	0.00	37.56	41-0
W3	0.00	16,302.56	22,311.99	0.00	0.00	9,627.00	37.56	43-0
V1S	0.00	16,302.56	0.00	0.00	0.00	1,540.15	33.52	46-5
W2	0.00	17,040.50	0.00	0.00	19,036.96	0.00	64.80	45-0

Standard Verticals

Member	Position	Max Tension	Max Comp.	Length
V2	Interior	0.00	969.05	28.89

STRESS ANALYSIS - PAGE 2

NEW MILLENNIUM BUILDING SYSTEMS

Job Number:	Job Name:	Date Run:
00-0-0576	SJI RESEARCH - SHOPORDERS	9/20/2022 4:34:44 PM

Location:	Joist Description:	Mark:
BUTLER, IN	Short Span Crimp 30K9	30K9W2

Chord Properties

Chord	Area	Rx	Rz	Ryy	Y	Ix	Q	Material
TC	0.6209	0.6011	0.3559	1.2877	0.5763	0.2243	1.0000	A34A = 1.9380 x 0.176
BC	0.5181	0.5633	0.3325	1.2357	0.5373	0.1644	1.0000	A30A = 1.8125 x .157

Axial and Bending Analysis

K:	Fy:	Fb:	Mom of Inertia:	LL 360:	LL 240:	Max Bridg TC:	Max Bridg BC:
0.75	50,000.00	45,000.00	472.11	143.96	215.94	17-3 1/8	24-8 1/2

Top Chord Check	End Panel LE	First Panel LE	Interior Panel	First Panel RE	End Panel RE
Length	41.00	41.00	24.00	41.00	41.00
Bending Load	367.00	367.00	367.00	367.00	367.00
Axial Load	17,040.50	16,302.56	47,010.39	16,302.56	17,040.50
fa	13,722.42	13,128.17	37,856.65	13,128.17	13,722.42
Maximum K L/r	68.21	115.20	33.72	115.20	68.21
Fcr	35,582.52	18,914.09	46,011.85	18,914.09	35,582.52
Fa	32,024.27	17,022.68	41,410.67	17,022.68	32,024.27
F'e	61,521.02	61,521.02	319,187.78	61,521.02	61,521.02
Cm	0.9256	0.9289	0.9473	0.9289	0.9256
Panel Point Moment	5,709.10	5,709.10	1,468.00	5,709.10	5,709.10
Mid Panel Moment	3,809.25	2,137.33	734.00	2,137.33	3,809.25
Panel Point fb	17,329.66	17,329.66	4,456.03	17,329.66	17,329.66
Mid Panel fb	4,893.61	2,745.75	942.94	2,745.75	4,893.61
Fillers	1	0	6	0	1
Panel Point Stress	31,052.08	30,457.83	42,312.68	30,457.82	31,052.08
Mid Panel Stress	0.5475	0.8373	0.9345	0.8373	0.5475

Gap Between Chords:	1.1250
Min Weld Len 2X:	0.5000
Max Load Fillers TC:	50,503.57
Max Load no Fillers TC:	45,528.86
TC OAL/Ryy:	462.85
BC OAL/Ryy:	482.33
BC Stress:	1.00
BC L/Rz:	144.3609
TC Shear Stress:	17,993.16
BC Shear Stress:	21,740.25

Web Design

Member	Web Tension	Allow Tension	Web Comp	Allow Comp	Weld	Qty	Material
* W2 *	19,036.96	14,742.43	0.00	3,629.88	6.38 x 0.134	1	C22AA = 1.125 x 1.086 x .134
W3	0.00	21,613.01	9,627.00	10,004.19	2.88 x 0.150	1	C28AA = 1.125 x 1.347 x .150
W4	8,756.77	11,808.24	0.00	5,632.08	3.74 x 0.105	1	C16AA = 1.125 x 0.943 x .105
W5	0.00	16,380.48	7,915.37	7,972.61	2.65 x 0.134	1	C22AA = 1.125 x 1.086 x .134
W6	7,102.79	8,420.89	0.00	2,410.64	3.54 x 0.090	1	C12AA = 1.125 x 0.715 x .090
W7	0.00	13,526.79	6,319.03	6,406.39	2.47 x 0.115	1	C18AA = 1.125 x 1.012 x .115
W8	5,564.09	7,177.20	66.55	2,001.93	3.26 x 0.077	1	C10AA = 1.125 x 0.700 x 0.07
W9	562.10	11,808.24	4,837.97	5,632.08	2.07 x 0.105	1	C16AA = 1.125 x 0.943 x .105
W10	4,140.67	7,177.20	1,086.48	2,001.93	2.42 x 0.077	1	C10AA = 1.125 x 0.700 x 0.07
W11	1,639.67	11,808.24	3,472.19	5,632.08	2.00 x 0.105	1	C16AA = 1.125 x 0.943 x .105
W12	2,962.26	8,420.89	2,221.69	2,410.64	2.00 x 0.090	1	C12AA = 1.125 x 0.715 x .090
W12	2,962.26	8,420.89	2,221.69	2,410.64	2.00 x 0.090	1	C12AA = 1.125 x 0.715 x .090
W11	1,639.67	11,808.24	3,472.19	5,632.08	2.00 x 0.105	1	C16AA = 1.125 x 0.943 x .105
W10	4,140.67	7,177.20	1,086.48	2,001.93	2.42 x 0.077	1	C10AA = 1.125 x 0.700 x 0.07
W9	562.10	11,808.24	4,837.97	5,632.08	2.07 x 0.105	1	C16AA = 1.125 x 0.943 x .105
W8	5,564.09	7,177.20	66.55	2,001.93	3.26 x 0.077	1	C10AA = 1.125 x 0.700 x 0.07
W7	0.00	13,526.79	6,319.03	6,406.39	2.47 x 0.115	1	C18AA = 1.125 x 1.012 x .115
W6	7,102.79	8,420.89	0.00	2,410.64	3.54 x 0.090	1	C12AA = 1.125 x 0.715 x .090
W5	0.00	16,380.48	7,915.37	7,972.61	2.65 x 0.134	1	C22AA = 1.125 x 1.086 x .134

* Continued on Next Page...

STRESS ANALYSIS - PAGE 2

NEW MILLENNIUM BUILDING SYSTEMS

Job Number:	Job Name:	Date Run:
00-0-0576	**SJI RESEARCH - SHOPORDERS**	**9/20/2022 4:34:44 PM**

Location:	Joist Description:	Mark:
BUTLER, IN	**Short Span Crimp 30K9**	**30K9W2**

Web Design, Continued...

Member	Web Tension	Allow Tension	Web Comp	Allow Comp	Weld	Qty	Material
W4	8,756.77	11,808.24	0.00	5,632.08	3.74 x 0.105	1	C16AA = 1.125 x 0.943 x .105
W3	0.00	21,613.01	9,627.00	10,004.19	2.88 x 0.150	1	C28AA = 1.125 x 1.347 x .150
W2	19,036.96	19,451.71	0.00	5,600.82	5.70 x 0.150	1	C28AA = 1.125 x 1.347 x .150
V1	0.00	7,177.20	1,540.15	2,513.36	2.00 x 0.077	1	C10AA = 1.125 x 0.700 x 0.07
V2	0.00	7,177.20	969.05	3,249.33	2.00 x 0.077	1	C10AA = 1.125 x 0.700 x 0.07

STRESS ANALYSIS - PAGE 3

NEW MILLENNIUM BUILDING SYSTEMS

Job Number:	Job Name:	Date Run:
00-0-0576	SJI RESEARCH - SHOPORDERS	9/20/2022 4:34:44 PM

Location:	Joist Description:	Mark:
BUTLER, IN	Short Span Crimp 30K9	30K9W2

TCX Design

961 TCX Left	
TCX Length	0-0
TCX Type	R
TCX Depth	2 1/2
BPL Length	0-4
Clear Bearing	0-4 5/8
BPL Material: 1714 = 1 3/4 x 1 3/4 x .143	

TCX Right	
TCX Length	0-0
TCX Type	R
TCX Depth	2 1/2
BPL Length	0-4
Clear Bearing	0-4 3/8
BPL Material: 1714 = 1 3/4 x 1 3/4 x .143	

Total Load	367.00
Reqd TL Def L/80	0.00
Live Load	225.60
Reqd LL Def L/120	0.00
Section Modulus	0.0000
Reqd SM	0.0000
Mom of Inertia	0.0000
Reqd MI	0.0000

Seat Type: Lapped

Total Load	367.00
Reqd TL Def L/80	0.00
Live Load	225.60
Reqd LL Def L/120	0.00
Section Modulus	0.0000
Reqd SM	0.0000
Mom of Inertia	0.0000
Reqd MI	0.0000

Seat Type: Lapped

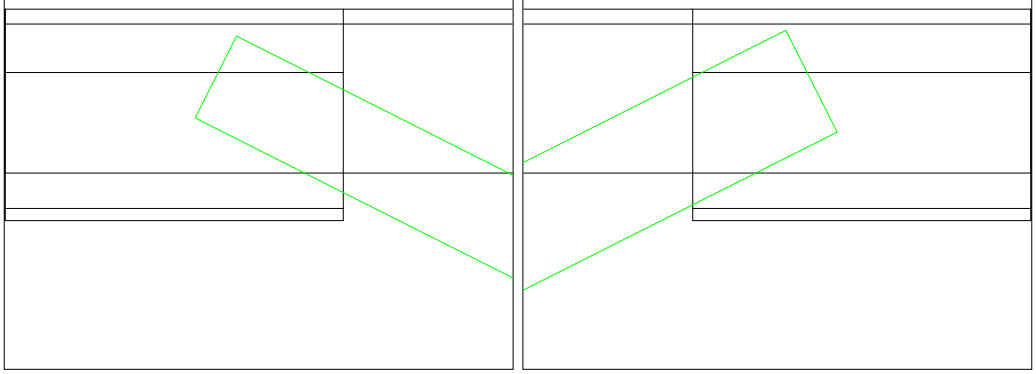

Load Combinations

Case 1a: DL
Case 1b: 1.4(DL)
Case 2a: LL
Case 2b: SL
Case 3a: 1.2(DL+CL)+1.6(TL+LL)
Case 3b: 1.2(DL+CL)+1.6(TL+SL)
Case 3c: 1.2(DL+CL)+1.6(TL+LL+FEM)
Case 3d: 1.2(DL+CL)+1.6(TL+SL+FEM)
Case 3e: DL+CL+TL+LL
Case 3f: DL+CL+TL+SL
Case 4a: 1.2(DL)+0.5(CL+LL)+1.6(WL+AX)+0.8(TL)
Case 4b: 1.2(DL)+0.5(CL+LL)+1.6(WL-AX)+0.8(TL)
Case 4c: 1.2(DL)+0.5(CL+LL)+1.6(WL+AX+IP)+0.8(TL)
Case 4d: 1.2(DL)+0.5(CL+LL)+1.6(WL-AX+IP)+0.8(TL)
Case 4e: 1.2(DL+CL)+1.6(WL+AX)+1.1(TL)+LL
Case 4f: 1.2(DL+CL)+1.6(WL-AX)+1.1(TL)+LL
Case 5a: 0.9(DL)+1.6(WL+AX)
Case 5b: 0.9(DL)+1.6(WL-AX)
Case 5c: 0.9(DL)+1.6(WL+AX+IP)
Case 5d: 0.9(DL)+1.6(WL-AX+IP)
Case 5e: 0.9(DL)+SM+AX
Case 5f: 0.9(DL)+SM-AX
Case 6a: 1.2(DL)+0.5(CL+SL)+1.6(WL+AX)+0.8(TL)
Case 6b: 1.2(DL)+0.5(CL+SL)+1.6(WL-AX)+0.8(TL)
Case 6c: 1.2(DL)+0.5(CL+SL)+1.6(WL+C+AX+IP)+0.8(TL
Case 6d: 1.2(DL)+0.5(CL+SL)+1.6(WL+C-AX+IP)+0.8(TL
Case 6e: 1.2(DL)+0.5(CL+SL)+1.6(WL+AX+IP)+0.8(TL)
Case 6f: 1.2(DL)+0.5(CL+SL)+1.6(WL-AX+IP)+0.8(TL)
Case 7a: 1.2(DL+CL)+0.8(WL+AX)+1.6(TL+LL)
Case 7b: 1.2(DL+CL)+0.8(WL-AX)+1.6(TL+LL)
Case 7c: 1.2(DL+CL)+0.8(WL+C+AX+IP)+1.6(TL+LL)
Case 7d: 1.2(DL+CL)+0.8(WL+C-AX+IP)+1.6(TL+LL)
Case 7e: 1.2(DL+CL)+0.8(WL+AX+IP)+1.6(TL+LL)
Case 7f: 1.2(DL+CL)+0.8(WL-AX+IP)+1.6(TL+LL)
Case 8a: 1.2(DL+CL)+0.8(WL+AX)+1.6(TL+SL)
Case 8b: 1.2(DL+CL)+0.8(WL-AX)+1.6(TL+SL)
Case 8c: 1.2(DL+CL)+0.8(WL+C+AX+IP)+1.6(TL+SL)
Case 8d: 1.2(DL+CL)+0.8(WL+C-AX+IP)+1.6(TL+SL)
Case 8e: 1.2(DL+CL)+0.8(WL+AX+IP)+1.6(TL+SL)
Case 8f: 1.2(DL+CL)+0.8(WL-AX+IP)+1.6(TL+SL)
Case 9a: 1.2(DL+CL)+0.7(LL)+0.9(TL)+SM+AX+FEM
Case 9b: 1.2(DL+CL)+0.7(LL)+0.9(TL)+SM-AX+FEM
Case 9c: 1.2(DL+CL)+0.7(SL)+0.9(TL)+SM+AX+FEM
Case 9d: 1.2(DL+CL)+0.7(SL)+0.9(TL)+SM-AX+FEM
Case 9e: 1.2(DL+CL)+LL+1.1(TL)+SM+AX+FEM
Case 9f: 1.2(DL+CL)+LL+1.1(TL)+SM-AX+FEM
Case 10a: 1.2(DL)+SM+AX
Case 10b: 1.2(DL)+SM-AX
Case 10c: 1.2(DL+CL)+SM+AX
Case 10d: 1.2(DL+CL)+SM-AX

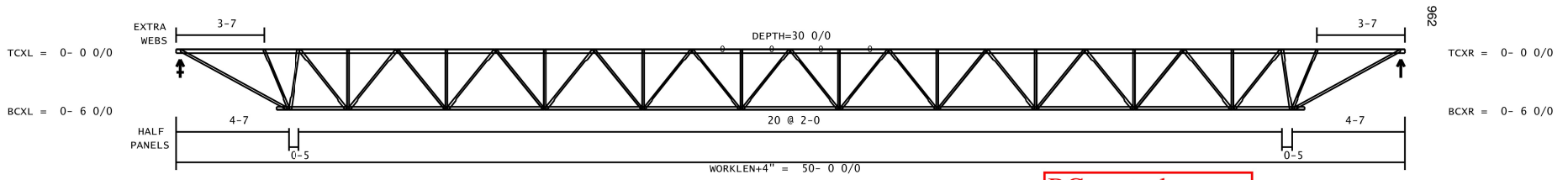

APPLIED LOADS

(D)Dead (Lr)Roof Live

**** UNFACTORED UNIFORM LOADS (PLF) ****

MAIN	START	LENGTH
DESIG: 245 UNFACTORED TOTAL / 141 DEFL L/Lr/S/R	0- 0 0/0	50- 0 0/0

LOAD COMBINATIONS
1=1.0D+1.0Lr 2=0.56D+1.0W 3=0.78D+0.75W

DEFLECTION DATA

DEFLECTION	-- MAINSPAN -- ----- Lr -----
LIMITS	(L/360) -1.66
MAXIMA	-1.67

ADDITIONAL DESIGN DATA

LOAD COMBINATIONS FROM: IBC 2018
JOIST DESIGNED WITH: ASD

JOIST IXX DEV = 458. IN^4 JOIST EFF. DEPTH= 29.00 IN

ALLOW LYY	STRESS	SLENDER
TOP CHORD=	4.5 FT	16.4 FT
BOT CHORD=		20.8 FT

TOP CHORD BRIDGING REQD= 2 ROWS HORZ., 1 ROW BOLTED-'EX'
BOT CHORD BRIDGING REQD= 3 ROWS

MAX LE END REACTION= 6084 lbs
MAX RE END REACTION= 6084 lbs

STANDARD SJI CAMBER= 1 0/0"

CHORD DATA

BC controls mat'l size reduced

TOP CHORD= 2L 2 X 2 X.163 FY= 50 KSI
BOT CHORD= 2L1-1/2X1-1/2X.170 FY= 50 KSI

TC MEM		REQ MP AXIAL	PP RATIO	MP RATIO
1	-	10497	0.67	0.83
2	-	10145	0.59	0.63
3	-	14877	0.52	0.51
4	-	14877	0.58	0.50
5	-	21358	0.67	0.71
6	-	21358	0.74	0.71
7	-	26223	0.80	0.87
8	-	26223	0.84	0.87
9	-	29467	0.88	0.97
10	-	29467	0.91	0.97
11	F -	31089	0.93	0.95
12	F -	31089	0.93	0.95
13	F -	31089	0.93	0.95
14	F -	31089	0.93	0.95
15	-	29467	0.91	0.97
16	-	29467	0.88	0.97
17	-	26223	0.84	0.87
18	-	26223	0.80	0.87
19	-	21358	0.74	0.71
20	-	21358	0.67	0.71
21	-	14877	0.58	0.50
22	-	14877	0.52	0.51
23	-	10145	0.59	0.63
24	-	10497	0.67	0.83

BC MEM		REQ MP AXIAL	PP RATIO	MP RATIO
1	+	10988	0.52	0.38
2	+	18314	0.74	0.63
3	+	23993	0.91	0.83
4	+	28048	1.02	0.97
5	+	30480	1.08	1.06
6	+	31291	1.08	1.08
7	+	30480	1.08	1.06
8	+	28048	1.02	0.97
9	+	23993	0.91	0.83
10	+	18314	0.74	0.63
11	+	10988	0.52	0.38

WEB DATA

WEB	QTY	DESCRIPTION	WELD SIZE	AXIAL	RATIO
1	1	1-1/16 ROUND	2.5 X 0.230	+ 11966.	0.50
2	1	L1-1/4x1-1/4x.109	1.5 X 0.109	- 1078.	0.35
3	1	L1-1/2x1-1/2x.170	2.0 X 0.170	- 5112.	0.63
4	1	L1-1/2x1-1/2x.123	3.5 X 0.123	+ 6416.	0.60
5	1	L 1 x 1 x.109	1.5 X 0.109	- 701.	0.40
6	1	L1-1/2x1-1/2x.170	2.3 X 0.170	- 5836.	0.79
7	1	L 1 x 1 x.109	3.3 X 0.109	+ 5275.	0.85
8	1	L 1 x 1 x.109	1.5 X 0.109	- 649.	0.37
9	1	L1-1/2x1-1/2x.123	2.6 X 0.123	- 4734.	0.88
10	1	L 1 x 1 x.109	2.6 X 0.109	+ 4212.	0.68
11	1	L 1 x 1 x.109	1.5 X 0.109	- 646.	0.37
12	1	L1-1/2x1-1/2x.123	2.0 X 0.123	- 3708.	0.69
13	1	L 1 x 1 x.109	2.0 X 0.109	+ 3224.	0.52
14	1	L 1 x 1 x.109	1.5 X 0.109	- 645.	0.37
15	1	L1-1/4x1-1/4x.109	1.7 X 0.109	- 2760.	0.92
16	1	L1-1/4x1-1/4x.109	1.5 X 0.109	- 1093.	0.36
17	1	L 1 x 1 x.109	1.5 X 0.109	- 645.	0.37
18	1	L1-1/4x1-1/4x.109	1.5 X 0.109	- 1974.	0.66
19	1	L1-1/4x1-1/4x.109	1.5 X 0.109	- 1974.	0.66
20	1	L 1 x 1 x.109	1.5 X 0.109	- 645.	0.37
21	1	L1-1/4x1-1/4x.109	1.5 X 0.109	- 1093.	0.36
22	1	L1-1/4x1-1/4x.109	1.7 X 0.109	- 2760.	0.92
23	1	L 1 x 1 x.109	1.5 X 0.109	- 645.	0.37
24	1	L 1 x 1 x.109	2.0 X 0.109	+ 3224.	0.52
25	1	L1-1/2x1-1/2x.123	2.0 X 0.123	- 3708.	0.69
26	1	L 1 x 1 x.109	1.5 X 0.109	- 646.	0.37
27	1	L 1 x 1 x.109	2.6 X 0.109	+ 4212.	0.68
28	1	L1-1/2x1-1/2x.123	2.6 X 0.123	- 4734.	0.88
29	1	L 1 x 1 x.109	1.5 X 0.109	- 649.	0.37
30	1	L 1 x 1 x.109	3.3 X 0.109	+ 5275.	0.85
31	1	L1-1/2x1-1/2x.170	2.3 X 0.170	- 5836.	0.79
32	1	L 1 x 1 x.109	1.5 X 0.109	- 701.	0.40
33	1	L1-1/2x1-1/2x.123	3.5 X 0.123	+ 6416.	0.60
34	1	L1-1/2x1-1/2x.170	2.0 X 0.170	- 5112.	0.63
35	1	L1-1/4x1-1/4x.109	1.5 X 0.109	- 1078.	0.35
36	1	1-1/16 ROUND	2.5 X 0.230	+ 11966.	0.50

WEBS FY= 50 KSI

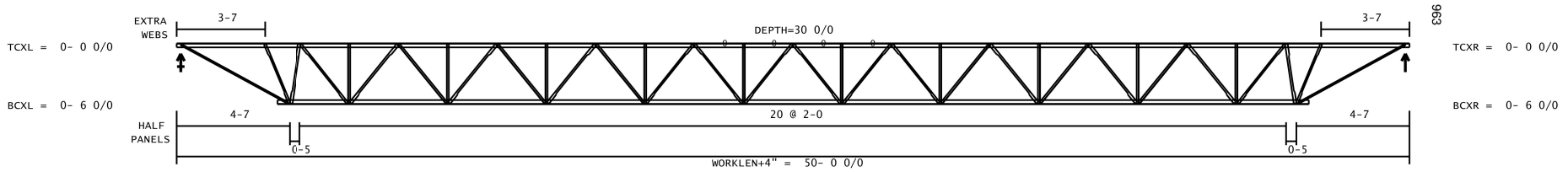

APPLIED LOADS

(D)Dead (Lr)Roof Live

**** UNFACTORED UNIFORM LOADS (PLF) ****

MAIN		START	LENGTH
DESIG: 245	UNFACTORED TOTAL / 141 DEFL L/Lr/S/R	0- 0 0/0	50- 0 0/0

LOAD COMBINATIONS
1=1.0D+1.0Lr 2=0.56D+1.0W 3=0.78D+0.75W

DEFLECTION DATA

DEFLECTION	-- MAINSPAN -- ----- Lr -----
LIMITS	(L/360) -1.66
MAXIMA	-1.60

ADDITIONAL DESIGN DATA

LOAD COMBINATIONS FROM: IBC 2018
JOIST DESIGNED WITH: ASD

JOIST IXX DEV = 479. IN^4 JOIST EFF. DEPTH= 28.89 IN

ALLOW LYY	STRESS	SLENDER
TOP CHORD=	4.4 FT	16.4 FT
BOT CHORD=		24.4 FT

TOP CHORD BRIDGING REQD= 2 ROWS HORZ., 1 ROW BOLTED-'EX'
BOT CHORD BRIDGING REQD= 3 ROWS

MAX LE END REACTION= 6084 lbs
MAX RE END REACTION= 6084 lbs

STANDARD SJI CAMBER= 1 0/0"

CHORD DATA

TOP CHORD= 2L 2 X 2 X.163 FY= 50 KSI
BOT CHORD= 2L 2 X 2 X.137 FY= 50 KSI

W2 controls mat'l size reduced

TC MEM		REQ AXIAL	PP RATIO	MP RATIO		MP AXIAL	MP RATIO
1	-	10539	0.67	0.83	1	+ 11031	0.35
2	-	10185	0.59	0.63	2	+ 18386	0.58
3	-	14935	0.52	0.51	3	+ 24087	0.76
4	-	14935	0.58	0.50	4	+ 28158	0.89
5	-	21441	0.67	0.71	5	+ 30600	0.96
6	-	21441	0.74	0.71	6	+ 31414	0.99
7	-	26326	0.80	0.87	7	+ 30600	0.96
8	-	26326	0.85	0.87	8	+ 28158	0.89
9	-	29582	0.89	0.98	9	+ 24087	0.76
10	-	29582	0.91	0.98	10	+ 18386	0.58
11	F -	31211	0.93	0.95	11	+ 11031	0.35
12	F -	31211	0.93	0.95			
13	F -	31211	0.93	0.95			
14	F -	31211	0.93	0.95			
15	-	29582	0.91	0.98			
16	-	29582	0.89	0.98			
17	-	26326	0.85	0.87			
18	-	26326	0.80	0.87			
19	-	21441	0.74	0.71			
20	-	21441	0.67	0.71			
21	-	14935	0.58	0.50			
22	-	14935	0.52	0.51			
23	-	10185	0.59	0.63			
24	-	10539	0.67	0.83			

WEB DATA

WEB	QTY	DESCRIPTION	WELD SIZE	AXIAL	RATIO
1	1	3/4 ROUND	2.9 X 0.200	+ 12003.	1.01
2	1	L1 1/4x1 1/4x.109	1.5 X 0.109	1079.	0.35
3	1	L1-1/2x1-1/2x.170	2.0 X 0.170	- 5113.	0.63
4	1	L1-1/4x1-1/4x.109	4.0 X 0.109	+ 6427.	0.82
5	1	L 1 x 1 x.109	1.5 X 0.109	- 702.	0.40
6	1	L1-1/2x1-1/2x.170	2.3 X 0.170	- 5846.	0.79
7	1	L 1 x 1 x.109	3.3 X 0.109	+ 5284.	0.85
8	1	L 1 x 1 x.109	1.5 X 0.109	- 650.	0.37
9	1	L1-1/2x1-1/2x.123	2.6 X 0.123	- 4741.	0.88
10	1	L 1 x 1 x.109	2.6 X 0.109	+ 4218.	0.68
11	1	L 1 x 1 x.109	1.5 X 0.109	- 646.	0.37
12	1	L1-1/2x1-1/2x.123	2.0 X 0.123	- 3714.	0.69
13	1	L 1 x 1 x.109	2.0 X 0.109	+ 3230.	0.52
14	1	L 1 x 1 x.109	1.5 X 0.109	- 646.	0.37
15	1	L1-1/4x1-1/4x.109	1.7 X 0.109	- 2764.	0.92
16	1	L1-1/4x1-1/4x.109	1.5 X 0.109	- 1095.	0.36
17	1	L 1 x 1 x.109	1.5 X 0.109	- 646.	0.37
18	1	L1-1/4x1-1/4x.109	1.5 X 0.109	- 1977.	0.66
19	1	L1-1/4x1-1/4x.109	1.5 X 0.109	- 1977.	0.66
20	1	L 1 x 1 x.109	1.5 X 0.109	- 646.	0.37
21	1	L1-1/4x1-1/4x.109	1.5 X 0.109	- 1095.	0.36
22	1	L1-1/4x1-1/4x.109	1.7 X 0.109	- 2764.	0.92
23	1	L 1 x 1 x.109	1.5 X 0.109	- 646.	0.37
24	1	L 1 x 1 x.109	2.0 X 0.109	+ 3230.	0.52
25	1	L1-1/2x1-1/2x.123	2.0 X 0.123	- 3714.	0.69
26	1	L 1 x 1 x.109	1.5 X 0.109	- 646.	0.37
27	1	L 1 x 1 x.109	2.6 X 0.109	+ 4218.	0.68
28	1	L1-1/2x1-1/2x.123	2.6 X 0.123	- 4741.	0.88
29	1	L 1 x 1 x.109	1.5 X 0.109	- 650.	0.37
30	1	L 1 x 1 x.109	3.3 X 0.109	+ 5284.	0.85
31	1	L1-1/2x1-1/2x.170	2.3 X 0.170	- 5846.	0.79
32	1	L 1 x 1 x.109	1.5 X 0.109	- 702.	0.40
33	1	L1-1/4x1-1/4x.109	4.0 X 0.109	+ 6427.	0.82
34	1	L1-1/2x1-1/2x.170	2.0 X 0.170	- 5113.	0.63
35	1	L1-1/4x1-1/4x.109	1.5 X 0.109	- 1079.	0.35
36	1	3/4 ROUND	2.9 X 0.200	+ 12003.	1.01

WEBS FY= 50 KSI

STRESS ANALYSIS - PAGE 1

NEW MILLENNIUM
A Steel Dynamics Company

Job Number:	Job Name:	Date Run:
00-0-0511	PHIL - SHOPORDERS	4/17/2024 10:00:20 AM

Location:	Joist Description:	Mark:
,	Short Span Crimp 30K162.8/162.8	CKUBI2

Geometry

Base Length:	Working Length:	Joist Depth:	Effective Depth:	BC Panel Length:	Shape:	TC Slope:
50-0	49-8	30.00	28.89	10 @ 4-0	Parallel Chords	0.0000

Variable	Left End	Right End
BC Panel	5-0	5-0
TC Panel	3-7	3-7
First Half	2-0	2-0
First Diag.	7-0	7-0
Depth	30.00	30.00
Trib Width	0-0	0-0

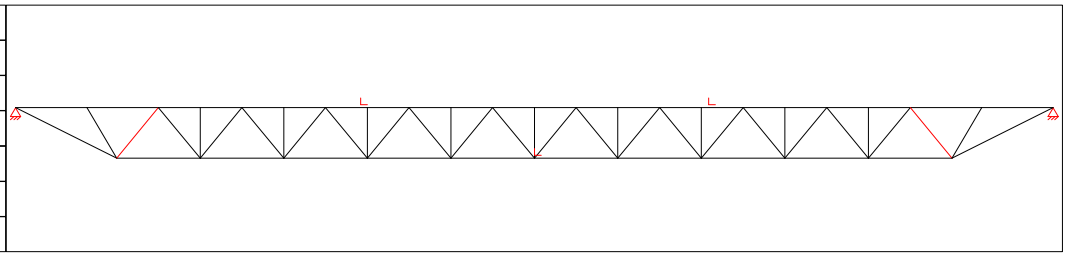

Loads

Load Type	Category	Load1	Load2	Position	Direction	Loc/Begin	Sp/End	Reference
Uniform (plf)	LL	162.80	162.80	TC	+	0-0	50-0	L-BL

Stress Analysis Summary

Int. Panel TC:	Max Panel BC:	Reaction LE:	Reaction RE:	Minimum Shear:	Max TC Comp.:	Max BC Tension
24.00	48.00	4,042.87	4,042.87	1,010.72	20,853.66	20,718.40

Member	TC Tension	TC Compresion	BC Tension	BC Compresion	Web Tension	Web Comp.	Web Length	PP Dist.
W2	0.00	7,559.11	0.00	0.00	8,444.73	0.00	64.80	0-2
V1S	0.00	7,231.76	0.00	0.00	0.00	683.21	33.52	3-7
W3	0.00	7,231.76	9,897.53	0.00	0.00	4,270.50	37.56	5-0
W4	0.00	12,196.96	9,897.53	0.00	3,884.48	0.00	37.56	7-0
W5	0.00	12,196.96	14,225.87	0.00	0.00	3,511.23	37.56	9-0
W6	0.00	15,984.27	14,225.87	0.00	3,150.77	0.00	37.56	11-0
W7	0.00	15,984.27	17,472.13	0.00	0.00	2,803.10	37.56	13-0
W8	0.00	18,689.49	17,472.13	0.00	2,468.21	29.52	37.56	15-0
W9	0.00	18,689.49	19,636.31	0.00	249.35	2,146.11	37.56	17-0
W10	0.00	20,312.61	19,636.31	0.00	1,836.79	481.96	37.56	19-0
W11	0.00	20,312.61	20,718.40	0.00	727.35	1,540.25	37.56	21-0
W12	0.00	20,853.66	20,718.40	0.00	1,314.05	985.54	37.56	23-0
W12	0.00	20,853.66	20,718.40	0.00	1,314.05	985.54	37.56	25-0
W11	0.00	20,312.61	20,718.40	0.00	727.35	1,540.25	37.56	27-0
W10	0.00	20,312.61	19,636.31	0.00	1,836.79	481.96	37.56	29-0
W9	0.00	18,689.48	19,636.31	0.00	249.35	2,146.11	37.56	31-0
W8	0.00	18,689.48	17,472.14	0.00	2,468.21	29.52	37.56	33-0
W7	0.00	15,984.27	17,472.14	0.00	0.00	2,803.10	37.56	35-0
W6	0.00	15,984.27	14,225.88	0.00	3,150.77	0.00	37.56	37-0
W5	0.00	12,196.96	14,225.88	0.00	0.00	3,511.23	37.56	39-0
W4	0.00	12,196.96	9,897.53	0.00	3,884.48	0.00	37.56	41-0
W3	0.00	7,231.76	9,897.53	0.00	0.00	4,270.50	37.56	43-0
V1S	0.00	7,231.76	0.00	0.00	0.00	683.21	33.52	46-5
W2	0.00	7,559.11	0.00	0.00	8,444.73	0.00	64.80	45-0

Standard Verticals

Member	Position	Max Tension	Max Comp.	Length
V2	Interior	0.00	429.87	28.89

STRESS ANALYSIS - PAGE 2

NEW MILLENNIUM
A Steel Dynamics Company

Job Number:	Job Name:	Date Run:
00-0-0511	PHIL - SHOPORDERS	4/17/2024 10:00:20 AM

Location:	Joist Description:	Mark:
,	Short Span Crimp 30K162.8/162.8	CKUBI2

Chord Properties

Chord	Area	Rx	Rz	Ryy	Y	Ix	Q	Material
TC	0.6209	0.6011	0.3559	1.2877	0.5763	0.2243	1.0000	A34A = 1.938 x 1.938 x 0.176
BC	0.5181	0.5633	0.3325	1.2357	0.5373	0.1644	1.0000	A30A = 1.813 x 1.813 x 0.157

Axial and Bending Analysis

K:	Fy:	Fb:	Mom of Inertia:	LL 360:	LL 240:	Max Bridg TC:	Max Bridg BC:
0.75	50,000.00	30,000.00	472.11	143.96	215.94	17-3 1/8	24-8 1/2

Top Chord Check	End Panel LE	First Panel LE	Interior Panel	First Panel RE	End Panel RE
Length	41.00	41.00	24.00	41.00	41.00
Bending Load	162.80	162.80	162.80	162.80	162.80
Axial Load	7,559.11	7,231.76	20,853.66	7,231.76	7,559.11
fa	6,087.22	5,823.61	16,793.09	5,823.61	6,087.22
Maximum K L/r	115.20	115.20	50.58	115.20	115.20
Fcr	18,914.09	18,914.09	41,470.98	18,914.09	18,914.09
Fa	11,348.46	11,348.46	24,882.59	11,348.46	11,348.46
F'e	61,521.02	61,521.02	319,187.78	61,521.02	61,521.02
Cm	0.9505	0.9527	0.9647	0.9527	0.9505
Panel Point Moment	2,532.54	2,532.54	651.20	2,532.54	2,532.54
Mid Panel Moment	1,689.77	948.11	325.60	948.11	1,689.77
Panel Point fb	7,687.38	7,687.38	1,976.68	7,687.38	7,687.38
Mid Panel fb	2,170.79	1,218.00	418.29	1,218.00	2,170.79
Fillers	0	0	0	0	0
Panel Point Stress	13,774.60	13,510.99	18,769.77	13,510.99	13,774.60
Mid Panel Stress	0.6096	0.5540	0.6880	0.5540	0.6096

Gap Between Chords: **1.1250**
Min Weld Len 2X: **0.5000**
Max Load Fillers TC: **33,946.65**
Max Load no Fillers TC: **30,599.07**
TC OAL/Ryy: **462.85**
BC OAL/Ryy: **482.33**
BC Stress: **0.67**
BC L/Rz: **144.3609**
TC Shear Stress: **8,744.15**
BC Shear Stress: **10,675.04**

Web Design

Member	Web Tension	Allow Tension	Web Comp	Allow Comp	Weld	Qty	Material
W2	8,444.73	12,967.80	0.00	3,733.26	3.79 x 0.150	1	C28AA = 1.125 x 1.347 x 0.150
* W3 *	0.00	9,017.86	4,270.50	4,270.22	2.50 x 0.115	1	C18AA = 1.125 x 1.012 x 0.115
W4	3,884.48	7,872.16	0.00	3,754.09	2.52 x 0.105	1	C16AA = 1.125 x 0.943 x 0.105
W5	0.00	10,920.32	3,511.23	5,314.19	2.00 x 0.134	1	C22AA = 1.125 x 1.086 x 0.134
W6	3,150.77	5,613.92	0.00	1,606.83	2.36 x 0.090	1	C12AA = 1.125 x 0.716 x 0.090
W7	0.00	9,017.86	2,803.10	4,270.22	2.00 x 0.115	1	C18AA = 1.125 x 1.012 x 0.115
W8	2,468.21	4,784.80	29.52	1,334.40	2.17 x 0.077	1	C10AA = 1.125 x 0.699 x 0.077
W9	249.35	7,872.16	2,146.11	3,754.09	2.00 x 0.105	1	C16AA = 1.125 x 0.943 x 0.105
W10	1,836.79	4,784.80	481.96	1,334.40	2.10 x 0.077	1	C10AA = 1.125 x 0.699 x 0.077
W11	727.35	7,872.16	1,540.25	3,754.09	2.00 x 0.105	1	C16AA = 1.125 x 0.943 x 0.105
W12	1,314.05	5,613.92	985.54	1,606.83	2.00 x 0.090	1	C12AA = 1.125 x 0.716 x 0.090
W12	1,314.05	5,613.92	985.54	1,606.83	2.00 x 0.090	1	C12AA = 1.125 x 0.716 x 0.090
W11	727.35	7,872.16	1,540.25	3,754.09	2.00 x 0.105	1	C16AA = 1.125 x 0.943 x 0.105
W10	1,836.79	4,784.80	481.96	1,334.40	2.10 x 0.077	1	C10AA = 1.125 x 0.699 x 0.077
W9	249.35	7,872.16	2,146.11	3,754.09	2.00 x 0.105	1	C16AA = 1.125 x 0.943 x 0.105
W8	2,468.21	4,784.80	29.52	1,334.40	2.17 x 0.077	1	C10AA = 1.125 x 0.699 x 0.077
W7	0.00	9,017.86	2,803.10	4,270.22	2.00 x 0.115	1	C18AA = 1.125 x 1.012 x 0.115
W6	3,150.77	5,613.92	0.00	1,606.83	2.36 x 0.090	1	C12AA = 1.125 x 0.716 x 0.090
W5	0.00	10,920.32	3,511.23	5,314.19	2.00 x 0.134	1	C22AA = 1.125 x 1.086 x 0.134

* Continued on Next Page...

STRESS ANALYSIS - PAGE 2

NEW MILLENNIUM
A Steel Dynamics Company

Job Number:	Job Name:	Date Run:
00-0-0511	**PHIL - SHOPORDERS**	**4/17/2024 10:00:20 AM**

Location:	Joist Description:	Mark:
,	**Short Span Crimp 30K162.8/162.8**	**CKUBI2**

Web Design, Continued...

Member	Web Tension	Allow Tension	Web Comp	Allow Comp	Weld	Qty	Material
W4	3,884.48	7,872.16	0.00	3,754.09	2.52 x 0.105	1	C16AA = 1.125 x 0.943 x 0.105
* W3 *	0.00	9,017.86	4,270.50	4,270.22	2.50 x 0.115	1	C18AA = 1.125 x 1.012 x 0.115
W2	8,444.73	12,967.80	0.00	3,733.26	3.79 x 0.150	1	C28AA = 1.125 x 1.347 x 0.150
V1	0.00	4,784.80	683.21	1,675.30	2.00 x 0.077	1	C10AA = 1.125 x 0.699 x 0.077
V2	0.00	4,784.80	429.87	2,165.86	2.00 x 0.077	1	C10AA = 1.125 x 0.699 x 0.077

STRESS ANALYSIS - PAGE 3

NEW MILLENNIUM
A Steel Dynamics Company

Job Number:	Job Name:	Date Run:
00-0-0511	PHIL - SHOPORDERS	4/17/2024 10:00:20 AM

Location:	Joist Description:	Mark:
,	Short Span Crimp 30K162.8/162.8	CKUBI2

TCX Design

967 TCX Left	
TCX Length	0-0
TCX Type	R
TCX Depth	2 1/2
BPL Length	0-4
Clear Bearing	0-4 3/8
BPL Material: 1714 = 1 3/4 x 1 3/4 x 0.143	

TCX Right	
TCX Length	0-0
TCX Type	R
TCX Depth	2 1/2
BPL Length	0-4
Clear Bearing	0-4 3/8
BPL Material: 1714 = 1 3/4 x 1 3/4 x 0.143	

Total Load	162.80
Reqd TL Def L/80	0.00
Live Load	162.80
Reqd LL Def L/120	0.00
Section Modulus	0.0000
Reqd SM	0.0000
Mom of Inertia	0.0000
Reqd MI	0.0000

Seat Type: Lapped

Total Load	162.80
Reqd TL Def L/80	0.00
Live Load	162.80
Reqd LL Def L/120	0.00
Section Modulus	0.0000
Reqd SM	0.0000
Mom of Inertia	0.0000
Reqd MI	0.0000

Seat Type: Lapped

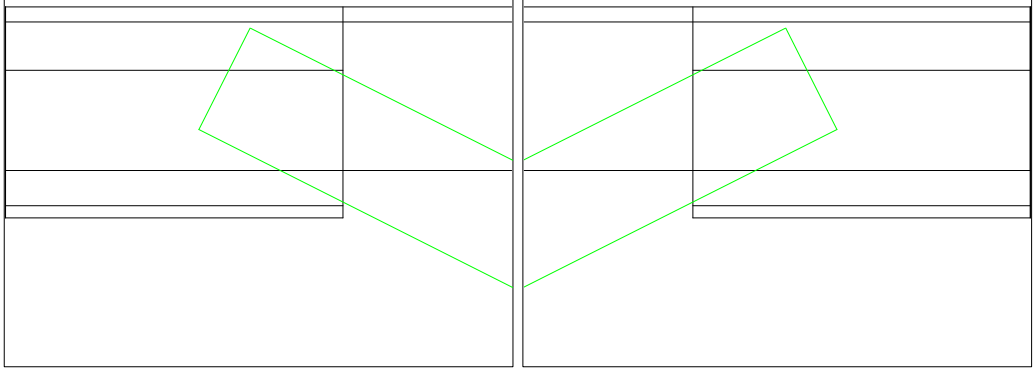

Load Combinations

Case 1: DL
Case 2a: LL
Case 2b: SL
Case 3a: DL+CL+TL+LL
Case 3b: DL+CL+TL+SL
Case 3c: DL+CL+TL+LL+FEM
Case 3d: DL+CL+TL+SL+FEM
Case 3e: DL+CL+TL+LL
Case 3f: DL+CL+TL+SL
Case 4a: DL+WL+AX
Case 4b: DL+WL-AX
Case 4c: DL+WL+AX+IP
Case 4d: DL+WL-AX+IP
Case 4e: DL+SM+AX
Case 4f: DL+SM-AX
Case 5a: 0.6(DL)+WL+AX
Case 5b: 0.6(DL)+WL-AX
Case 5c: 0.6(DL)+WL+AX+IP
Case 5d: 0.6(DL)+WL-AX+IP
Case 5e: 0.6(DL)+WL+AX+SM
Case 5f: 0.6(DL)+WL-AX+SM
Case 6a: DL+CL+0.85(TL)+WL+AX
Case 6b: DL+CL+0.85(TL)+WL-AX
Case 6c: DL+CL+0.85(TL)+WL+C+AX+IP
Case 6d: DL+CL+0.85(TL)+WL+C-AX+IP
Case 6e: DL+CL+0.85(TL)+WL+AX+IP
Case 6f: DL+CL+0.85(TL)+WL-AX+IP
Case 6g: DL+CL+0.85(TL)+SM+AX
Case 6h: DL+CL+0.85(TL)+SM-AX
Case 7a: DL+CL+0.85(TL)+0.75(WL+AX+LL)
Case 7b: DL+CL+0.85(TL)+0.75(WL-AX+LL)
Case 7c: DL+CL+0.85(TL)+0.75(WL+C+AX+LL+IP)
Case 7d: DL+CL+0.85(TL)+0.75(WL+C-AX+LL+IP)
Case 7e: DL+CL+0.85(TL)+0.75(WL+AX+LL+IP)
Case 7f: DL+CL+0.85(TL)+0.75(WL-AX+LL+IP)
Case 7g: DL+CL+0.85(TL)+0.75(SM+AX+LL)
Case 7h: DL+CL+0.85(TL)+0.75(SM-AX+LL)
Case 8a: DL+CL+0.85(TL)+0.75(WL+AX+SL)
Case 8b: DL+CL+0.85(TL)+0.75(WL-AX+SL)
Case 8c: DL+CL+0.85(TL)+0.75(WL+C+AX+SL+IP)
Case 8d: DL+CL+0.85(TL)+0.75(WL+C-AX+SL+IP)
Case 8e: DL+CL+0.85(TL)+0.75(WL+AX+SL+IP)
Case 8f: DL+CL+0.85(TL)+0.75(WL-AX+SL+IP)
Case 8g: DL+CL+0.85(TL)+0.75(WL+AX+SL+SM)
Case 8h: DL+CL+0.85(TL)+0.75(WL-AX+SL+SM)
Case 9a: 1.2(DL)+0.5(LL)+0.8(TL)+SM+AX+FEM
Case 9b: 1.2(DL)+0.5(LL)+0.8(TL)+SM-AX+FEM

STRESS ANALYSIS - PAGE 1

NEW MILLENNIUM
A Steel Dynamics Company

Job Number:	Job Name:	Date Run:
00-0-0511	PHIL - SHOPORDERS	5/13/2024 4:53:19 PM

Location:	Joist Description:	Mark:
,	Short Span Crimp 30K152.5/152.5	HKUBI

Geometry

Base Length:	Working Length:	Joist Depth:	Effective Depth:	BC Panel Length:	Shape:	TC Slope:
50-0 (968)	49-8	30.00	28.88	11 @ 4-0	Parallel Chords	0.0000

Variable	Left End	Right End
BC Panel	4-7	4-7
TC Panel	3-7	3-7
First Half	0-5	0-5
First Diag.	5-0	5-0
Depth	30.00	30.00
Trib Width	0-0	0-0

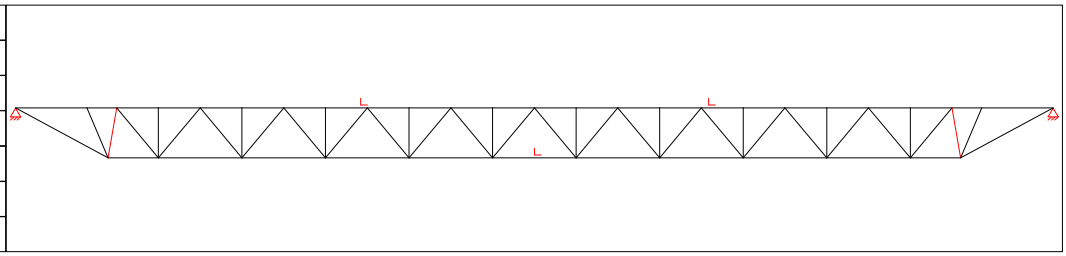

Loads

Load Type	Category	Load1	Load2	Position	Direction	Loc/Begin	Sp/End	Reference
Uniform (plf)	LL	152.50	152.50	TC	+	0-0	50-0	L-BL

Stress Analysis Summary

Int. Panel TC:	Max Panel BC:	Reaction LE:	Reaction RE:	Minimum Shear:	Max TC Comp.:	Max BC Tension
24.00	48.00	3,787.08	3,787.08	946.77	19,412.29	19,539.03

Member	TC Tension	TC Compresion	BC Tension	BC Compresion	Web Tension	Web Comp.	Web Length	PP Dist.
W2	0.00	6,472.01	0.00	0.00	7,370.45	0.00	60.36	0-2
V1S	0.00	6,318.87	0.00	0.00	0.00	431.45	31.27	3-7
W3	0.00	6,318.87	6,865.63	0.00	0.00	3,205.00	29.31	4-7
W4	0.00	9,273.58	6,865.63	0.00	4,000.71	0.00	37.55	5-0
W5	0.00	9,273.58	11,428.06	0.00	0.00	3,639.07	37.55	7-0
W6	0.00	13,329.07	11,428.06	0.00	3,289.41	0.00	37.55	9-0
W7	0.00	13,329.07	14,976.60	0.00	0.00	2,951.72	37.55	11-0
W8	0.00	16,370.68	14,976.60	0.00	2,626.01	0.00	37.55	13-0
W9	0.00	16,370.68	17,511.29	0.00	27.66	2,312.28	37.55	15-0
W10	0.00	18,398.42	17,511.29	0.00	2,010.53	233.59	37.55	17-0
W11	0.00	18,398.42	19,032.09	0.00	451.51	1,720.75	37.55	19-0
W12	0.00	19,412.29	19,032.09	0.00	1,442.95	681.40	37.55	21-0
W13	0.00	19,412.29	19,539.03	0.00	923.27	1,231.03	37.55	23-0
W13	0.00	19,412.29	19,539.03	0.00	923.27	1,231.03	37.55	25-0
W12	0.00	19,412.29	19,032.09	0.00	1,442.95	681.40	37.55	27-0
W11	0.00	18,398.42	19,032.09	0.00	451.51	1,720.75	37.55	29-0
W10	0.00	18,398.42	17,511.28	0.00	2,010.53	233.59	37.55	31-0
W9	0.00	16,370.68	17,511.28	0.00	27.66	2,312.28	37.55	33-0
W8	0.00	16,370.68	14,976.61	0.00	2,626.01	0.00	37.55	35-0
W7	0.00	13,329.06	14,976.61	0.00	0.00	2,951.72	37.55	37-0
W6	0.00	13,329.06	11,428.06	0.00	3,289.41	0.00	37.55	39-0
W5	0.00	9,273.58	11,428.06	0.00	0.00	3,639.07	37.55	41-0
W4	0.00	9,273.58	6,865.63	0.00	4,000.71	0.00	37.55	43-0
W3	0.00	6,318.88	6,865.63	0.00	0.00	3,205.00	29.31	45-0
V1S	0.00	6,318.88	0.00	0.00	0.00	431.45	31.27	46-5
W2	0.00	6,472.01	0.00	0.00	7,370.45	0.00	60.36	45-5

Standard Verticals

Member	Position	Max Tension	Max Comp.	Length
V2	Interior	0.00	402.06	28.88

STRESS ANALYSIS - PAGE 2

NEW MILLENNIUM
A Steel Dynamics Company

Job Number:	Job Name:	Date Run:
00-0-0511	PHIL - SHOPORDERS	5/13/2024 4:53:19 PM

Location:	Joist Description:	Mark:
,	Short Span Crimp 30K152.5/152.5	HKUBI

Chord Properties

Chord	Area	Rx	Rz	Ryy	Y	Ix	Q	Material
TC	0.6254	0.6208	0.3951	1.2830	0.5603	0.2410	0.9528	2016 = 2 x 2 x 0.163
BC	0.6254	0.6208	0.3951	1.2830	0.5603	0.2410	0.9528	2016 = 2 x 2 x 0.163

Axial and Bending Analysis

K:	Fy:	Fb:	Mom of Inertia:	LL 360:	LL 240:	Max Bridg TC:	Max Bridg BC:
0.75	50,000.00	30,000.00	522.56	159.35	239.02	17-2 3/8	25-7 7/8

Top Chord Check	End Panel LE	First Panel LE	Interior Panel	First Panel RE	End Panel RE
Length	41.00	17.00	24.00	17.00	41.00
Bending Load	152.50	152.50	152.50	152.50	152.50
Axial Load	6,472.01	6,318.87	19,412.29	6,318.88	6,472.01
fa	5,174.30	5,051.87	15,519.90	5,051.87	5,174.30
Maximum K L/r	103.77	43.03	45.56	43.03	103.77
Fcr	22,499.07	41,875.14	41,226.14	41,875.14	22,499.07
Fa	13,499.44	25,125.08	24,735.69	25,125.08	13,499.44
F'e	65,619.59	381,683.47	340,452.22	381,683.47	65,619.59
Cm	0.9606	0.9934	0.9695	0.9934	0.9606
Panel Point Moment	2,009.45	2,009.45	610.00	2,009.45	2,009.45
Mid Panel Moment	1,703.82	1,434.01	305.00	1,434.01	1,703.82
Panel Point fb	6,002.08	6,002.07	1,822.03	6,002.07	6,002.08
Mid Panel fb	1,980.60	4,283.28	354.55	4,283.28	1,980.60
Fillers	0	0	0	0	0
Panel Point Stress	11,176.37	11,053.94	17,341.93	11,053.94	11,176.38
Mid Panel Stress	0.4514	0.3364	0.6390	0.3364	0.4514

Gap Between Chords: **1.1250**
Min Weld Len 2X: **0.5000**
Max Load Fillers TC: **33,255.84**
Max Load no Fillers TC: **30,690.51**
TC OAL/Ryy: **464.54**
BC OAL/Ryy: **464.54**
BC Stress: **0.52**
BC L/Rz: **121.4882**
TC Shear Stress: **8,204.01**
BC Shear Stress: **8,054.47**

Web Design

Member	Web Tension	Allow Tension	Web Comp	Allow Comp	Weld	Qty	Material
W2	7,370.45	26,972.16	0.00	5,102.58	2.62 x 0.245	1	R112 = round 1 1/8
* W3 *	0.00	7,857.08	3,205.00	3,203.90	2.00 x 0.109	1	1210 = 1 1/4 x 1 1/4 x 0.109
W4	4,000.71	7,857.08	0.00	2,593.86	2.47 x 0.109	1	1210 = 1 1/4 x 1 1/4 x 0.109
W5	0.00	13,296.14	3,639.07	5,819.16	2.00 x 0.155	1	1515 = 1 1/2 x 1 1/2 x 0.155
W6	3,289.41	7,857.08	0.00	2,593.86	2.43 x 0.109	1	1210 = 1 1/4 x 1 1/4 x 0.109
W7	0.00	10,670.07	2,951.72	4,097.33	2.00 x 0.123	1	1512 = 1 1/2 x 1 1/2 x 0.123
W8	2,626.01	7,857.08	0.00	2,593.86	2.43 x 0.109	1	1210 = 1 1/4 x 1 1/4 x 0.109
W9	27.66	10,670.07	2,312.28	4,097.33	2.00 x 0.123	1	1512 = 1 1/2 x 1 1/2 x 0.123
W10	2,010.53	7,857.08	233.59	2,593.86	2.43 x 0.109	1	1210 = 1 1/4 x 1 1/4 x 0.109
W11	451.51	7,857.08	1,720.75	2,593.86	2.00 x 0.109	1	1210 = 1 1/4 x 1 1/4 x 0.109
W12	1,442.95	7,857.08	681.40	2,593.86	2.00 x 0.109	1	1210 = 1 1/4 x 1 1/4 x 0.109
W13	923.27	7,857.08	1,231.03	2,593.86	2.00 x 0.109	1	1210 = 1 1/4 x 1 1/4 x 0.109
W13	923.27	7,857.08	1,231.03	2,593.86	2.00 x 0.109	1	1210 = 1 1/4 x 1 1/4 x 0.109
W12	1,442.95	7,857.08	681.40	2,593.86	2.00 x 0.109	1	1210 = 1 1/4 x 1 1/4 x 0.109
W11	451.51	7,857.08	1,720.75	2,593.86	2.00 x 0.109	1	1210 = 1 1/4 x 1 1/4 x 0.109
W10	2,010.53	7,857.08	233.59	2,593.86	2.43 x 0.109	1	1210 = 1 1/4 x 1 1/4 x 0.109
W9	27.66	10,670.07	2,312.28	4,097.33	2.00 x 0.123	1	1512 = 1 1/2 x 1 1/2 x 0.123
W8	2,626.01	7,857.08	0.00	2,593.86	2.43 x 0.109	1	1210 = 1 1/4 x 1 1/4 x 0.109
W7	0.00	10,670.07	2,951.72	4,097.33	2.00 x 0.123	1	1512 = 1 1/2 x 1 1/2 x 0.123

* Continued on Next Page...

STRESS ANALYSIS - PAGE 2

NEW MILLENNIUM
A Steel Dynamics Company

Job Number:	Job Name:	Date Run:
00-0-0511	**PHIL - SHOPORDERS**	**5/13/2024 4:53:19 PM**

Location:	Joist Description:	Mark:
,	**Short Span Crimp 30K152.5/152.5**	**HKUBI**

Web Design, Continued...

Member	Web Tension	Allow Tension	Web Comp	Allow Comp	Weld	Qty	Material
W6	3,289.41	7,857.08	0.00	2,593.86	2.43 x 0.109	1	1210 = 1 1/4 x 1 1/4 x 0.109
W5	0.00	13,296.14	3,639.07	5,819.16	2.00 x 0.155	1	1515 = 1 1/2 x 1 1/2 x 0.155
W4	4,000.71	7,857.08	0.00	2,593.86	2.47 x 0.109	1	1210 = 1 1/4 x 1 1/4 x 0.109
* W3 *	0.00	7,857.08	3,205.00	3,203.90	2.00 x 0.109	1	1210 = 1 1/4 x 1 1/4 x 0.109
W2	7,370.45	26,972.16	0.00	5,102.58	2.62 x 0.245	1	R112 = round 1 1/8
V1	0.00	7,857.08	431.45	3,061.03	2.00 x 0.109	1	1210 = 1 1/4 x 1 1/4 x 0.109
V2	0.00	6,213.91	402.06	1,432.68	2.00 x 0.109	1	1010 = 1 x 1 x 0.109

STRESS ANALYSIS - PAGE 3

NEW MILLENNIUM
A Steel Dynamics Company

Job Number:	Job Name:	Date Run:
00-0-0511	PHIL - SHOPORDERS	5/13/2024 4:53:19 PM

Location:	Joist Description:	Mark:
,	Short Span Crimp 30K152.5/152.5	HKUBI

TCX Design

971 TCX Left	
TCX Length	0-0
TCX Type	R
TCX Depth	2 1/2
BPL Length	0-4
Clear Bearing	0-4 1/2
BPL Material: 1714 = 1 3/4 x 1 3/4 x 0.143	

TCX Right	
TCX Length	0-0
TCX Type	R
TCX Depth	2 1/2
BPL Length	0-4
Clear Bearing	0-4 5/8
BPL Material: 1714 = 1 3/4 x 1 3/4 x 0.143	

Total Load	152.50
Reqd TL Def L/80	0.00
Live Load	152.50
Reqd LL Def L/120	0.00
Section Modulus	0.0000
Reqd SM	0.0000
Mom of Inertia	0.0000
Reqd MI	0.0000

Seat Type: Lapped

Total Load	152.50
Reqd TL Def L/80	0.00
Live Load	152.50
Reqd LL Def L/120	0.00
Section Modulus	0.0000
Reqd SM	0.0000
Mom of Inertia	0.0000
Reqd MI	0.0000

Seat Type: Lapped

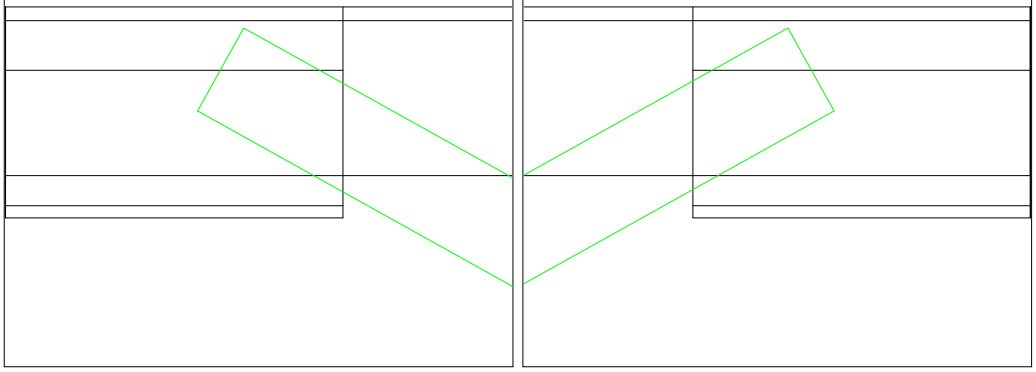

Load Combinations

Case 1: DL
Case 2a: LL
Case 2b: SL
Case 3a: DL+CL+TL+LL
Case 3b: DL+CL+TL+SL
Case 3c: DL+CL+TL+LL+FEM
Case 3d: DL+CL+TL+SL+FEM
Case 3e: DL+CL+TL+LL
Case 3f: DL+CL+TL+SL
Case 4a: DL+WL+AX
Case 4b: DL+WL-AX
Case 4c: DL+WL+AX+IP
Case 4d: DL+WL-AX+IP
Case 4e: DL+SM+AX
Case 4f: DL+SM-AX
Case 5a: 0.6(DL)+WL+AX
Case 5b: 0.6(DL)+WL-AX
Case 5c: 0.6(DL)+WL+AX+IP
Case 5d: 0.6(DL)+WL-AX+IP
Case 5e: 0.6(DL)+WL+AX+SM
Case 5f: 0.6(DL)+WL-AX+SM
Case 6a: DL+CL+0.85(TL)+WL+AX
Case 6b: DL+CL+0.85(TL)+WL-AX
Case 6c: DL+CL+0.85(TL)+WL+C+AX+IP
Case 6d: DL+CL+0.85(TL)+WL+C-AX+IP
Case 6e: DL+CL+0.85(TL)+WL+AX+IP
Case 6f: DL+CL+0.85(TL)+WL-AX+IP
Case 6g: DL+CL+0.85(TL)+SM+AX
Case 6h: DL+CL+0.85(TL)+SM-AX
Case 7a: DL+CL+0.85(TL)+0.75(WL+AX+LL)
Case 7b: DL+CL+0.85(TL)+0.75(WL-AX+LL)
Case 7c: DL+CL+0.85(TL)+0.75(WL+C+AX+LL+IP)
Case 7d: DL+CL+0.85(TL)+0.75(WL+C-AX+LL+IP)
Case 7e: DL+CL+0.85(TL)+0.75(WL+AX+LL+IP)
Case 7f: DL+CL+0.85(TL)+0.75(WL-AX+LL+IP)
Case 7g: DL+CL+0.85(TL)+0.75(SM+AX+LL)
Case 7h: DL+CL+0.85(TL)+0.75(SM-AX+LL)
Case 8a: DL+CL+0.85(TL)+0.75(WL+AX+SL)
Case 8b: DL+CL+0.85(TL)+0.75(WL-AX+SL)
Case 8c: DL+CL+0.85(TL)+0.75(WL+C+AX+SL+IP)
Case 8d: DL+CL+0.85(TL)+0.75(WL+C-AX+SL+IP)
Case 8e: DL+CL+0.85(TL)+0.75(WL+AX+SL+IP)
Case 8f: DL+CL+0.85(TL)+0.75(WL-AX+SL+IP)
Case 8g: DL+CL+0.85(TL)+0.75(WL+AX+SL+SM)
Case 8h: DL+CL+0.85(TL)+0.75(WL-AX+SL+SM)
Case 9a: 1.2(DL)+0.5(LL)+0.8(TL)+SM+AX+FEM
Case 9b: 1.2(DL)+0.5(LL)+0.8(TL)+SM-AX+FEM

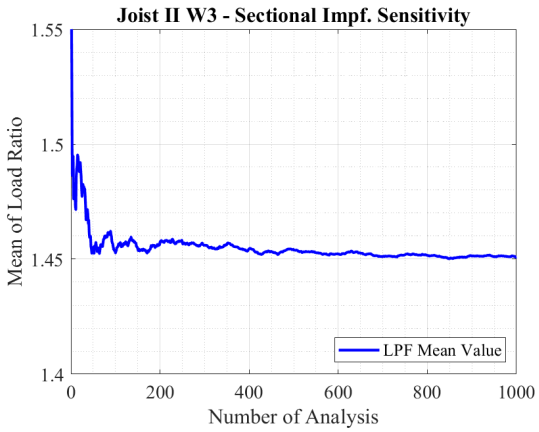

(a) PDF of LPF values

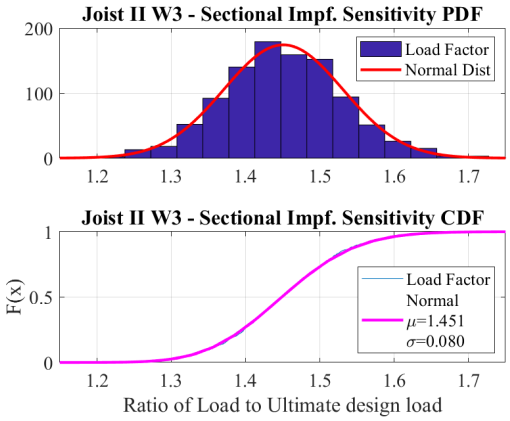

(b) Fitted distribution type for LPF results

Figure B.24: Joist II W3 cross-sectional imperfection sensitivity analyses results and fitted distribution

Bibliography

[1] Leroy Gardner and Xiang Yun. Description of stress-strain curves for cold-formed steels. *Construction and Building Materials*, 189:527–538, 2018.

[2] Xiang Yun and Leroy Gardner. Stress-strain curves for hot-rolled steels. *Journal of Constructional Steel Research*, 133:36–46, 2017.

[3] Joseph Robert Yost, David W Dinehart, Shawn P Gross, Joseph J Pote, and Brian Gargan. Strength and design of open web steel joists with crimped-end web members. *Journal of Structural Engineering*, 130(5):715–724, 2004.

[4] Theodore V Galambos. Systems reliability and structural design. *Structural Safety*, 7(2-4):101–108, 1990.

[5] Samer Hendawi and Dan M Frangopol. System reliability and redundancy in structural design and evaluation. *Structural safety*, 16(1-2):47–71, 1994.

[6] American Iron and Steel Institute. *S100-16 (R2020): North American Specification for the Design of Cold-formed Steel Structural Members*. The American Iron and Steel Institute (AISI), Washington, DC, U.S.A., 2020.

[7] AISC 360-16. *Specification for Structural Steel Buildings*. ANSI/AISC, 2016.

[8] International Code Council. *2021 International Building Code (IBC)*. International Code Council, Washington, D.C., 2020.

[9] Edward J Sippel, Ronald D Ziemian, and Hannah B Blum. Buckling behavior of open-web steel joists and joist girders. In *Proceedings of the 2022 SSRC Annual Stability Conference. Denver, CO: SSRC*, pages 1–21, 2022.

[10] Rohola Rahnavard, Hélder D Craveiro, Rui A Simões, Shahabeddin Torabian, and Benjamin W Schafer. Built-up cold-formed steel lightweight concrete (cfs-lwc) composite beams: applicability of en 1994-1-1 and aisc-360. *Thin-Walled Structures*, 214:113301, 2025.

[11] Sándor Ádány and Benjamin W Schafer. Finite tube method for buckling analysis of tubular members using fourier-approximation for the displacements. *Thin-Walled Structures*, 206:112672, 2025.

[12] Divyansh R Kapoor, Brian Bogh, and Kara D Peterman. Influence of support attachment pattern on the out-of-plane buckling capacity of steel deck. 2023.

[13] Edward J Sippel, Ronald D Ziemian, and Hannah B Blum. Influence of torsional stiffness in double-angle open-web joist and joist girder chords. *Journal of Constructional Steel Research*, 199:107595, 2022.

[14] Kubilay Cicek, Thomas Sputo, and Hannah B Blum. The impact of analysis assumptions on buckling prediction in open-web steel joists. In *Annual Stability Conference, Structural Stability Research Council*, 2024.

[15] NS Trahair and GJ Hancock. Steel member strength by inelastic lateral buckling. *Journal of structural Engineering*, 130(1):64–69, 2004.

[16] Merih Kucukler, Leroy Gardner, and Lorenzo Macorini. A stiffness reduction method for the in-plane design of structural steel elements. *Engineering Structures*, 73:72–84, 2014.

[17] Xi Zhang, Kim JR Rasmussen, and Hao Zhang. Beam-element-based analysis of locally and/or distortionally buckled members: Application. *Thin-Walled Structures*, 95:127–137, 2015.

[18] Kim JR Rasmussen, Xi Zhang, and Hao Zhang. Beam-element-based analysis of locally and/or distortionally buckled members: Theory. *Thin-Walled Structures*, 98:285–292, 2016.

[19] AISC 360-22. *Specification for Structural Steel Buildings*. ANSI/AISC, 2022.

[20] ASTM International. Standard specification for general requirements for rolled structural steel bars, plates, shapes, and sheet piling. Technical Report ASTM A6/A6M-24, ASTM Interna-

tional, West Conshohocken, PA, 2024.

[21] American Iron and Steel Institute. North american standard for cold-formed steel structural framing. Technical Report AISI S240-20, American Iron and Steel Institute, Washington, DC, 2020.

[22] Kubilay Cicek, Thomas Sputo, and Hannah B Blum. Sensitivity of open-web steel joist stability to material and geometric property variability. In *Annual Stability Conference, Structural Stability Research Council*, 2025.

[23] Andrzej S Nowak and Kevin R Collins. *Reliability of structures*. CRC press, 2012.

[24] Bruce R Ellingwood. *Development of a probability based load criterion for American National Standard A58: Building code requirements for minimum design loads in buildings and other structures*, volume 577. US Department of Commerce, National Bureau of Standards, 1980.

[25] VZ Meimand and BW Schafer. Impact of load combinations on structural reliability determined from testing cold-formed steel components. *Structural Safety*, 48:25–32, 2014.

[26] American Society of Civil Engineers. Minimum design loads and associated criteria for buildings and other structures. American Society of Civil Engineers, 2017.